Dynamic Characteristics of Bare Conductors

By

Ojo Evans Eshiemogie

(Student No: 206520793)

In *partial* * Fulfillment of the requirements for the degree

Masters of Science in Electrical Engineering

School of Electrical, Electronics and Computer Engineering
Faculty of Engineering
University of KwaZulu-Natal
Supervisor : Professor N.M. Ijumba
Co-supervisor : Professor D. Muftic
Durban, South Africa
June, 2011

PREFACE

The work described in this dissertation was carried out through the school of Electrical, Electronic and Computer Engineering, University of KwaZulu-Natal (UKZN). The experimental work used in this study was done at Vibration Research and Testing Centre (VRTC) located at the Westville campus of University of KwaZulu-Natal.

The author hereby confirms that the material presented in this dissertation is my own work, except where specific acknowledgment is made by name or in the form of a reference.

DECLARATION
I, Ojo Evans Eshiemogie declare that:

(i) The research reported in this dissertation/thesis, except where otherwise indicated, is my original work.
(ii) This dissertation/thesis has not been submitted for any degree or examination at any other university.
(iii) This dissertation/thesis does not contain other persons' data, pictures, graphs or other information, unless specifically acknowledged as being sourced from other persons.
(iv) This dissertation/thesis does not contain other persons' writing, unless specifically acknowledged as being sourced from other researchers. Where other written sources have been quoted, then:
a) their words have been re-written but the general information attributed to them has been referenced;
b) where their exact words have been used, their writing has been placed inside quotation marks, and referenced.
(v) Where I have reproduced a publication of which I am an author, co-author or editor, I have indicated in detail which part of the publication was actually written by myself alone and have fully referenced such publications.
(vi) This dissertation/thesis does not contain text, graphics or tables copied and pasted from the Internet, unless specifically acknowledged, and the source being detailed in the dissertation/thesis and in the References sections.

Signed_____ Date _____
E. E. Ojo

"As the candidate's supervisor I agree/do not agree to the submission of this dissertation"

Signed_____ Date _____
Prof. N. M Ijumba (Supervisor)

ACKNOWLEDGEMENTS

My sincere gratitude goes to my supervisor and co-supervisor, Professor N.M. Ijumba and Professor D. Muftic for their invaluable support and guidance throughout this study.
I am highly grateful to my mentor, Professor M. A. E. Kaunda for his immense support and also for being the source of my inspiration.

I own my sincere gratitude to a number of individuals whom in one form or the other contributed to the successful completion of this project among them Dr R. Loubser, Prof E. Boje, Dr M. Gafarri, Cosmai Umbato, Prof Dan Iman, Dr. K. Arunakirinathar and others too numerous to mention.

I would like to thank the former business manager of High Voltage and Direct Current (HVDC) centre, Leena Rajpal for being there to lend me her support and to the coordinator of the VRTC, Pravesh Moodley for his immense contribution to this study. My thanks go to all past postgraduate administrators: Neetu, Precious, Nicolas, and Kerry-Ann.

My gratitude goes to the Engineering Faculty Officer, Fiona Higginson for her guidance during the course of my study.

I gratefully acknowledge the financial support from the HVDC centre and VRTC during the course of my study

My sincere thanks go to my all my colleagues and friends for their moral support. I want to use this opportunity to remember my late friend and colleague Don Chamagini, the biggest question that still remain unanswered, ‘why must this happen’. I believe it is only God that knows why such a tragic event has to happen to an innocent person like you, rest in peace my bosson friend.

I dedicate this dissertation to my father and mother Mr. Moses and Mrs. Magdalene Ojo and to the entire Ojo’s family especially Cyril, for their constant source of inspiration and if not for them it would have not been possible for me to complete my studies.

Finally, I would like to thank all those who have contributed, either directly or indirectly to the preparation, research and compilation of this project report.

Abstract

The dynamic characteristic of transmission line conductors is very important in designing and constructing a new line or upgrading an existing one. This concept is an impediment to line design and construction because it normally determines the tension at which the line is strung and this in respect affects the tower height and the span length. Investigations into the phenomenon of mechanical oscillation of power line conductors have been extensively looked into by many researchers using concepts from mechanics and aerodynamics to try and predict the conductor dynamic behaviour. Findings have shown that precise prediction of conductor wind-induced vibration is very difficult i.e. non-linearity.

Over the years, various analytical models have been developed by researchers to try and predict the mechanical vibration of transmission line conductors. The first part of this dissertation considers the analysis of the model describing the transverse vibration of a conductor as a long, slender, simply supported beam, isotropic in nature and subjected to a concentrated force. The solution of this beam equation was used to obtain the conductor natural frequencies and mode shapes. Conductor self-damping was obtained by the introduction of both external and internal damping models into the equation of motion for the beam.

Next, also using the same beam concept was the application of the finite element method (FEM) for the dynamic analysis of transmission line conductors. A finite element formulation was done to present a weak form of the problem; Galerkin's method was then applied to derive the governing equations for the finite element. Assembly of these finite element equations, the equation of motion for the transverse vibration of the conductor is obtained. A one dimensional finite element simulation was done using ABAQUS software to simulate its transverse displacement. The eigenvalues and natural frequencies for the conductors were calculated at three different tensions for two different conductors. The damping behaviour of the conductors was evaluated using the proportional damping (Rayleigh damping) model. The results obtained were then compared with the results from the analytical model and the comparison showed a very good agreement.

An electrical equivalent for the conductor was developed based on the concept of mechanical-electrical analogy, using the discrete simply supported beam model. The developed electrical equivalent circuit was then used to formulate the transfer function for the conductor. Matlab software was used to simulate the free response of the developed transfer function.

Finally, the experimental study was conducted to validate both the analytical model and the FEM. Tests were done on a single span conductor using two testing methods i.e. free and force vibration. The test results are valid only for Aeolian vibration. From the test results the conductor's natural frequencies and damping were determined. The experimental results, as compared with the analytical results were used to validate the finite element simulation results obtained from the ABAQUS simulation.

CONTENTS

4. MODEL VERIFICATION: FINITE ELEMENT ANALYSIS AND MECHANICAL EQUIVALENCE

5. TESTING AND RESULTS

6. CONCLUSIONS AND RECOMMENDATIONS

CHAPTER 1

INTRODUCTION

1.1 Background

South Africa is presently experiencing power crises because the current generation capacity is less than the load. This has prompted the nation utility to increase the power output from all aspects of its operation. The power system in the country is divided into generation, transmission and distribution. The transmission networks are used to transfer power from the generation stations to the distribution networks.

Economic and environmental pressure, coupled with the difficulty in acquiring lines right-of-way (servitude) has greatly influenced the design of overhead transmission lines. The pressure resulting from these conditions has necessitated the construction of long, high-capacity, high-voltage transmission lines [1].

Transmission lines are designed to ensure availability, reliability of power, safety for the public and maintenance personnel and can be constructed at optimal cost. Lines in South Africa are designed to meet standards set in accordance with the code of practice described in the SABS document [2]. This code of practice specifies the minimum clearance of the conductor from the ground, public roads, railway lines as well as other power lines under varying weather conditions such as temperature and wind. Based on these criteria; it is very expensive to construct a new line, upgrade or maintain existing ones. Hence, the cost of designing and constructing transmission lines continues to increase over the years. Overhead power lines usually consist of the following: steel towers, conductors, insulators and associated attachment hardware.

The conductor whose function is to transfer power in power lines is considered to be the most expensive component. Therefore, its contribution towards the cost of the power line is significant. Conductor costs (material cost and installation costs) associated with the capital investment of a new over head power line contributes up to 40% of the total capital costs of the line [3]. Consequently, much attention has to be given to the selection of a conductor configuration to meet both present and predicted future load requirements. Transmission line components are usually exposed to dynamic forces (mechanical power) and motions. Out of all the line components, cables are normally susceptible to forces that cause both static and dynamic action due to its flexible structure. The dynamic action is mostly caused by wind loading.

Probably no other large structure so continuously exposed to the forces of the wind has as much of its mass in such a highly flexible form [1][4]. This makes the line susceptible to the development of sustained cyclic conductor motions. The continuous exposure of conductors to mechanical power from wind can possibly lead to damage or fatigue failure of conductors and also to other line components.

1.2 Motivation

In utilities all over the world, power is normally transferred using overhead transmission lines from the generation stations, which are usually sited in remote areas and are connected to load centers which are a few kilometers to hundreds of kilometers away, passing through different terrains. This power is transferred by bare conductors. Bare conductors are non-insulated, and are made of numbers of aluminum stands with or without steel wires at the core. The conductors can withstand higher level of current compared to the insulated conductors of the same cross-sectional area and this is why they are widely used in long-span transmission line.

In transmission lines, the most important component used to convey power is the bare conductor and before it is put into service, the line designers have to ascertain its electrical properties, thermal limits, mechanical properties and other factors which affect the performance of the line. This process will help the line designers to design an optimal power line that will guarantee availability, reliability of power, safety to the public and maintenance personnel and will also meet the cost/benefit of constructing the line.

As the lines passes through various terrains, they are usually subjected to mechanical loading from wind which is dynamic in nature and also a function of the type of terrain [1]. Loading causes mechanical oscillations in the high-voltage transmission lines, and prolonged exposure of conductors to vibrations will eventually result in fatigue, fretting and other failure modes.

Over the years, numerous research projects have been conducted to try and understand the dynamic behaviour of conductors when subjected to mechanical loading from wind. Investigations into the phenomenon of mechanical oscillation of power line conductors have been extensively looked into using concepts from rigid body, analytical, fluid mechanics and aerodynamics to try and predict the conductor dynamic behaviour. Based on findings, the mechanical vibrations of a conductor when it receives loading from wind exhibits a complex dynamic and also the system response is non-linear. Thus, precise modeling of the dynamics

involved is difficult due to the fact that the behaviour of the system is non-linear. Therefore, in line with the above, there is a need to continue to study this form of conductor motion in order to be able to adequately predict the system response to some degree of accuracy, especially with respect to self-damping when subjected to the dynamic forces from wind.

The aims and objectives of this research project are:

- To analyse the model describing the transverse vibration of bare conductors
- To evaluate the self-damping capability of bare conductors
- To evaluate the analytical model using finite element analysis
- To develop an electrical equivalence for the vibrating conductor
- To verify experimentally the analytical model

1.3 Research Question

Based on the inference made in [5] in which it was stated that the accurate information on how to determine the power line self-damping capability is very important because it can be used to assess a method of estimating the maximum amplitude that occurs on the line. Conversely, in the same report it was suggested that if the value of the conductor self-damping was small enough to be ignored, consequently the analysis of the principle modes of the undamped system could then also be used for the damped systems. However, the dynamic analysis of systems shows that the damping force of a system may be considered small as compared to mass and stiffness but its influence on the system's dynamic characteristic is very significant. Therefore, it is imperative to know the accurate amount of conductor self-damping before ignoring it or its contribution when carrying out dynamic analysis of power line conductors.

In line with the above, the research question that needs to be answered is

"How can we effectively determine bare conductors' self-damping?"

1.4 Hypothesis

Wind-induced vibration, due to its catastrophic nature and engineering implication on power has led to extensive research work over the years. Ever since mechanical oscillation of power line conductors was noticed on transmission lines, investigations have been carried out by many

researchers. This has led to extensive studies using theoretical, field, and also from both outdoor and indoor vibration testing laboratory experimental studies to try and predict the conductor dynamic behaviour.

Based on findings emanating from other researchers, various bodies, such as IEEE, Gigré, and IEC have come with standards in constructing power lines. These standards normally specify the stringing tension with respect to the conductor ultimate tensile strength (UTS) and also vibration absorber suitable for certain climatic conditions and the nature of the terrain. The main goal of this study is to determine damping of line conductors at tensions higher than that stipulated, as its string tension and also ascertain whether it is desirable to adopt a higher conductor tension than the one currently being used by line designers. Thus, this will help determine the conductor self-damping at that tension and in respect help to ascertain its influence on the dynamic characteristics of the vibrating conductor. Conversely, this will help determine the type and amount of vibration absorbers (dampers) that will be needed on the lines.

1.5 Importance of This Study

As highlighted above, standards are set by various bodies on the specific tension (as a percentage of its UTS) which the line should be strung. In accordance, designing an overhead line, transmission line engineers normally string the line conductor at 25% of its ultimate tensile strength for aluminium conductor steel reinforced (ACSR) conductors based on recommendation in the Gigré report on Aeolian vibration [6] and 20% of its ultimate tensile strength for Aero-Z conductors based on the recommendation in the IEC standard [7]. These standards have been adopted by line designers based on outcomes from years of research and experience with overhead lines. Based on this, it has been ascertained that using these standards; the dynamic loading from the wind can be curtailed thereby ensuring a good fatigue life for the conductor.

In adopting these standards in designing a line, conductor self-damping capability is usually ignored. This is due to the fact that the self-damping by a conductor is assumed to be very small and also the value is not normally specified by conductor manufacturers. Thus, line design is normally done ignoring the contribution of conductor self-damping. However, if the conductor self-damping can be adequately ascertained, and also can be determined above the tension at which the lines are strung, by an increase of 5% above the value recommended above with

respect to its ultimate tensile strength i.e. 30% and 25% respectively. This will result in reducing sag with the following implications:

1) The line can be designed with a shorter tangential tower while the span length is kept the same.
2) The line can be designed with longer span length while the height of the tower is still kept the same.

The result will be a higher cost benefit on the part of power utilities both in designing and construction of new lines or upgrading existing lines.

1.6 Dissertation Outline

The background of this study has been elaborated on in this chapter. Chapter 2 gives the literature review of the mechanical vibration of systems with single degree-of-freedom (SDOF) and how the analysis of these systems can be used to describe conductor's mechanical vibrations when it receives loading from wind. Chapter 3 describes the analytical model describing the dynamic characteristics of bare conductors. Chapter 4 will be used for verification of the model using finite element method. Also in this chapter an electrical equivalence was also developed for the conductor. The aim of developing the conductor equivalent circuit is to provide an alternative in determining the conductor self-damping by means of electrical elements. Chapter 5 will describe the procedure used to carry out tests in Vibration Research and Testing Centre (VRTC) in line with IEEE standard on conductor self-damping. Also results from vibration tests and finite element method were presented and analyses of the results done. In Chapter 6, concluding remarks and future scope of the study was discussed.

CHAPTER 2

LITERATURE REVIEW

2.1 Waves

Waves are phenomena that are common to most aspects of our physical world and they are everywhere in nature. Based on the concept of physics, waves are created when an external energy (disturbance) is imposed on a system and this sets the system into back-and-forth vibrations about its equilibrium or rest position. When a wave is set up in a system, a pulse travels through the system continuously and periodically transporting energy away from the point the impulse was imposed on the system. Hence, waves are said to be an energy transport phenomenon in a medium without transporting the matter.

There are basically two types of wave with regards to energy transportation; electromagnetic and mechanical. A mechanical wave is a wave that requires a medium to transport energy while an electromagnetic wave does not require a medium. Waves are usually described by the following properties:

1) Amplitude (A)
2) Wavelength (λ)
3) Frequency (f)
4) Speed or Velocity (V)
5) Period (T)

The wave properties are illustrated using the diagram below.

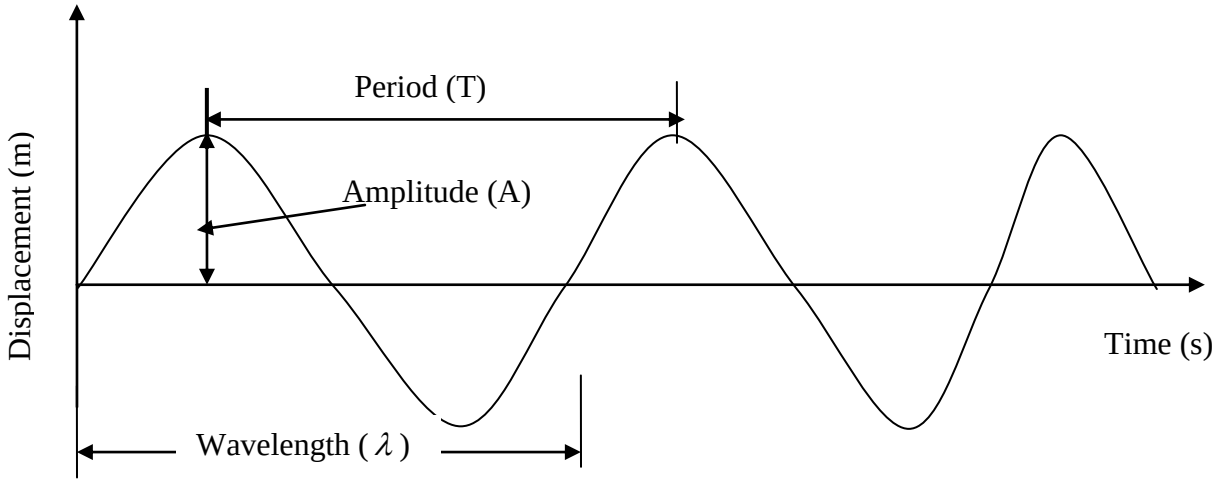

Figure 2.1 Graphical representations of wave motion and its properties

In the study of waves and vibration of systems, the vibration of the system is caused by the waves that travel through it and also the amplitude of vibration of the system is a function of the quantity of energy being transported through it i.e. the greater the energy the higher the amplitude of vibration of the system. Therefore, the quantity of energy that passes through the system determines the level of vibration.

For a system, a vibrating body with varying wave properties as mentioned above will not have effects on the speed. But for any system experiencing change in tension, this change will affect the speed of the wave. This is because a change in tension will have effects on the system's material properties such as the system's stiffness and density and this ultimately affect the speed at which the wave travels through the system.

In this study, the physics of waves is very important because the vibration of the system in focus is due to the transportation of energy through the system and analysis of the system will be done at different tensions. The varying of the tension of the system tends to have an effect on properties of the wave that travels through the system. As more energy is added to the system due to loading, the more energetic the vibration becomes. This can result to a phenomenon called resonance which will be discussed later in this chapter. This phenomenon is very important because some analysis that will be done in this study will be around the region in which it occurs.

2.2 Mechanical Vibration

Vibration is a fluctuating motion brought by fluctuating forces due to waves traveling through a system. The concept of vibration is a common phenomenon in mechanical systems and it is evidence in most systems in our physical world. Mechanical oscillation of a system is the motion about an equilibrium point and this oscillation may be periodic or non-periodic. The concept of vibration in any system may be beneficial, but in most cases it is a limiting factor in engineering design and careful design usually minimises unwanted vibrations.

2.2.1 Linear and Non-linear Systems

Vibrating mechanical systems can be analysed as either linear systems or non-linear systems. Linear systems vibrate in a periodic form and can be analysed using the superposition principle.

Therefore, the equations of motion are such that a linear combination of input to the system leads to the same linear combination of outputs (response) i.e. superposition principle. Examples of equations describing such systems are:-

$$m\ddot{x} + c\dot{x} + kx = 0 \qquad \text{..... (2.1)}$$

$$\ddot{x} + \frac{l}{g}x = 0 \qquad \text{..... (2.2)}$$

Non-linear systems are systems that oscillate in a non-periodic manner and all properties of linear systems are violated by non-linear systems. Non-linearity in a vibrating system is due to its mass, stiffness, damping and geometry. For time invariant system, non-linearity can be of two types: non-linear damping and non-linear stiffness [8]. Modal analysis does not apply to non-linear systems because it depends on super-position of solutions. Examples of equations describing non-linear systems are:-

$$m\ddot{x} + \dot{x} - \beta^2 x^3 = 0 \qquad \text{.....(2.3)}$$

$$m\ddot{x} + 2c(x^2 - 1)\dot{x} + kx = 0 \text{ (Van der Pol's equation)} \qquad \text{..... (2.4)}$$

It worthwhile to note that vibrations experienced in any real physical systems are non-linear which therefore implies that the assumption of small angles of oscillation restricts the system to linear case as well as simplifies the problem. This concept will be used in all analysis in this study.

2.3 Vibration Analysis

In the area of vibration analysis, understanding the response of both simple and complex systems can be achieved by studying and analysing the simple mass-spring–damper models. The vibration of this form of system can be described by single-degree-of-freedom and also the excitation of the system can be brought about by a harmonic force, *f*, as shown in figure 2.2. The formulation of the equation of motion for this system and its analysis, the following will be used:

- Based on Newton's second law of motion, the force produced is proportional to the acceleration of the mass

- The force applied to the mass by the spring is proportional to the length the spring is stretched. The proportionality constant is the stiffness of the spring in (N/m)
- The energy dissipated by the system is proportional to its velocity (i.e. viscous damping) in (Ns/m)
- The response of the system at $t = 0$ is x_0 (initial displacement) and v_0 (initial velocity) and are known as initial conditions.

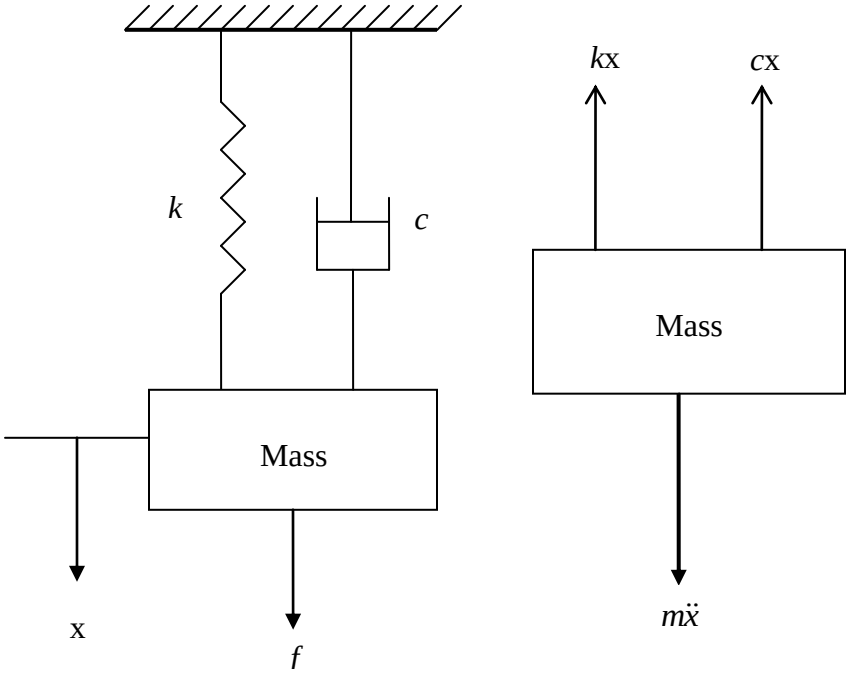

Figure 2.2 (a) Showing the mass-spring-damper system with one degree of freedom and figure 2.2 (b) showing its free body diagram

2.3.1 Types of Mechanical Vibration

The system of mass-spring-damper system shown in figure 2.2 can be used to analyse the following different types of mechanical vibrations usually experienced by vibrating systems.

- Free vibration without damping
- Free vibration with damping

- Forced vibration without damping
- Forced vibration with damping.

Free vibration without damping occurs when a mechanical system is set into vibration with an initial input and allowed to vibrate freely assuming damping is negligible and excitation force is zero i.e. c and f equal zero.

From figure 2.2, the equation describing the free vibration for the system is given as:

$m\ddot{x} + kx = 0$ or

$\ddot{x} + \omega^2 x = 0$ …….. ……. (2.5)

Where $\omega^2 = \frac{k}{m}$ and it is natural frequency for the system

The response of the system is given as

$x(t) = A\sin(\omega t + \phi)$ …… (2.6)

Where $A = \frac{\sqrt{\omega^2 x_0 + v_0}}{\omega}$ and $\phi = \tan^{-1}\frac{\omega x_0}{v_0}$

For free vibration with damping, the vibrating system has damping mechanism to dissipate energy which makes the initial amplitude decay with time.

Also using figure 2.2, the equation for the system becomes

$m\ddot{x} + c\dot{x} + kx = 0$

$\ddot{x}(t) + 2\xi\omega\dot{x}(t) + \omega^2 x(t) = 0$ ……..……. (2.7)

Where $\zeta = \sqrt{\frac{c}{m}} = \frac{c}{2m\omega}$

The response of the system is given as

$x(t) = Ae^{-\zeta\omega t}\sin(\omega_d t + \phi)$ …… (2.8)

Where $\omega_d = \omega\sqrt{1-\zeta^2}$, $A = \sqrt{\frac{(v_0 + \zeta\omega x_0)^2 + (x_0\omega_d)^2}{{\omega_d}^2}}$ and $\phi = \tan^{-1}\frac{x_0\omega_d}{v_0 + \zeta\omega x_0}$

A system is said to experience forced vibration without damping, with the assumption that the system damping is negligible. When the system is set into vibration by the application of an external force, the frequency of the vibration of the system is the same as the frequency of the driving force, but the magnitude of the vibration is strongly dependent on the dynamic characteristics of the mechanical system itself.

Using figure 2.2, if the external force, *f*, which is harmonic in nature is applied, the equation describing the system becomes:-

$$m\ddot{x}(t) + kx = f\sin\omega_{dr}t$$

$$\ddot{x} + \omega^2 x = F\sin\omega_{dr}t \qquad \ldots\ldots\ldots\ldots (2.9)$$

Where ω_{dr} frequency of the driving force

$$F = \frac{f}{m}$$

The response of the system is given as

$$x(t) = A\sin(\omega t + \phi) + \frac{F}{\omega^2 - \omega_{dr}}\cos\omega_{dr}t \qquad \ldots\ldots\ldots\ldots\ldots (2.10a)$$

or

$$x(t) = \frac{v_0}{\omega}\sin\omega t + \left(x_0 - \frac{F}{\omega^2 - {\omega_{dr}}^2}\right)\cos\omega t + \frac{F}{\omega^2 - {\omega_{dr}}^2}\cos\omega t \qquad \ldots\ldots\ldots\ldots\ldots (2.10b)$$

For forced vibration with damping, when set into vibration by a harmonic force *f*, the amplitude decays with time.

The equation of motion describing the system becomes

$$m\ddot{x} + c\dot{x} + kx = f\sin\omega_{dr}t$$

$$m\ddot{x} + 2\xi\omega\dot{x} + \omega x = F\sin\omega_{dr}t \qquad \ldots\ldots\ldots\ldots\ldots\ldots (2.11)$$

Whose general response is give as

$$x(t) = Ae^{-\zeta\omega_n t}\sin(\omega_d t + \phi) + X\cos(\omega t - \theta) \quad \text{..... (2.12)}$$

Where

$$A = \frac{x_0 - X\cos\theta}{\sin\phi}\ ,\ \phi = \tan^{-1}\frac{\omega_d(x_0 - X\cos\theta)}{v_0 + (x_0 - X\cos\theta)\zeta\omega_n - \omega X\sin\theta},\ \theta = \tan^{-1}\frac{2\zeta\omega_n\omega}{\omega_n{}^2 - \omega^2}$$

And $X = \dfrac{F}{\sqrt{\left(\omega_n{}^2 - \omega^2\right)^2 + \left(2\zeta\omega_n\omega\right)^2}}$

2.3.2 Beats and Resonance

For a system experiencing forced vibration without damping as shown in figure 2.2, as described by equation (2.8). As explained by the author [9], for such a system to maintain a constant-amplitude, a force *f*, has to be applied that is harmonic in nature. As the frequency (ω_{dr}) of the driving force is being varied, a condition is reached in which the frequency of the driving force approaches the natural frequency of the system (ω) and two very important phenomena occur. The first is the beats.

Beats are rapid oscillations with slowly varying amplitude and they occur when the frequencies are slightly different. Applying the principle of superposition, the summation of their displacements at each instance with time equals to the total displacement at that time, as shown in figure 2.3 below.

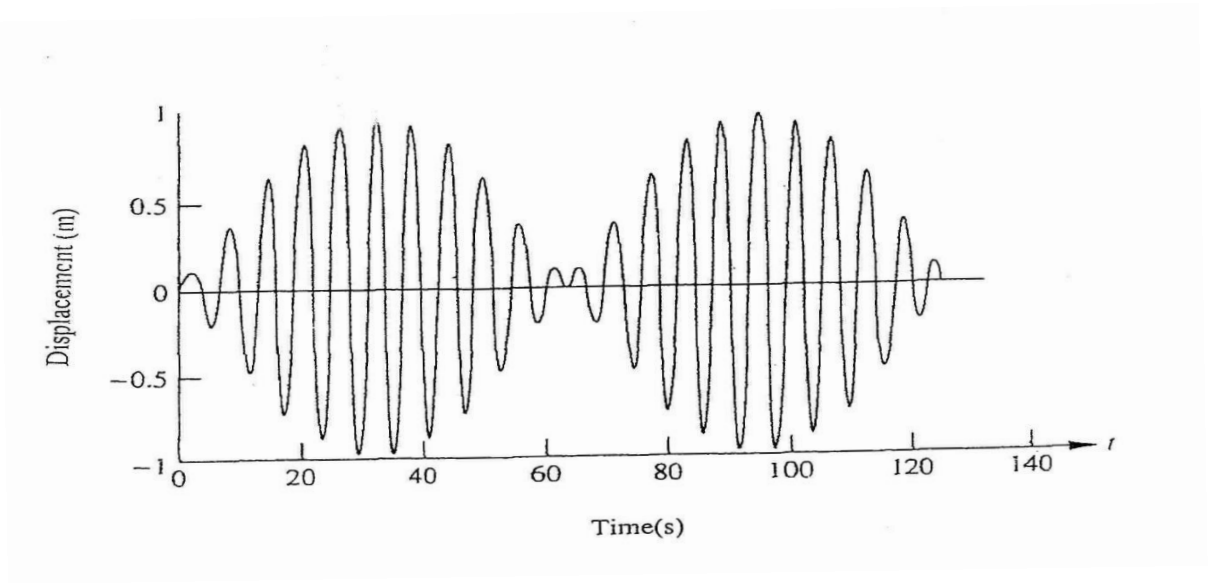

Figure 2.3 Beats [9]

The second is resonance and it occurs when the driving frequency ω_{dr} becomes exactly equal to the system's natural frequency (ω_{dr} = ω). When a system is at resonance, the system experiences oscillation which is an amplitude peak i.e. the amplitude of vibration becomes unbound as shown in figure 2.4. The frequency at which this occurs is called the resonance frequency.

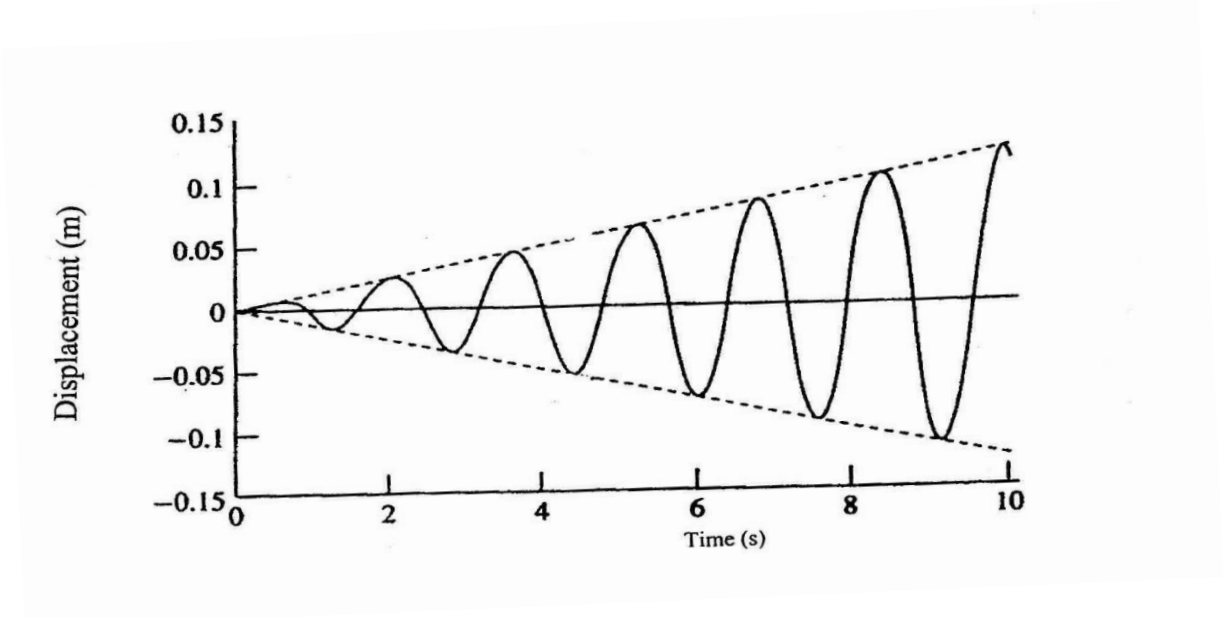

Figure 2.4 Forced response of a spring-mass system driven harmonically at its natural frequency [9]

2.4 Damping

Damping is the term used to define the non-conservative forces used by mechanical systems to dissipate energy. It is responsible for the decrease in amplitude with time as the system undergoes oscillation. In real-world systems there is an inherent mechanism, in which imposed external energy is removed from the system without which the system will continue to oscillate without coming to rest.

There are three main types of damping present in any mechanical system:

- Internal damping in which damping is caused by a microstructure defects, thermoelastic, effects of dislocation in metals etc. This form of damping can either be viscoelastic or hysteretic damping.
- Structural damping, where damping occurs from rubbing friction or contact between different elements in a mechanical system.
- Fluid damping, this occurs when a material is immersed in a fluid and there is relative motion between the material and the fluid, and the material is subjected to drag force resulting in damping.

Using the mass-spring-damper systems with damping described in section 2.3.1, the solution to these equations depends on the amount of damping. Systems vibrating with some form of damping can be experiencing one of the following types of damping:

- ❖ Critical damping: This occurs when the system no longer oscillates but returns to its equilibrium position without oscillation when it is displaced and released.
- ❖ Over damping: In this condition the system does not oscillate, but returns to its equilibrium position more slowly than with critical damping.
- ❖ Under damping: In this condition the system oscillates with steadily decreasing amplitude.

In this study, the system that was analysed is an example of a system that experiences under-damping but with very low inherent damping characteristics that made it prone to vibration.

In analysing vibrating mechanical systems, several forms of damping models were available for modeling a particular mechanical device or structure. These are:

1) Viscous damping
2) Coulomb damping
3) Hysteretic damping, solid damping or structural damping.

It is common to study damping mechanisms by examining the energy dissipated per cycle under a harmonic loading. Often, force versus displacement curve, or stress versus strain curves are used to measure the energy lost and hence, determine a measure of damping in the system.

Energy lost ΔE, per cycle is defined by

$$\Delta E = \int F_d \, dx \qquad \text{…….. (2.13)}$$

Where F_d is the damping force

2.4.1 Effects of damping

The vibration of systems usually slows down and eventually dies out with the presence of damping. In modern engineering, damping is a design parameter because the amplitude of vibration will be determined by the amount of damping present in the system. Reference [10], with relation to damping, gave the explanation of the effect of the other two parameters: mass and stiffness. This implies that to optimise any system for maximum damping consideration should be given to the variation of all three parameters invoved these are damping, mass and stiffness.

For systems executing harmonic excitation, increasing damping will affect the response only while an increase in stiffness (increase in frequency) will result in a decrease in amplitude. Also change in mass of the system results in change in frequency but little or no change in the response of the system.

2.4.2 Conductor damping

Generally, any system or body that is subjected to mechanical vibration can damp-out energy in the following ways:

Firstly, by internal damping where the damping is by internal friction at the molecular level due to microstructures- impurities, grain boundaries, etc in the system. Secondly, is by structural damping as a result of inter-strand friction (rubbing friction) and contact among different

components and assemblies of the system. Thirdly, by fluid damping where the relative motion between the wind and the body subjects the body to a drag force thereby returning the energy back to the wind.

In transmission lines when conductors are exposed to transverse vibration by mechanical loading that is dynamic and harmonic in nature, conductors can damp out this energy by internal friction at the molecular level; by inter-strand friction within the conductor; by transference to clamps, dampers, spacers, spacer-dampers, and suspension assemblies; by transference to adjoining sub-conductors (in the case of bundled conductors); or by return of energy to the wind. [1] [11]

The internal energy losses at microscopic (molecular) level within the core and individual strands of the conductor are known as metallurgical or material damping [12]. When a conductor flexes, the strands of the conductor slip against each other; this relative motion generates frictional forces that provide damping [11]. The combination of these energy dissipative processes by a conductor is known as conductor self-damping.

2.5 Conductor Mechanical Vibration

In an overhead transmission line, conductors are used to transfer power from one point to another. When these conductors are exposed to nature's dynamic forces, they are set into vibration. Wind loading is the most common form of loading that causes mechanical oscillations of conductor in high-tension transmission lines. This form of dynamic motion includes those types that are repetitive or cyclic in motion and there are three major types of wind-induced conductor motion that affect the transmission lines. These are Aeolian vibration, Conductor galloping and Wake-induced vibration. It is important to note that this motion exhibited by a conductor when it is exposed to wind loading is a function of the following:

a) Wind velocity
b) Line tension
c) Diameter of conductor
d) Temperature
e) Conductor self-damping
f) Terrain

2.5.1 Strouhal and Scruton Numbers

Strouhal [13] was the first person to describe the vortex-shedding phenomenon resulting from wind flowing across a stationary cylindrical structure. This phenomenon can be described by a non-dimensional number, known as Strouhal number. This number is given as:

$$S = \frac{f_s d}{V} \quad \text{…… …….. (2.14)}$$

Where

f_s = the frequency of vortex shedding

d = the diameter of the cylindrical structure

V = velocity of the smooth flow of wind.

The Strouhal number is taken to be 0.185 to 0.2 for vibrating conductors

The Scruton number [14] is another important parameter when considering vortex excitation of wind-induced vibrations of power line conductors. This number is given as:

$$S_c = \frac{m\zeta}{\rho d^2} \quad \text{……. (2.15)}$$

where

m = is mass of cable per unit length (kg/m),

ζ = damping as ratio of critical damping,

ρ = air density (kg/m^3), and

d = cable diameter (m).

This relationship shows that increasing the mass density and damping of the conductor, increases the Scruton number. Most types of wind-induced oscillation on a conductor tend to be mitigated by increasing the Scruton number because the amplitude of the conductor oscillations is inversely proportional to the Scruton number S_c.

Therefore, increasing the mass and damping of the conductor increases the Scruton number and therefore reduces oscillation amplitudes. Thus, its value is a measure of the conductor damping when subjected to aerodynamic excitation (vortex shedding) at the Strouhal frequency.

2.5.2 Classification of Conductor Oscillation

As mentioned earlier, there are three major types of wind-induced conductor vibration which are cyclic in nature that will affect the transmission lines conductors:

1) Aeolian vibration
2) Conductor galloping
3) Wake-induced vibration

2.5.2.1 Aeolian vibration

Aeolian vibration [1][4] is caused by the flow of laminar (smooth) streams of wind over a conductor. Based on the research using the concept from fluid mechanics and aerodynamics, it occurs as the wind stream passes over the conductor, causing a formation of alternating vortices (eddies) behind. This creates vortex induced air pressure fluctuations in the downstream wake side of the conductor which tends to produce motion at right angle to the direction of the wind as shown in figure 2.6. Aeolian vibration is characterised by a frequency range which is usually between 3 and 200Hz and the vibration amplitude could be one conductor diameter peak-to-peak. It occurs at low wind velocities between 1 to 7m/s.

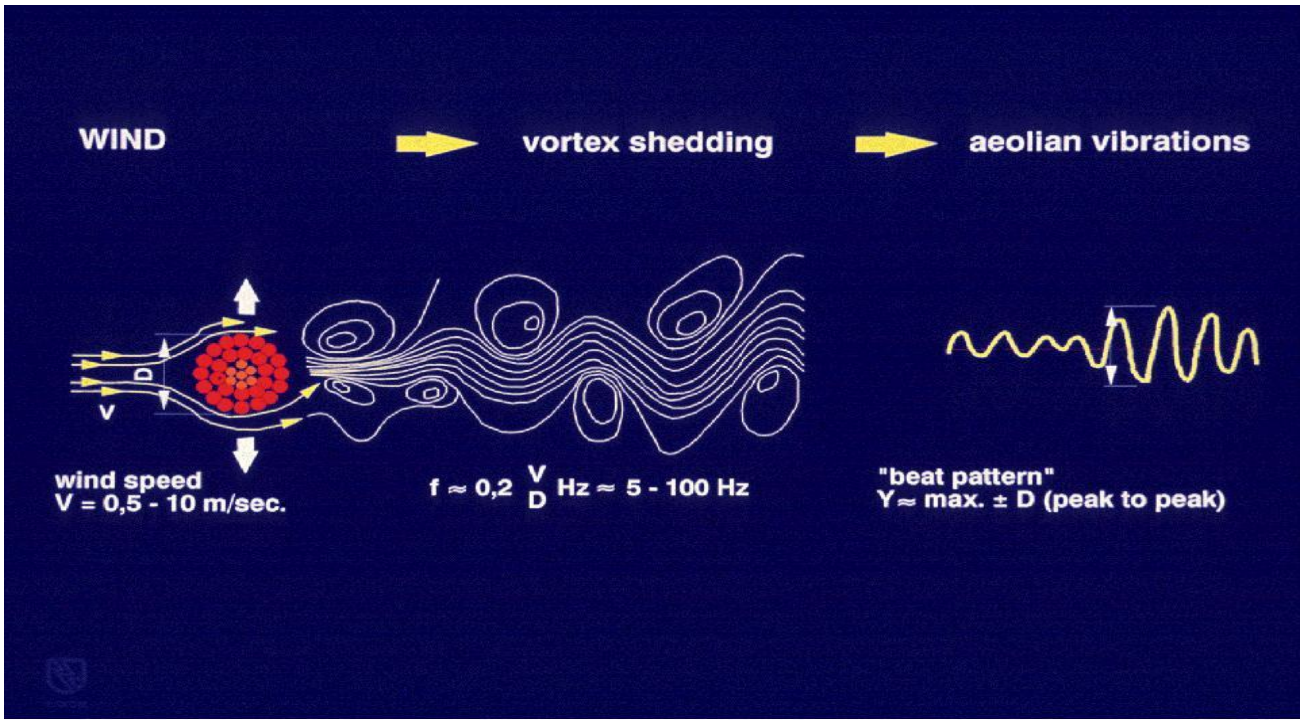

Figure 2.6 Aeolian vibration vortex formations [1]

2.5.2.2 Conductor galloping

Conductor galloping [1][4] is a cyclic conductor oscillation that is common to areas that experiences snow. It is usually caused by ice deposited on the conductor, modifying its cross-sectional circular shape to an asymmetrically-iced conductor surface as shown in figure 2.7 below. As wind blows across the conductor, because the asymmetrically-iced conductor is aerodynamically unstable, conductor galloping does occur. It is a low frequency (from 0.1 to 1Hz), high amplitude (± 0.1 to ±1 times the sag of the span) form of vibration and it is usually caused by a moderate, steady crosswind acting upon an asymmetrically iced conductor surface. Galloping takes one of two basic forms, standing waves and traveling waves or a combination of them.

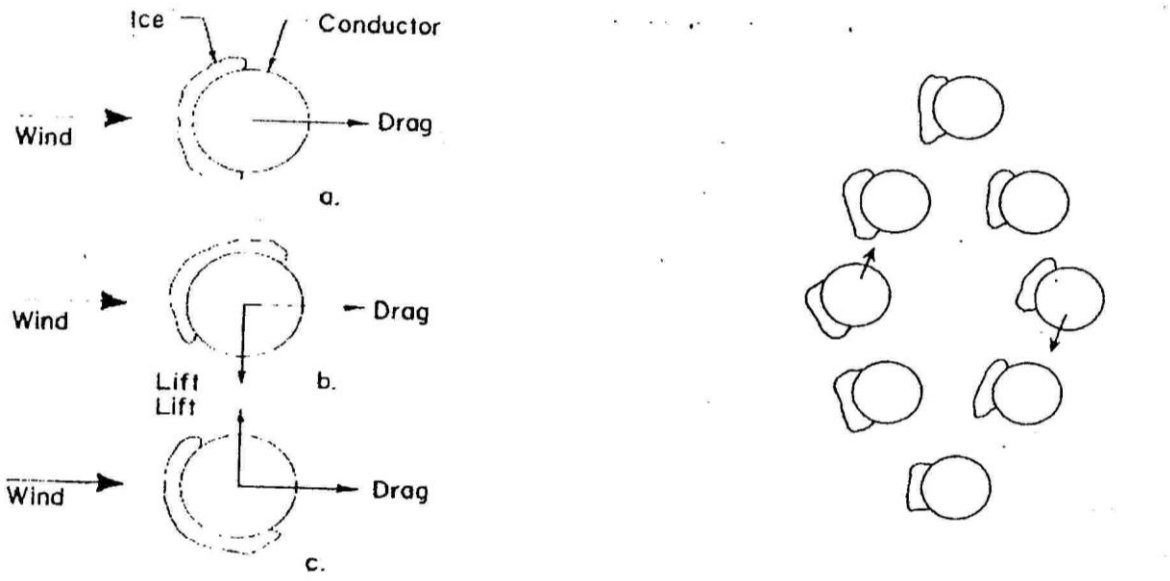

Figure 2.7 Asymmetric iced conductor [1] [4]

2.5.2.3 Wake-induced vibration

Wake-induced vibration or bundle conductor oscillation [1][4] is associated with bundle conductors of a transmission line. It is caused by the aerodynamic shielding of leeward conductors by windward conductors. The vibration occurs in moderate to strong winds (range of 7 to 18m/s) and it takes place when the wake from the windward line induces lower drag and creates lifting forces on the leeward line. Also because the bundle is held together by a spacer, a combination of motion can occur due to spacer effect. The wake-induced vibration is observed when the conductors are dry, but it also occurs during icy and rainy conditions. The major four bundle conductor oscillations are shown in the diagram below.

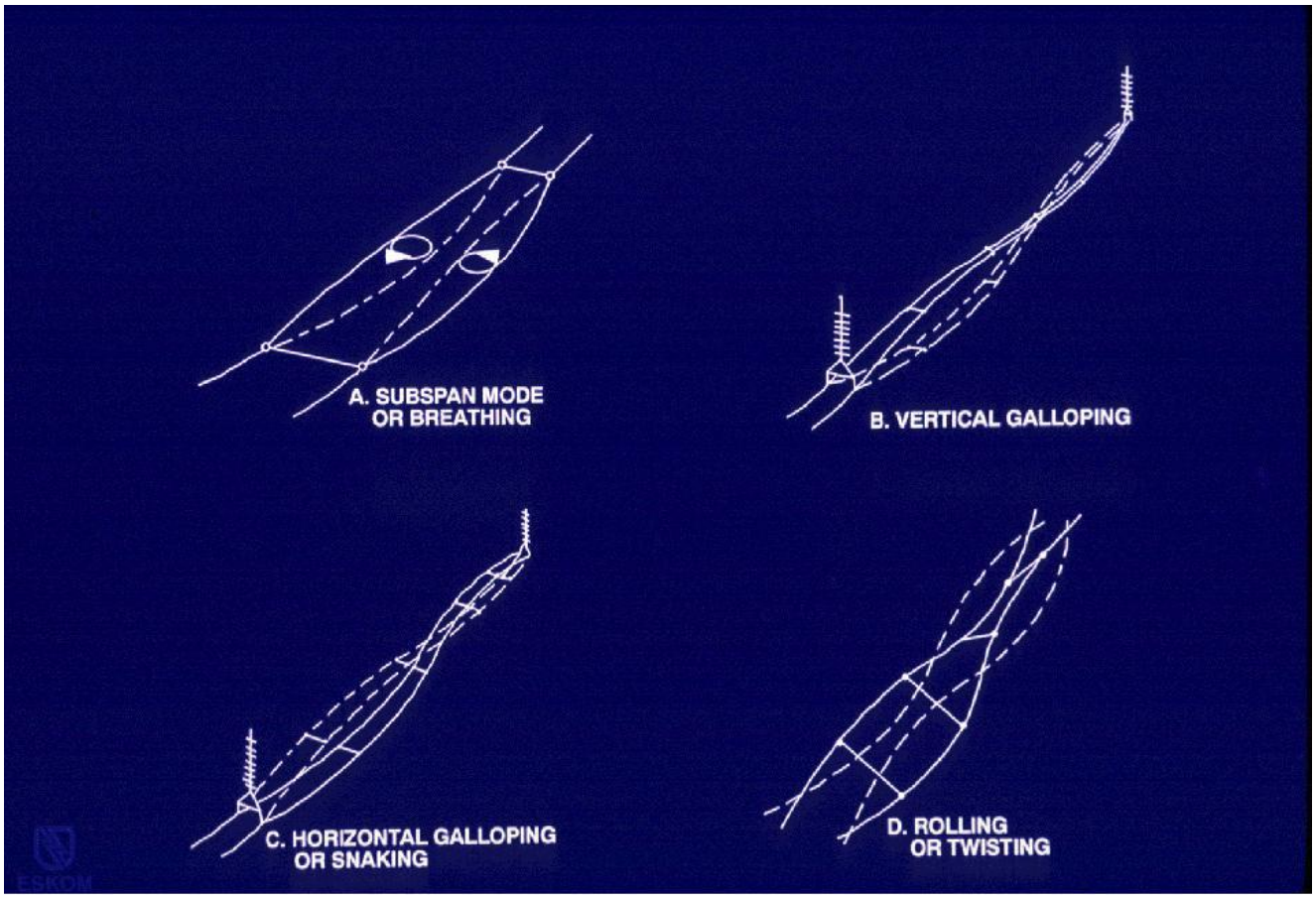

Fig 2.8 Wake-induced vibration [1][4]

The table in the next page gives a summary of the comparison of the three types of wind induced vibration normally experienced in overhead transmission lines

Table 2.1 Comparison of types of cyclic conductor motion [1] [4]

	Aeolian Vibration	Conductor Galloping	Wake-induced Oscillation
Types of Overhead Lines Affected	All	All	Limited to lines with bundled conductors
Approx. Frequency Range (Hz)	3 to 150	0.08 to 3	0.15 to 10
Approx. Range of Vibration Amplitudes (Peak-to-Peak) (Expressed in conductor diameters)	0.01 to 1	5 to 300	Rigid-Body Mode: 0.5 to 80 Sub span Mode: 0.5 to 20
Weather Conditions Favoring Conductor Motion			
Wind Character	Steady	Steady	Steady
Wind Velocity	1 to7m/s (2 to 15mph)	7 to 18m/s (15 to 40mph)	4 to l8m/s (10 to 40mph)
Conductor Surface	Bare or uniformly iced (i.e. hoarlrost)	Asymmetrical ice deposit on conductor	Bare, dry
Design Conditions Affecting Conductor Motion	Line tension, conductor self-damping, use of dampers, armor rods	Ratio of vertical natural frequency to torsion natural frequency; sag ratio and sup-port conditions	Subconductor separation, tilt of bundle, subconductor arrangement sub span staggering
Damage			
Approx, time required for severe damage to develop	3 months to 20 + years	1 to 48 hours	1 months to 8 + years
Direct causes of damage	Metal fatigue due to cyclic bending	High dynamic loads	Conductor clashing, accelerate ate wear in hardware
Line components most affected by damage	Conductor and shield wire strands	Conductor, all hardware, insulators, structures	Suspension hardware, spacers, dampers, conductor strands

2.6 Fatigue Failure

Based on the early investigation by a German engineer named August Wöhler, he was able to establish that fatigue occurs if the alternating stress was only slightly less than the static stresses which would cause failure of the metal, and only a few cycles of loading were required to cause failure [15]. Fatigue of conductor is caused by dynamic stresses that result from alternating bending of the conductors where their motion is restrained. Fatigue is enhanced when both stresses and fretting increase with the amplitude of bending i.e. the greater the amplitude, the more quickly fatigue occurs.

Fatigue failure of conductor and its associated line hardware in overhead line is the most common form of damage from wind induced vibration especially from Aeolian vibration. This is because this form of wind induced vibration produces several numbers of standing waves which induces bending stresses at points which motion is restrained and many million cycles can be accumulated. Hence, fatigue of conductor strands occurs at points where motion of a conductor is constrained against transverse vibration and its occurrence at these points is directly linked to the rigidity with which conductor motion is restrained [1][4]. These points include support location, suspension clamps, line hardware.

To counter fatigue and other effects resulting from wind-induced vibration, during the design stage, vibration absorbers (dampers) are usually included. Example of a vibration absorber is the Stockbridge damper [4] shown below in figure 2.9, which has been proven to be very effective against Aeolian vibration.

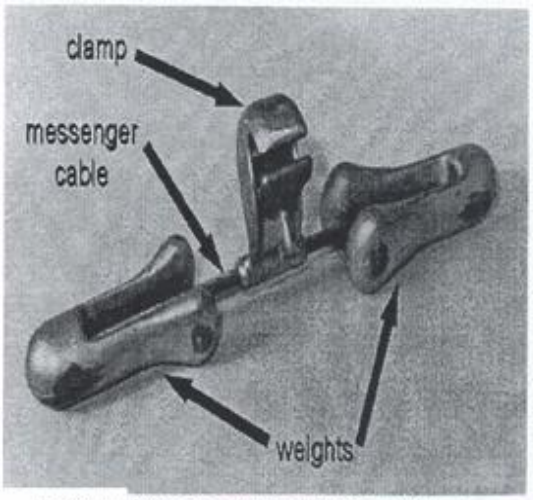

Fig 2.9 (a) Vibration damper of Stockbridge type [4]

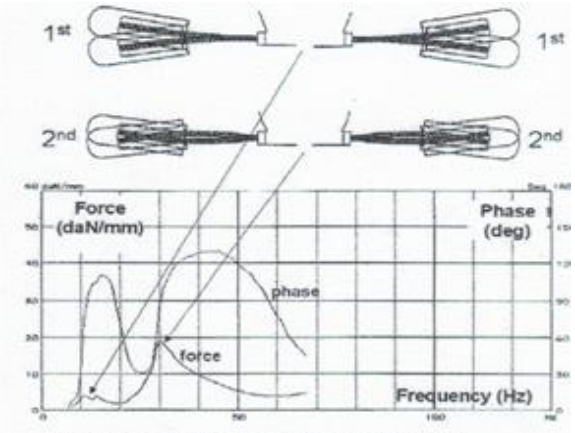

Fig 2.9 (b) Dynamic response of symmetric Stockbridge-type damper. Test performed at constant displacement of 2 mm peak-to-peak up to 14 Hz and 1 mm peak-to-peak above 14 Hz (courtesy U. Cosmai) **[4]**

CHAPTER 3

ANALYTICAL MODELLING

3.1 INTRODUCTION

This chapter presents the methodology used in the study of wind-induced vibration experienced by conductors on overhead transmission lines. The concept that is addressed in this aspect of the study is divided into two phases: free and forced vibration. These include the explanation of the physical nature of the phenomenon as well as the analysis of the power line cable model as a beam, the finite element method equation formulation and the determination of bending stiffness for the conductor.

3.2 PHYSICAL ASPECT AND MODELLING CONCEPT

Generally, the solution to any engineering problem normally proceeds through four stages: first, a real-world problem is identified; second, with proper assumptions the problem is modeled; third, the model is analysed and last, the results are applied to the original physical problem. This process enables the prediction of the system response, thereby helping in developing a mechanism to find a solution to this identified physical problem. The first three stages in terms of the conductor experiencing transverse vibration will be applied in this chapter and in the next. The last stage will be addressed in chapter five.

In the physical world, wind-induced conductor oscillation can be caused by wind excitation and the loading which is distributed throughout the conductor span. This can be reproduced in a wind tunnel experiment when the conductor is subjected to wind at varying conditions. Based on explanations given for experiments conducted in wind tunnels with regard to fluid–solid interaction reported in publications and in literatures by researchers and which detailed explanations can be found in references [1][2][4][13][16][17][18]. In these research publications, it was established that the wind that flows across the conductor in the horizontal plane will cause the conductor to vibrate in vertical plane perpendicular to the direction of the wind. In modeling the above as discussed earlier, contrary to what happened in the physical world and in wind tunnel experiments, in an indoor laboratory the vibration is assumed to be caused by an effective

or integrated wind loading that is concentrated at a point and this can produce the same effect as that of the distributed loading found in the real world as illustrated in figure 3.1 shown below. In the diagram, a single span conductor is exposed to a stream of wind in the horizontal plane. To analyse this form of vibration, the resultant force is assumed to be harmonic in nature, thus expressed as a single frequency sinusoidal force. This assumption is made because the input loading from vibrator (shaker) is set at fixed vibration frequency and this is allowed to vibrate or sweep across the conductor within a certain frequency range to determine the various conductor resonance frequencies.

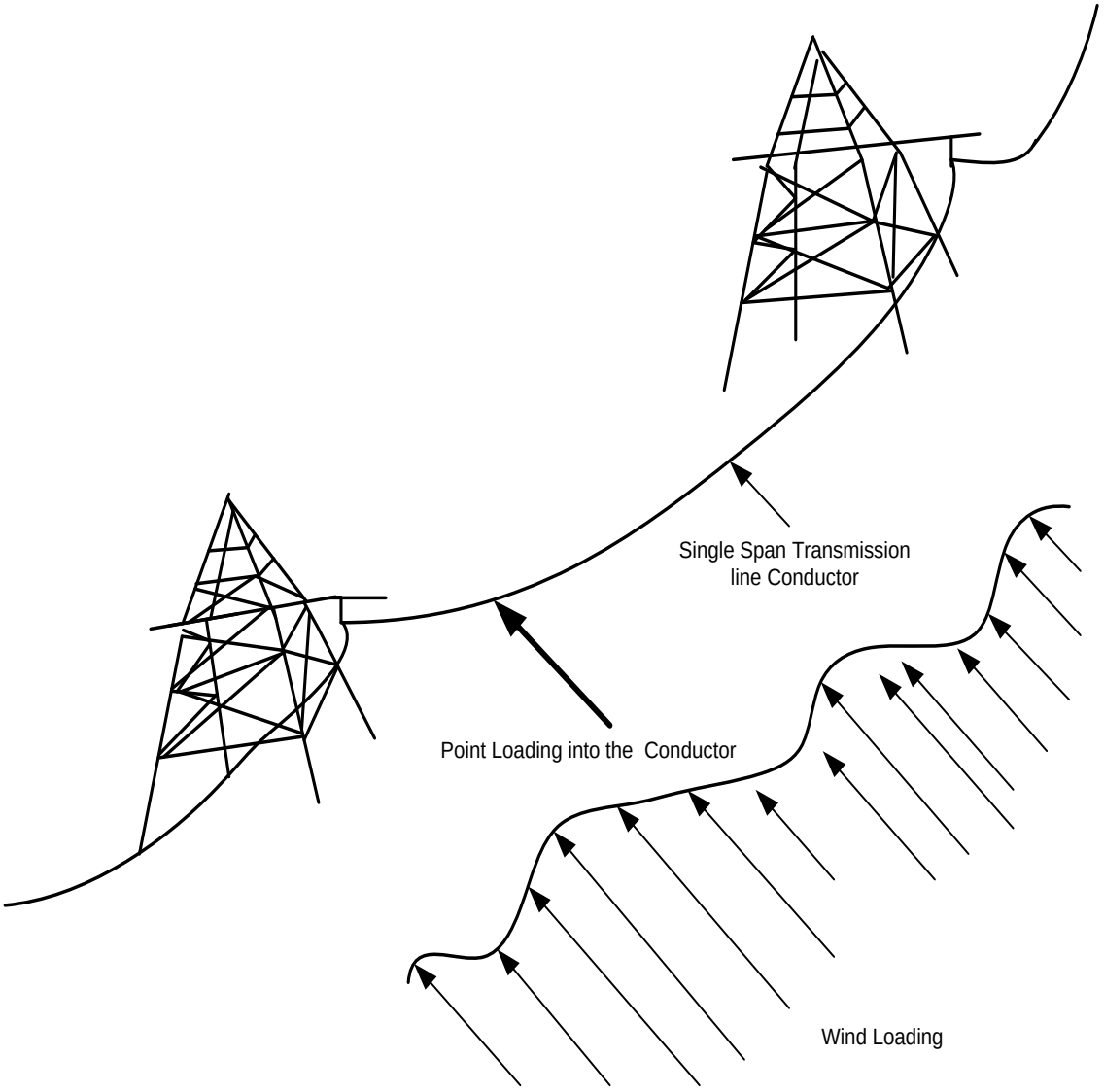

Fig 3.1. Shows the conductor wind loading in the physical world and the point loading concept used in modeling.

3.3 Conductor Input Power (Wind Loading)

In the real world, the vibration of a conductor is caused by vortex formation as the wind flows across the conductor and this effect is known as Koman effect. For Aeolian vibration, the frequency of vibration is calculated using strouhal fomula as given by equation (2.14). Investigations into this fluid–dynamic excitation force causing this form of oscillation has been done using wind tunel experiments [17][18]. Findings from these experiments have helped produce an emperical formulae to calculate the wind input force and this is specific for a particular conductor. Based on these findings, reference [4] provides empirical formulae to calculate the wind input power to the conductor.

The exitation of a conductor in an indoor testing laboratory is different compared to that done in the wind turnel which tends to produce the same excitation similar to that of the real world scenerio (distributed loading). In the indoor testing laboratory, a concentrated force, *F,* is used to cause the conductor to oscillate and this will replicate the same effect as the distributed force which a conductor in wind turnel experiment or in the physical world would be subjected to. This point loading is simulated with a shaker (vibrator) in the laboratory and inputing this force to the conductor as modeled by damper-spring system attached to the conductor illustrated in fugure 3.2 shown below.

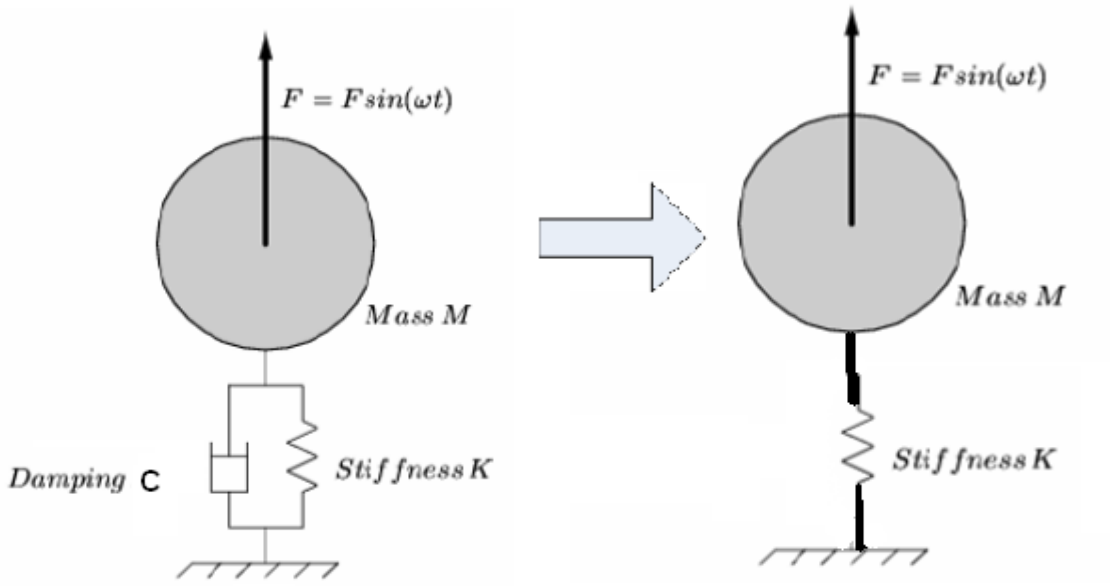

Figure 3.2 (a and b).The mass-spring-damper model for Shaker-Conductor flexible link connection

The flexible link connection is used in the laboratory to connect the shaker and the conductor is modeled with the stiffness and the damping as shown above. Figure 3.2a represents the actual physical model in which not all the power is transferred from the vibrator to the conductor. Due to the negligible energy that is lost as well as the complication caused by the presences of the damping constant with regard to its phase shift, it is then assumed that no power is lost between the vibrator and the conductor. Thus, setting the damping constant to zero, then transforming the model to a pure spring coupling shown in figure 3.2b. This model will be used to calculate the input force for a single span conductor or determine the amount of force impacted by the shaker to the conductor.

3.4 Concepts of Bare Conductor Modeling

Conductor vibrations have been a subject of intensive studies for a long time. Over the years, various analytical models have been developed by researchers and used to try and predict the mechanical vibration of transmission line conductors. These developed models are either based on modeling the conductor as beam or taut string. Also the beam or string model is either considered a continuous or lump mass. The taut string model of the vibrating conductor neglects the bending stiffness of the cable that is known to have some effect on the dynamics of the conductor.

In this study, the modeling of the transverse (flexural) vibration of a bare conductor is done using the concept of bending vibration of a beam. This concept also considers the beam to be a distributed-parameter (continuous or infinite-dimensional) systems i.e. mass of the system is considered to be distributed throughout the structure as a series of infinitely small elements. Hence, when there is vibration, each of these infinite numbers of elements move relative to each other in a continuous manner [9]. To understand the concept of bending vibration of a beam, see appendix A for the derivation of simple beam equation also known as the Euler-Bernoulli equation.

From literature, most researchers' model the conductor as beam clamped at both ends i.e. rigidly fixed and permits no motion. In [19] it was pointed out that this assumption was only valid for earth wires. In transmission lines, the conductors are attached to suspension insulators which permit some degree of motion in the longitudinal direction. Hence, based on the above inference,

the transverse vibration of the conductor was modeled as a long, slender, simply supported beam, isotropic in nature and subjected to a concentrated force.

3.4.1 The Equation of Motion

The equation of motion of a conductor using the beam as explained above, experiencing transverse vibration has been investigated by many researchers and authors. Figure 3.3 shows the static profile of the beam, sag by a given tensile force, S, that can be approximately determined by the parabolic curve subjected to wind loading. From this profile, the wind loading is assumed to be a concentrated force, *f (x, t)*, with a single harmonic frequency and this is used as the basis to model the transverse vibration of transmission line conductor

The formulation of the equation of motion is based on the following assumptions [12]:

- Uniformity along the span (length) and slender (thin Beam theory)
- Conductor is regarded as a solid, cylindrical body composed of linear, homogeneous physical properties throughout its cross-sectional area i.e. tension, flexural rigidity, cross-sectional area assumed uniform throughout the conductor.
- Such that the plane of symmetry of the beam is also the plane of vibration so that rotation and translation are decoupled. Hence, the deformation will be small that the shear deformation is much smaller than the transverse displacement and also the slope of line of the tangent to the conductor that is $\partial y(x, t)/\partial x << 1$

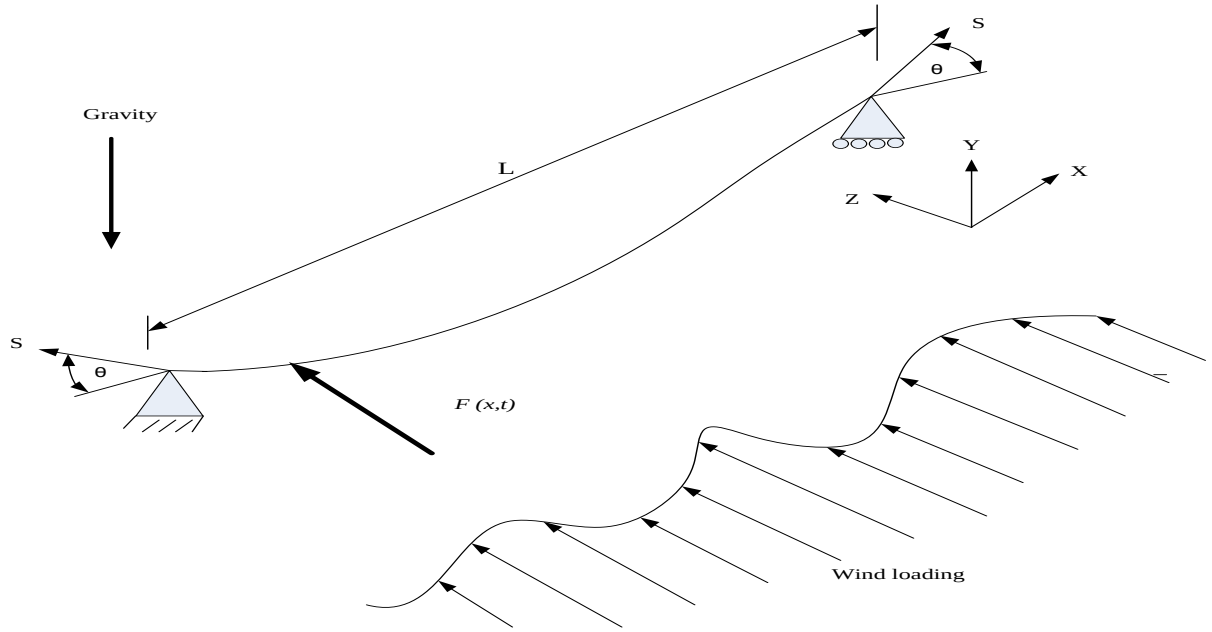

Fig 3.3. Static profile of the simply supported beam subjected to wind dynamic loading and the loading is assumed to be an equivalent concentrated force *F(x ,t)* with the same resultant effect as the wind

Based on the above assumptions, the equation of motion of a conductor with axial loading (tensioned at both ends) as described in research publications in terms of wind-induced vibration experienced by transmission lines conductors as a beam, documented in publications[5][20][21] [22] is given as

$$EI\frac{\partial^4 y(x,t)}{\partial x^4} - S\frac{\partial^2 y(x,t)}{\partial x^2} + \rho A\frac{\partial^2 y(x,t)}{\partial t^2} = f(x,t) \qquad \ldots\ldots\ldots\ldots\ldots\ldots (3.1)$$

for x$\epsilon(0,l)$, t > 0 , with the boundary conditions at

$y(0,t) = \frac{\partial^2 (0,t)}{\partial x^2} = 0$ simply supported or pinned end x = 0

$y(l,t) = \frac{\partial^2 (l,t)}{\partial x^2} = 0$ simply supported or pinned end x = l

And initial conditions.

$y(x,0) = y_0(x)$ at $t = 0$

$\dot{y}(x,0) = \dot{y}_0(x)$ at $t = 0$

Where

E = young modulus

I = area moment of inertia

EI = flexural rigidity or conductor bending stiffness

S = the tension (axial loading)

ρ = the conductor density

$y(x, t)$ = transverse displacement position x, time t

A = the cross-sectional area

$F(x, t)$ = the external force

Substituting the conductor mass per unit length, $m = \rho A$

$$EI\frac{\partial^4 y(x,t)}{\partial x^4} - S\frac{\partial^2 y(x,t)}{\partial x^2} + m\frac{\partial^2 y(x,t)}{\partial t^2} = f(x,t) \qquad \ldots\ldots\ldots\ldots\ldots\ldots (3.2)$$

Expressing this equation for the transverse vibration in dimensionless form as expressed in reference [12]

If expressing the following dimensionless form as $Y = \frac{y(x,t)}{D}$ $X = \frac{x}{L}$ $\tau = \frac{t}{f}$

Also expressing the excitation in Dirac delta function, then equation (3.2) becomes

$$M_p.\frac{\partial^4 Y}{\partial X^4} - S_p \frac{\partial^2 Y}{\partial X^2} + I_p \frac{\partial^2 Y}{\partial \tau^2} = \frac{1}{\gamma}[F(X,\tau) + \sum_n \delta(X - X_n)F_n(\tau)] \quad \text{..... (3.3)}$$

Where $M_p = \frac{EI.D}{\gamma L^4}$, $S_p = \frac{S.D}{\gamma L^2}$ and $I_p = \frac{Df^2}{g}$

Where g is the gravitational constant,

γ is the conductor weight per unit length (i.e. *mg),*

$F(X,\tau)$ represents the net, transverse force per unit length acting on the conductor,

$F_n(\tau)$ represents the *n*th concentrated force acting transversely on the conductor at location X_n

$\delta(X-X_n)$ represents the Dirac delta function

3.4.2 Solution to the Equation of Motion

The solution to equation (3.1), whose general solution is assumed to be the same as Euler-Bernoulli equation, see appendix A. The particular solution to this equation of motion of a conductor modeled as a beam with axial load, S experiencing transverse vibration, ignoring the external force and damping can be obtained as a series of product of two functions.

Using separation of variables

$$Y(x,t) = X(x)T(t) \quad \text{..... (3.4)}$$

Where the normalized functions *X(x)* is mode shapes for equation and it satisfy the orthogonality condition

Hence substituting into equation 3.1 results in two equations given as follows

$$EI\overset{////}{X}(x) - S\overset{//}{X}(x) - \omega^2 \rho A X(x) = 0 \quad \text{..... (3.5)}$$

$$\ddot{T}(t) + \omega^2 T(t) = 0 \quad \text{..... (3.6)}$$

Where $\overset{////}{X}(x) = \frac{d^4 y}{dx^4}$ $\overset{//}{X}(x) = \frac{d^2 y}{dx^2}$ $\ddot{T}(t) = \frac{d^2 y}{dt^2}$

and ω^2 is the constant which equate the variable of *x* and *t*

Assuming that $X(x) = Ze^{\Psi x}$ equation 3.4 becomes

$$Ze^{\Psi x}\left(EI\Psi^4 - S\Psi^2 - \rho A\omega^2\right) = 0 \qquad \ldots\ldots\ldots\ldots\ldots\ldots (3.7)$$

$Ze^{\Psi x} \neq 0$ Therefore $\left(EI\Psi^4 - S\Psi^2 + \rho A\omega^2\right) = 0$

In relation to the general solution of the Euler-Bernoulli equation, the solution to the above equation becomes

$$\Omega^2, \Psi^2 = -\frac{(-S) \pm \sqrt{S^2 - 4(EI)(-\rho A\omega^2)}}{2EI}$$

$$\Omega, \Psi = (\pm)\sqrt{\frac{S \pm \sqrt{S^2 + 4EI(\rho A\omega^2)}}{2EI}}$$

The values of Ω, and Ψ are the solutions for the general equation describing the transverse vibration of the conductor and because a conductor is an example of distributed-parameter systems which has infinite number of solutions. Thus Ω, and Ψ is indexed to be Ω_n and Ψ_n respectively

$$\Psi_n = \sqrt{-\frac{S}{2EI} + \sqrt{\frac{S^2}{(2EI)^2} + m_L\frac{(2\pi f_n)^2}{EI}}} \qquad \ldots\ldots\ldots\ldots\ldots (3.8)$$

$$\Omega_n = \sqrt{\frac{S}{2EI} + \sqrt{\frac{S^2}{(2EI)^2} + m_L\frac{(2\pi f_n)^2}{EI}}} \qquad n = 1,2,3,... \qquad \ldots\ldots\ldots\ldots\ldots (3.9)$$

Where $\omega_n = 2\pi f_n$

To find the infinite natural frequencies of the conductor (distributed system) is by solving equation (3.1), assuming that the mode shape is the same as the pinned-pinned beam eigenfunction (mode shape) and no external force.

$$Y_n(x,t) = \sin\frac{n\pi x}{l}\cos\omega_n t \qquad \text{where } n = 1, 2\ 3, ... \qquad \ldots\ldots\ldots\ldots\ldots (3.10)$$

$$EI\left(\frac{n\pi}{l}\right)^4 \sin\frac{n\pi x}{l}\cos\omega_n t - S\left(-\frac{n\pi}{l}\right)^2 \sin\frac{n\pi x}{l}\cos\omega_n t + \rho A(-\omega_n)\sin\frac{n\pi x}{l}\cos\omega_n t = 0$$

$$\sin\frac{n\pi x}{l}\cos\omega_n t\left[\frac{EI}{\rho A}\left(\frac{n\pi}{l}\right)^4 + \frac{S}{\rho A}\left(\frac{n\pi}{l}\right)^2 - {\omega_n}^2\right] = 0$$

The natural frequencies for the conductor is obtained as

$$\omega_n^2 = \left(\frac{n\pi}{l}\right)^2 \frac{S}{A\rho} + \left(\frac{n\pi}{l}\right)^4 \frac{EI}{A\rho}$$

$$\omega_n = \sqrt{\left(\frac{n\pi}{L}\right)^2 \frac{S}{m_L}\left[1+\left(\frac{n\pi}{L}\right)^2 \frac{EI}{S}\right]} \qquad \text{in rad/s} \qquad \ldots\ldots\ldots\ldots\ldots\ldots (3.11)$$

If $F_n = \dfrac{\omega}{2\pi}$

$$F_n = \frac{1}{2\pi}\sqrt{\left(\frac{n\pi}{L}\right)^2 \frac{S}{m_L}\left[1+\left(\frac{n\pi}{L}\right)^2 \frac{EI}{S}\right]} \quad \text{in Hz} \qquad \ldots\ldots\ldots\ldots\ldots\ldots (3.12)$$

3.5 Analytical Modeling of Conductor Self-damping

To model the damped equation of motion for bare conductor is by inserting damping model(s) into the partial differential equation i.e. equation (3.1) of the beam pinned at both ends. Reference [23] gave the explanation of the various damping mechanism that can be found in cantilever beams with tip mass at the free end and how it can be used to evaluate the various contribution each make to the total damping of the beam. In a similar manner, the damping models were incorporated into the beam equation of motion based on the analysis of the two types of damping mechanism found in a vibrating conductor as explained in section 2.4.2 and also on the concept proportional damping in which external and internal damping were distinguished as explained by the authors [20] [21]. In modeling conductor damping, the following concepts were used:

- The conductor inter-strand motion and fluid damping (both form the external damping) of the conductor is proportional to its velocity and it is represented by viscous damping model.

- The internal damping is proportional to the rate of strain in the conductor.

Incorporating the above into equation (3.1), the equation describing the damped model for the conductor becomes

$$EI\frac{\partial^4 y(x,t)}{\partial x^4} - S\frac{\partial^2 y(x,t)}{\partial x^2} + \beta I\frac{\partial^5 y(x,t)}{\partial x^4 \partial t} + C\frac{\partial y(x,t)}{\partial t} + \rho A\frac{\partial^2 y(x,t)}{\partial t^2} = f(x,t) \quad \text{..... ..... (3.13)}$$

Where

β and C are damping constant parameters.

The above equation is the equation of motion for the vibrating conductor with the presence of axial load (tension) S, with viscous air damping (external) and strain rate of damping (internal). The strain rate damping is also called Kelvin-Voigt damping. Thus, the above equation is simply the damped equation of motion for the conductor.

3.5.1 Free Vibration

The above equation for modeling the conductor self-damping can be used to analyse its free vibration where the forcing function becomes zero as given below

$$EI\frac{\partial^4 y(x,t)}{\partial x^4} - S\frac{\partial^2 y(x,t)}{\partial x^2} + \beta I\frac{\partial^5 y(x,t)}{\partial x^4 \partial t} + C\frac{\partial y(x,t)}{\partial t} + \rho A\frac{\partial^2 y(x,t)}{\partial t^2} = 0 \quad \text{..... (3.14)}$$

Using the separation of variables of equation (3.4), equation (3.14) becomes

$$EI\overset{////}{X}(x)T(t) - S\overset{//}{X}(x)T(t) + \beta I\overset{////}{X}(x)\dot{T}(t) + CX(x)\dot{T}(t) + \rho A\ddot{T}(t))X(x) = 0$$

Where $\overset{////}{X}(x) = \frac{d^4 y}{dx^4}$ $\overset{//}{X}(x) = \frac{d^2 y}{dx^2}$ $\ddot{T}(t) = \frac{d^2 y}{dt^2}$ $\dot{T}(t) = \frac{dy}{dt}$

Using the eigenfunction of

$$X_n(x) = \sin\left(\frac{n\pi x}{l}\right)$$

$$EI\left[\left(\frac{n\pi}{l}\right)^4 \sin\left(\frac{n\pi x}{l}\right)\right]T(t) - S\left[\left(\frac{-n\pi}{l}\right)\sin\left(\frac{n\pi x}{l}\right)\right]T(t) + \beta I\left[\left(\frac{n\pi}{l}\right)^4 \sin\left(\frac{n\pi x}{l}\right)\right]\dot{T}(t)$$

$$+ C\left[\sin\left(\frac{n\pi x}{l}\right)\right]\dot{T}(t) + \rho A\left[\sin\left(\frac{n\pi x}{l}\right)\right]\ddot{T}(t) = 0$$

$$\sin\left(\frac{n\pi x}{l}\right)\left[EI\left(\frac{n\pi}{l}\right)^4 T(t) + S\left(\frac{n\pi}{l}\right)^2 \dot{T}(t) + \beta I\left(\frac{n\pi}{l}\right)^4 T(t) + C\dot{T}(t) + \rho A\ddot{T}(t)\right] = 0$$

$$\rho A\ddot{T}(t) + \left[\beta I\left(\frac{n\pi}{l}\right)^4 + C\right]\dot{T}(t) + \left[S\left(\frac{n\pi}{l}\right)^2 + EI\left(\frac{n\pi}{l}\right)\right]T(t) = 0$$

$$\ddot{T}(t) + \left[\frac{\beta I}{\rho A}\left(\frac{n\pi}{l}\right)^4 + \frac{C}{\rho A}\right]\dot{T}(t) + \left[\frac{S}{\rho A}\left(\frac{n\pi}{l}\right)^2 + \frac{EI}{\rho A}\left(\frac{n\pi}{l}\right)^4\right]T(t) = 0 \qquad \text{.. ……..} \quad (3.15)$$

Comparing equation (3.15) with equation (2.7)

$$\omega_n^2 = \frac{S}{\rho A}\left(\frac{n\pi}{l}\right)^2 + \frac{EI}{\rho A}\left(\frac{n\pi}{l}\right)^4$$

$$2\xi\omega_n{}^2 = \left[\frac{\beta I}{\rho A}\left(\frac{n\pi}{l}\right)^4 + \frac{C}{\rho A}\right]$$

The solution to the temporal equation (3.15) becomes

$$T_n = A_1 e^{-\xi_n \omega_n t}\sin\left(\omega_d t + \phi\right)$$

Or

$$T_n = e^{-\xi_n \omega_n t}\left(B_1 \sin\,\omega_d t + B_2 \cos\omega_d t\right) \qquad \text{…….} \quad (3.16)$$

Where $\omega_d = \omega_n\sqrt{1-\xi^2}$

The response will be

$$y(x,t) = \sum_{n=1}^{\infty} A_1 e^{-\xi_n \omega_n t}\sin\left(\omega_d t + \varphi\right)\sin\frac{n\pi x}{l}$$

Or

$$y(x,t) = \sum_{n=1}^{\infty}\left[e^{-\xi_n \omega_n t}\left(B_1\,\sin\,\omega_d t + B_2\cos\omega_d\right)\right]\sin\frac{n\pi x}{l} \qquad \text{…….} \quad (3.17)$$

3.5.2 Forced Vibration

When a transmission line conductor is exposed to loading on the field from wind, the actual system represents a distributed loading on the entire span of the conductor. As mentioned before, this is simulated as point loading where the force is assumed to concentrate at a point. Evaluation of the actual response of the conductor to this specific excitation can be achieved by solving the equation of motion for the damped case i.e. equation (3.13) with the excitation function present. This will help determine the dynamic stress for a range of inputs, for example harmonic motion. Solving equation (3.13) with the driving force using the separation of variable of equations (3.4)

$$EI\frac{\partial^4 y(x,t)}{\partial x^4} - S\frac{\partial^2 y(x,t)}{\partial x^2} + \beta I\frac{\partial^5 y(x,t)}{\partial x^4 \partial t} + C\frac{\partial y(x,t)}{\partial t} + \rho A\frac{\partial^2 y(x,t)}{\partial t^2} = f(x,t)$$

$$\sin\left(\frac{n\pi x}{l}\right)\left[EI\left(\frac{n\pi}{l}\right)^4 T(t) + S\left(\frac{n\pi}{l}\right)^2 \dot{T}(t) + \beta I\left(\frac{n\pi}{l}\right)^4 T(t) + C\dot{T}(t) + \rho A\ddot{T}(t)\right] = F\sin\omega_{dr}t$$

$$\ddot{T}(t) + \left[\frac{\beta I}{\rho A}\left(\frac{n\pi}{l}\right)^4 + \frac{C}{\rho A}\right]\dot{T}(t) + \left[\frac{S}{\rho A}\left(\frac{n\pi}{l}\right)^2 + \frac{EI}{\rho A}\left(\frac{n\pi}{l}\right)^4\right]T(t) = F\sin\omega_{dr}t \qquad \text{..... (3.18)}$$

Comparing equation (3.18) with equation (2.11)

Hence

$$T(t) = Ae^{-\zeta\omega_n t}\sin(\omega_d t + \phi) + X\cos(\omega t - \theta)$$

Where

$$\omega_n^2 = \frac{S}{\rho A}\left(\frac{n\pi}{l}\right)^2 + \frac{EI}{\rho A}\left(\frac{n\pi}{l}\right)^4$$

$$2\xi\omega_n{}^2 = \left[\frac{\beta I}{\rho A}\left(\frac{n\pi}{l}\right)^4 + \frac{C}{\rho A}\right]$$

The solution becomes

$$y(x,t) = \sin\frac{n\pi x}{l}\left[Ae^{-\zeta\omega t}\sin(\sin\ \omega t + \phi) + X\cos(\omega t - \theta)\right]$$

3 .6 Bending Stiffness, *EI* Value

Most researchers in this area of wind-induced vibration tend to adopt a constant bending stiffness value for vibrating (ACSR) conductor based on the recommendation by Cigrè Study Committee [6]. This value is chosen such that the effective bending stiffness EI_{eff} is a constant value between the minimum and maximum values of bending stiffness. But in reference [24] the author presented the concept of how the *EI* value varies with the length along the conductor and on this basis, the *EI* value of the conductor then depends on conductor bending curvature. Also from his findings, the *EI* value varies non-linearly with wire helical geometry, interlayer friction and slip during bending.

Due to the fact that the linear concept is used in this study, the constant bending stiffness value was used for the ACSR conductor.

The equations to calculate for both the maximum and minimum bending stiffness for ACSR conductors can be found in references [4] [6] [24]

The minimum value ($EI_{\min}$) is obtained by considering the conductor as a bundle of individual wires free to move relative to each other

The calculation of EI_{min} is given as:

$$EI_{min} = n_s E_s \frac{\pi d_s^4}{64} + n_a E_a \frac{\pi d_a^4}{64} \qquad \text{..... (3.19)}$$

Wherein:

n_s and n_a = number of strands of steel and aluminium, respectively

E_s and E_a = modulus of elasticity of steel and aluminium

d_s and d_a = diameter of steel and aluminium strands

The maximum value ($EI_{\max}$) is obtained by considering the conductor as a bundle of individual wires unable to move relative to each other due to contact pressure

In the computation of $EI_{max,}$ the displacement of each strand from the conductor axis must be considered according to the formula:

$$I_x = I_c + AD^2 \qquad \text{..... (3.20)}$$

Where

I_x = moment of inertia about new axis
I_c = moment of inertia about original axis
A = area
D = distance between original and new axes

For the strands within a given lay of the conductor, the distance D may be computed as the sine of the angle as shown in the diagram.

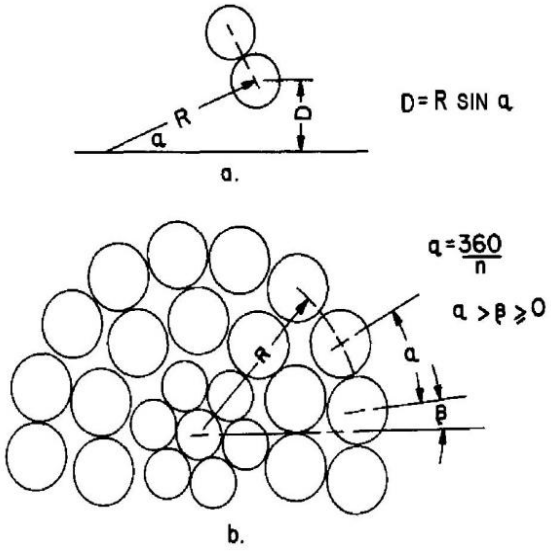

The moment of inertia for each strand in a given lay becomes:

$$I_x = \frac{\pi d^4}{64} + \frac{\pi d^2}{4}(R\sin\alpha)^2 \qquad \text{..... (3.21)}$$

$$I_x = \frac{\pi d^4}{64} + \frac{\pi d^2}{4}R^2(\sin\alpha)^2$$

$$I_{max} = \frac{n\pi d^2}{8}\left(\frac{d^2}{8} + R^2\right) \qquad \text{..... (3.22)}$$

Hence, the calculation of EI_{max} is given as:

$$EI_{max} = E_s \sum_{i=1}^{n_s} I_{max,i} + E_a \sum_{j=1}^{n_a} I_{max,j} \qquad \text{..... (3.23)}$$

The first conductor used for analysis in this study is the ACSR conductor with code name Tern which consists of the steel wires at the core and aluminum wires at the outer layers. The calculation of this maximum bending stiffness is given in appendix B as well as its physical properties as obtained from Aberdare Power cables Catalogue [25]. For both the analytical analysis and the finite element simulation of the transverse vibration, the value of the constant bending stiffness that was used is that for calculated maximum bending stiffness value. This value is chosen in line with the recommended value for bending stiffness suggested in [26] for a vibrating ACSR conductor.

The second conductor used for this study is the Aero-Z conductor and physical properties for the conductor, were obtained from referene [27] and the details are given in table-B-2 in appendix B. This conductor consist of two parts; the round wires at the core and the z-shaped wires that form the outer layers. For this conductor, because the exact value for the Young's modulus can be found in [27], the value for the bending stiffness can easily be calculated. To obtain the value of the bending stiffness the following process was used with regards to the moment of inertia.

For the round wires that constitute the centre wire and the next two inner layers, equation (3.22) was used to calculate for the moment of inertia, while for the region of the z-shaped wires, the assumption was made in which the two z-shaped wire layers were combined and treated as a hollow circular solid. Combining the above resulted to the equation given as

$$EI = EI_x + EI_{zs} = E(I_x + I_{zs}) \qquad \text{……(3.24)}$$

Where $I_x = \frac{n\pi d^2}{8}\left(\frac{d^2}{8} + R^2\right)$

$$I_{zs} = \frac{\pi(d_o^4 - d_i^4)}{64}$$

The calculated value for the bending stiffness of the Aero-z conductor is given in appendix B.

CHAPTER 4

MODEL VERIFICATION: FINITE ELEMENT ANALYSIS AND ELECTRICAL EQUIVALENCE

4.1 Discrete Modeling

As indicated in chapter 3, in which the conductor transverse vibration was modeled as a bending vibration of a beam and also considered to be a distributed parameter model, the same concept was used for the finite element method (FEM) but the beam was considered a lump mass model. Carrying out the finite element analysis (FEA), involves converting this distributed model to its equivalent lump mass model. Hence, by discrete modeling of conductor vibration means converting distributed mass to its equivalent lump mass by a method known as discretisation. The finite-element discretise model of the pinned-pinned (simply supported) beam which is made up of its finite element is shown in figure 4.1 below. This model was used for the finite element analysis of conductor transverse vibration. The modeling of the dynamic behaviour of the conductor will involve the use of both the static properties such as stiffness with the dynamic properties such as mass, damping and dynamic loading to try and predict its response.

4.1.1 Discretisation of the Domain into Finite Elements

FEA begins with formulation of domain for the discretise finite element model; the finite element formulation consideration assumes a domain limited to geometry and time. The domain of the conductor is given as (0, *l*) which is divided into *n* number of finite elements mesh of equal space as shown below in figure 4.1 and the conductor masses are lump at the nodes

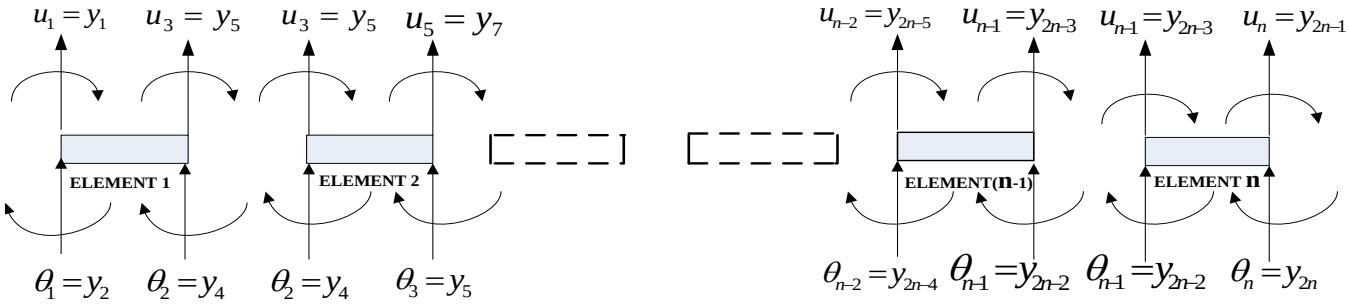

Figure 4.1 The discretise model of beam

This model shown in the previous page will be used for the finite element equation formulation and also in the analysis of the system equation.

4.2 Finite Element Analysis

The concept of finite element method (FEM) has provided opportunities for the development of procedures for the evaluation of both static and dynamic systems problems. This method is a computational technique that can be employed to evaluate both the static and the dynamic responses of systems. Although, a conductor is a continuous system, to evaluate the analytical model describing its transverse vibration using the FEM method involves discretising the system into finite elements in order to obtain the equation for each. Assembling these finite element equations, including the boundary conditions, was then used to formulate the equation of motion for the system. This resultant equation is obtained as the equation of inertial, stiffness, and applied force in matrix and vector forms. To obtain the damping force in vector form, for mathematical convenience, the mechanisms of the damping models are included in the global finite element equation obtained by assembly of these equations for the finite elements. This was used to evaluate the total damping of the system or the system's self-damping.

Using concepts from system dynamics and vibration modal analysis, the mass, stiffness and damping matrices for the system will then be used to solve for the required system parameters such as mode shapes, modal frequencies and damping. Hence, using these parameters for the vibrating conductor, its dynamic response can then be determined and analysed.

The solution to the resultant or the global equation of the system can be accomplished by using the numerical integration method such as those developed in references [28] [29] [30] to directly solve the equation. The numerical method that was used for the FEM is the Galerkin's method. Using concepts from analytical mechanics, matrix and vector, and vibration, these system parameters obtained was then used to carry out analysis on the response of the system within a range in line with the analytical model describing the same system.

4.2.1 Semi-discrete FEM

Some physical phenomena can be described by differential equation that relates certain quantities to their derivatives with respect to time and space variables. Conductor transverse vibration is an example of such practical problems in which the position and time dimensions have to be

considered. The method of finite element approximation of this type of time dependent equation (time dimension) is the semi-discrete method. In this method the time dimension is approximated by finite difference and for accuracy with respect to time a higher-order approximation is used i.e. cubic polynomial. To this regard the finite element interpolation functions as time dependent such that *u* is approximated by

$$u = y = \sum_{i=1} c_i N_i \qquad = c_1 x^3 + c_2 x^2 + c_3 x + c_4 \qquad \text{..... (4.1)}$$

$$u(x) = H_1(x)u_1 + H_2(x)u_2 + H_3(x)u_3 + H_4(x)u_4 \qquad \text{..... (4.2)}$$

Where

$$H_1(x) = 1 - \frac{3x^2}{l^2} + \frac{2x^3}{l^3} \qquad H_2(x) = x - \frac{2x^2}{l} + \frac{x^3}{l^2}$$

$$H_3(x) = \frac{3x^2}{l^2} - \frac{2x^3}{l^3} \qquad H_4(x) = -\frac{x^2}{l} + \frac{x^3}{l^2}$$

4.3 Finite Element Formulation

The development of the computational technique used to analyse the transverse vibration of power conductors starts with the finite element formulation. This involves the formation of the equation for a finite element from the discretise model of the conductor. The basic idea of the finite element formulation is to linearise the weak form of the equation of the problem and solve this equation for the finite elements discretised domain. The weak form or weak formulation of the problem is usually derived from the principle of virtual work. Therefore, for the conductor, the finite element formulation will be to transform the partial differential equation of motion into its variational form and then determine the approximate solution using variational method.

4.3.1 Weak Formulation

The weak formulation for the power line cables is obtained by transforming the equation of motion describing the conductor transverse vibration into its integral form using the test function of equation (4.1) and equation (4.2). Thus, using the Galerkin's method (method of weighted

residual or variational method) [31] [32] [33], the finite element formulation for the system can then be developed in integral form. Then, by applying the Galerkin's variational principle to this time dependent problem and considering the boundaries conditions, the finite element model equation was obtained. The weak formulation for the equation of motion was formulated using cubic displacement fields with respect to time because of the degree of freedom of the model.

The equation for the transverse vibration as given by equation (3.1):

$$EI\frac{\partial^4 y(x,t)}{\partial x^4} - S\frac{\partial^2 y(x,t)}{\partial x^2} + \rho A\frac{\partial^2 y(x,t)}{\partial t^2} = f(x,t)$$

Where $f(x,t) = F\sin\omega_d t$

The homogenous part of the equation is given as

$$EI\frac{\partial^4 y(x,t)}{\partial x^4} - S\frac{\partial^2 y(x,t)}{\partial x^2} + \rho A\frac{\partial^2 y(x,t)}{\partial t^2} = 0$$

Let $y(x,t) = X(x)e^{-i\omega t}$ $\quad i = \sqrt{-1}$

The homogenous part is transformed into

$$EI\frac{d^4 X}{dx^4} - S\frac{d^2 X}{dx^2} + \rho A\omega^2 X = 0 \qquad \text{..... (4.3)}$$

Using the same boundary and initial conditions used for the analytical analysis as given below.

Boundary conditions:

$y(0,t) = EI\dfrac{\partial^2 y(0,t)}{\partial x} = 0$, pinned end at x = 0

$y(l,t) = EI\dfrac{\partial^2 y(l,t)}{\partial x} = 0$, pinned end at x = l

Initial conditions:

$y(x,0) = y_0(x)$ at x = 0

$\dfrac{\partial(x,0)}{\partial t} = \dot{y}_0(x)$ at x = 0

The weak formulation for the semi-discrete finite element method can be obtained as follows. Firstly by multiplying equation (3.1) by the finite element interpolation functions defined by equation (4.1) to obtain

$$\int_0^l \left(EI\frac{\partial^4 y}{\partial x^4}u - S\frac{\partial^2 y}{\partial x^2}u + \rho A\frac{\partial^2 y}{\partial t^2}u - fu \right) dx = 0 \qquad \text{..... (4.4)}$$

The weak formulation is then obtained by carrying out the integration by parts twice on equation (4.4) and taking into account the finite-element discretise model shown in figure 4.1, which define the number of finite element in the system domain.

Hence, the resultant equation is obtained as

$$EI\int_{\Re}\frac{\partial^2 y}{\partial x^2}.\frac{\partial^2 u}{\partial x^2}\,dx + S\int_{\Re}\frac{\partial y}{\partial x}.\frac{\partial u}{\partial x}\,dx + \rho A\int_{\Re}\frac{\partial^2 y}{\partial t^2}u dx - \int_{\Re} fu dx +$$

$$\left[-Su\frac{\partial y}{\partial x} + \left(\frac{\partial^3 y}{\partial x^3}u - \frac{\partial u}{\partial x}.\frac{\partial^2 y}{\partial x^2} \right) \right]_{x_0}^{x_l} = 0$$

..... (4.5)

Where $\Re$ is the element domain

From the weak formulation above, the equations for the finite element in terms of the stiffness, mass matrices and force vector are given as:

$$\left[K^e\right] = EI\int_{\Re}\frac{\partial^2 y}{\partial x^2}.\frac{\partial^2 u}{\partial x^2}\,dx + S\int_{\Re}\frac{\partial y}{\partial x}.\frac{\partial u}{\partial x}\,dx \qquad \text{..... (4.6a)}$$

$$\left[M^e\right] = \rho A\int_{\Omega}\frac{\partial^2 y}{\partial t^2}u dx \qquad \text{..... (4.6b)}$$

$$\left[F^e(t)\right] = \int_{\Omega} f(x,t)\left[H\right]^T \qquad \text{..... (4.6c)}$$

From equation (4.2), given that

$$[H] = [H_1, H_2, H_3, H_4]$$

Then

$$[A] = [H_1', H_2', H_3', H_4']$$

$$[B] = [N_1'', N_2'', N_3'', N_4'']$$

Then equation (4.6) becomes

$$\left[K^e\right]=\left(EI\int_{\Re}B^TB+S\int_{\Re}A^TA\right)dx \qquad \text{…….. (4.7a)}$$

$$\left[M^e\right]=\left(\rho A\int_{\Re}\frac{\partial^2 y}{\partial t^2}udx\right)=\left(\rho A\int_{\Re}H^TH\right)\ddot{y} \qquad \text{…..... (4.7b)}$$

$$\left[F^e(t)\right]=\int_{\Re}f(x,t)\left[H\right]^T \qquad \text{…….. (4.7c)}$$

4.4 The System Matrix

The system or the global matrix is usually obtained by the assembly of finite element equations define by equations 4.7 (a, b and c). In assembling all of the finite elements equations requires the satisfaction of the boundary conditions and from the diagram of the discretise domain (figure 4.1), to satisfy the boundaries conditions of the simply supported beam i.e. $y_1 = y_2 = y_{2n-1} = y_{2n} = 0$

Thus, global matrix will be in the form:-

$$[\boldsymbol{M}]\{\ddot{\boldsymbol{y}}\} + [\boldsymbol{K}]\{\boldsymbol{y}\} = [\boldsymbol{F}(\boldsymbol{t})] \qquad \text{…….. (4.8)}$$

[$\boldsymbol{M}$] and **[K]** represent the system (or structure) stiffness matrix
{y} is the system displacement vector
[**F (t)]** represents the system force vector

4.4.1 Numerical Computation for Natural frequencies

Finding the natural frequencies for the system is by making force vector in the above undamped equation equal zero.

Equation (4.8) becomes

$$[\boldsymbol{M}]\{\ddot{\boldsymbol{y}}\} + [\boldsymbol{K}]\{\boldsymbol{y}\} = [\boldsymbol{0}] \qquad \text{..... (4.9)}$$

If $\left[y(t)\right]=\left[y\right]e^{j\omega t}$

Then $[\ddot{y}(t)] = [y](-\omega^2)e^{j\omega t}$

$\therefore -[M]\omega^2[y]e^{j\omega t} + [K]\{y\}e^{j\omega t} = [0]$

$e^{j\omega t}\{y\}([K] - \omega^2[M]) = [0]$

This result to eigenvalues problem as given

$$|[K] - \omega^2[M]| = |[K] - \lambda[M]| = [0] \quad \text{..... (4.10)}$$

Where

ω^2 $= \lambda$

ω = natural frequencies

λ = eigenvalues

4.4. 2. Numerical Computation for Damping

The formulation of the damping matrix for the conductor vibration was also based on the concept explained in section 2.4.2 which was also used in the formulation of the conductor damped equation in section 3.5. Hence, using equation (3.13) and also applying the Galerkin's method, the weak form of the equation becomes

$$EI\int_{\Re}\frac{\partial^2 y}{\partial x^2}.\frac{\partial^2 u}{\partial x^2}dx + S\int_{\Re}\frac{\partial y}{\partial x}.\frac{\partial u}{\partial x}dx + \beta.I\int_{\Re}\frac{\partial^3 y}{\partial x^2\partial t}\frac{\partial^2 u}{\partial x^2} + C\int_{\Re}\frac{\partial y}{\partial t}u + \rho A\int_{\Re}\frac{\partial^2 y}{\partial t^2}udx - \int_{\Re} fudx = 0$$

…… (4.11)

To obtain the damping matrix that conforms to the linear concept used for this study, the non-linear element is removed by simply equating the time partial differentiating variable to equal one.

This then results in damping equation for the finite element as

$$[D^e] = \beta.I\int_{\Re}\frac{\partial^2 y}{\partial x^2}.\frac{\partial^2 u}{\partial x^2}dx + C\int_{\Re}\frac{\partial y}{\partial t}udx$$

$$\left[D^e\right] = \beta.I\int_{\Re} B^T B + \left(C\int_{\Re} H^T H\right)\dot{y} \qquad \text{…….(4.12)}$$

Substituting equation (4 a and b) into equation (4.12), the damping matrix equation becomes

$$\left[D^e\right] = \beta.I\int_{\Re} \frac{\partial^2 y}{\partial x^2}.\frac{\partial^2 u}{\partial x^2}\,dx + \frac{C}{\rho A}\left[M^e\right] = \frac{\varepsilon}{E}\left[K^e\right] - \frac{\beta.S}{E}\int_{\Re}\frac{\partial y}{\partial x}.\frac{\partial u}{\partial x} + \frac{C}{\rho A}\left[M^e\right]$$

$$\left[D^e\right] = \frac{\beta}{E}\left[K^e\right] - \frac{\beta.S}{E}\int_{\Re} A^T A. + \frac{C}{\rho A}\left[M^e\right] \qquad \text{……..…… (4 .13)}$$

Incorporating the above equation into equation (4.8), the damped equation for the system becomes

$$[\boldsymbol{M}]\{\ddot{\boldsymbol{y}}\} + [\boldsymbol{D}]\{\dot{\boldsymbol{y}}\} + [\boldsymbol{K}]\{\boldsymbol{y}\} = [\boldsymbol{F}] \qquad \text{……. (4.14)}$$

Where [D] is the damping matrix

4.4.3 Evaluation of Damping

The evaluation of the amount of damping from the system was done by the comparison of the damping matrix of equation (4.13) to the proportional damping developed by Rayleigh.

The proportional damping equation is given as

$$D = \alpha M + \beta * K \qquad \text{…….. (4.15)}$$

$$D' = \alpha\, I * + \beta * \phi \quad \text{and} \quad D' = U^T D U \qquad \text{…….. (4.16)}$$

Where

α and $\beta *$ = real scalar constants
$I *$ = identity matrix
U = the orthonormal matrix of eigenvector
ϕ = the diagonal matrix of eigenvalues

The value of the damping ratio can be evaluated using the proportional damping, which is given as

$$\zeta = \frac{\alpha + \beta^* \omega_i^2}{2\omega_i} \qquad \text{..... (4.17)}$$

The values of α and β^* are usually evaluated using the values of natural frequencies obtained from experimental results.

In comparing equation (4.15) with equation (4.13)

$$\alpha = \frac{C}{\rho A} \quad \text{and} \quad \beta^* = \frac{\beta}{E}$$

In chapter 3, it was stated that conductor self-damping is a contribution of the internal damping modeled by Kelvin-Voigt damping model and external damping due to fluid to drag and inter-strand motion, modeled by viscous damping. Based on the classical work done by H.H Cudney and D.J. Inman [34], in which the values for each damping model and a combination of the both models were evaluated for a quasi-isotropic pultruded cantilever beam.

For the first case is the internal damping or the strain-rate damping, in this case damping is proportional to the mass matrix and from equation (4.15), β^* equal to zero. Thus, the percentage of the critical damping is inversely proportional to the natural frequency of each mode. This will give decreasing damping as their frequencies increase.

$$\zeta = \frac{\alpha + \beta^* \omega_i^2}{2\omega_i} = \frac{\alpha}{2\omega_i} \qquad \text{..... (4.18)}$$

Where $\beta^* = 0$

The second case is for the damping from fluid drag and inter-strand motion; the damping is proportional to the stiffness matrix and from equation (4.15), α equal to zero. Recognizing that the higher modes of vibration damp out quickly, this form of damping is proportional to frequencies in normal modes.

Hence $$\zeta = \frac{\alpha + \beta^* \omega_i^2}{2\omega_i} = \frac{\beta^* \omega_i}{2} \qquad \text{..... (4.19)}$$

Where $\alpha = 0$

The third case is the combination of both viscous and strain-rate damping which were evaluated by equation (4.15) to determine the total damping from the system.

The evaluation of the damping constants α and $\beta*$ was done by the least squares method also known as the pseudo-inverse routine.

To determine the estimated value for parameter α when $\beta*= 0$, is by finding the least-square solution to

$$\begin{bmatrix}\zeta_1\\ \zeta_2\\ \vdots\\ \zeta_n\end{bmatrix} = \begin{bmatrix}\frac{1}{2\omega_1}\\ \frac{1}{2\omega_2}\\ \vdots\\ \frac{1}{2\omega_n}\end{bmatrix}[\alpha] \qquad \text{..... (4.20)}$$

Also the value for $\beta*$ when $\alpha = 0$ is obtained by

$$\begin{bmatrix}\zeta_1\\ \zeta_2\\ \vdots\\ \zeta_n\end{bmatrix} = \begin{bmatrix}\frac{\omega_1}{2}\\ \frac{\omega_2}{2}\\ \vdots\\ \frac{\omega_n}{2}\end{bmatrix}[\beta*] \qquad \text{..... (4.21)}$$

For the values of both α and $\beta*$ is evaluated by

$$\begin{bmatrix}\zeta_1\\ \zeta_2\\ \vdots\\ \zeta_n\end{bmatrix} = \begin{bmatrix}\frac{1}{2\omega_1} & \frac{\omega_1}{2}\\ \frac{1}{2\omega_2} & \frac{\omega_2}{2}\\ \vdots & \vdots\\ \frac{1}{2\omega_n} & \frac{\omega_n}{2}\end{bmatrix}\begin{bmatrix}\alpha\\ \beta*\end{bmatrix} \qquad \text{..... (4.22)}$$

4.5 Electrical Equivalence: Electrical Equivalent Circuit

Although the transverse vibration of conductor is an example of a mechanical system that is dynamic in nature, the understanding and analysis of its dynamics can also be achieved by developing and analysing its electrical equivalence. The electrical equivalence is developed using the mechanical-electrical analogy, from which a corresponding equivalent circuit of the mechanical vibration of the conductor is obtained.

The electrical equivalence has the advantage that it can be constructed easily from which the results can be conveniently obtained and analysed to predict the system's dynamic response. This is based on the fact that much work has been done with respect to dynamics of electrical circuit especially in the area of resonance. Thus, results obtained from the equivalent circuit analysis can be used to determine the system parameters like natural frequencies, mode shapes and damping of mechanical systems. Also the mechanical-electrical analogy can help in further understanding the complex nature of the conductor's dynamic characteristics.

The conductor is a continuous model, but its electrical equivalence is developed from its lump-mass or discrete model similar to that of FEM. The discrete model of mass-spring–damper system of the equivalent continuous model of the pinned-pinned beam is shown in figure 4.2 (a and b) below. In this model, the first few modes of vibration are used to model the system response as shown in figure 4.2b, with the resultant force from the wind loading, perpendicular to the beam that produces the vertical oscillation. To develop the electrical equivalent, three degrees of freedom of the lump mass was used to describe the system response and the geometry of its domain of the lumped mass model is used to derive the equation of motion for the system.

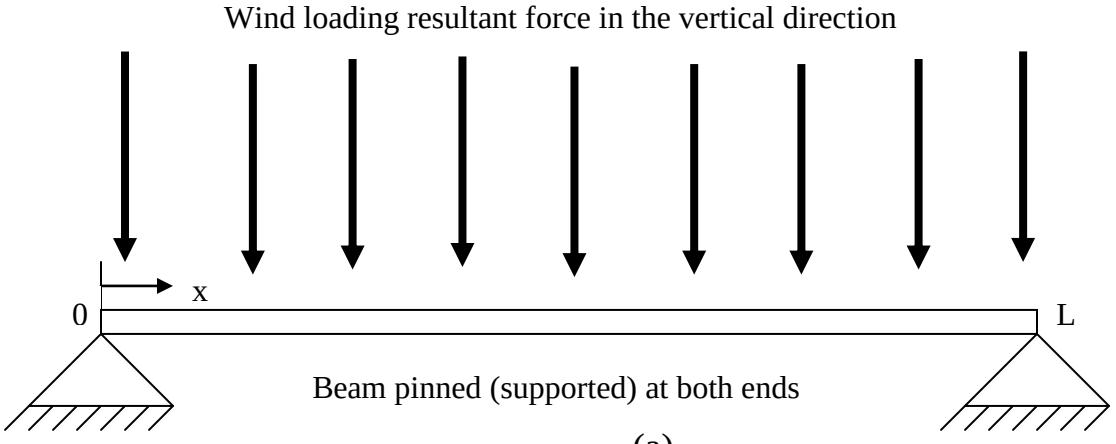

(a)

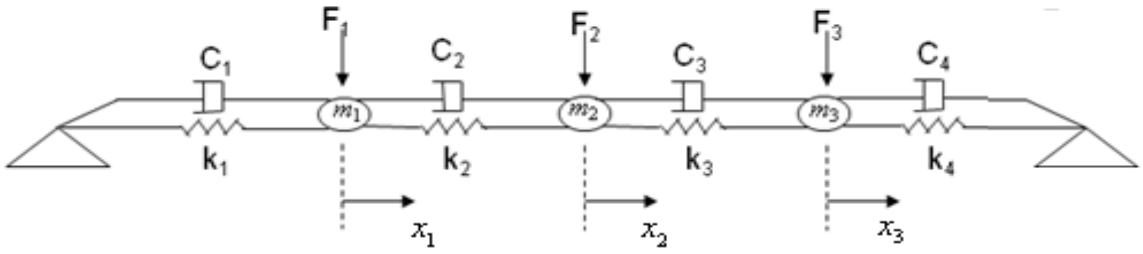

(b)

Fig 4.2 (a) Distributed model of a simply supported beam (b) its equivalent lump-mass model

In line with the concept mentioned in chapter 3, with regards to figure 4.2b, because it is assumed that the distributed loading on the conductor will have a resultant effect at a point, F_1, thus F_2, and F_3 are equal to zero.

Employing Newton's laws of motion, the equation for the discrete system will be in the form

$$m_1\ddot{x}_1 + (c_1 + c_2)\dot{x}_1 - c_2\dot{x}_2 + (k_1 + k_2)x_1 - k_2x_2 = F_1 \quad \text{..... (4.23a)}$$

$$m_2\ddot{x}_2 - c_2\dot{x}_1 + (c_2 + c_3)\dot{x}_2 - c_3\dot{x}_3 - k_2x_1 + (k_2 + k_3)x_2 - k_3x_3 = 0$$
… ..... (4.23b)

$$m_3\ddot{x}_3 - c_3\dot{x}_2 + (c_3 + c_4)\dot{x}_3 - k_3x_2 + (k_3 + k_4)x_x = 0 \quad \text{..... (4.23c)}$$

To obtain the differential equation in electrical form from equation of motion for the mechanical system is done by using the electrical analogies for mechanical systems listed in table 4.1. There are generally two types of mechanical- electrical analogies [35, 36]:

1. The voltage –force or mass-inductance analogy and
2. The current –force or mass capacitance analogy

In general, the following rule is used for developing an electrical equivalent circuit for mechanical systems. If the forces act in series in the mechanical system, the electric elements

representing these forces are put in parallel. Forces in parallel are represented by elements in the series in the electric circuits [35].

The table 4.1 below shows the analogies that exist between mechanical systems and electrical systems in terms of voltage-force analogy and current-force analogy.

Table 4.1 Mechanical-electrical analogies [35]

Mechanical Systems	**Electrical systems**	
	Voltage-force Analogy	**Current-force Analogy**
D'Alembert's principle	Kirchhoff's voltage law	Kirchhoff's current law
Degree of freedom	Loop	Node
Force applied	Switch closed	Switch closed
Force F, (N)	Voltage v, (volt)	Current I (ampere)
Mass m,(Kg)	Inductance L, (henry)	Capacitance C (farad)
Displacement x, (m)	Charge q, (coulomb)	$\Phi = \int v dt$
Velocity $\dot{x}$, (m/s)	Loop current I, (ampere)	Node voltage v (volt)
Damping c, (Ns/m)	Resistance R(ohms)	Conductance 1/R (mho)
Spring k, (N/m)	1/Capacitance 1/C (1/farad)	1/Inductance 1/L (1/henry)
Coupling element	Element common to two loop	Element between nodes

From table 4.1, using the voltage-force or mass-inductance analogy and comparing this with the mechanical equation, the electrical equivalent differential equations will be in the form given below

$$L_1 \frac{di_1}{dt} + (R_1 + R_2)i_1 - R_2 i_2 + (1/c_1 + 1/c_2) \int i_1 dt - \frac{1}{c_2} \int i_2 dt = V_1(t) \quad \ldots\ldots\ldots\ldots (4.24a)$$

$$L_2 \frac{di_2}{dt} - R_2 i_1 + (R_2 + R_3)i_2 - R_3 i_3 \; - \frac{1}{c_2} \int i_1 dt + (1/c_2 + 1/c_3) \int i_2 dt - 1c3i3dt=0 \quad \ldots\ldots\ldots\ldots (4.24b)$$

$$L_3 \frac{di_3}{dt} - R_3 i_2 + (R_3 + R_4)i_3 - \frac{1}{c_3} \int i_2 dt + (1/c_3 + 1/c_4) \int i_3 dt = 0 \quad \ldots\ldots\ldots\ldots\ldots (4.24c)$$

Based on Kirchhoff's voltage law and using electrical differential equation given above, the resultant electrical equivalent circuit for the vibrating conductor was constructed as shown in fig 4.5 below.

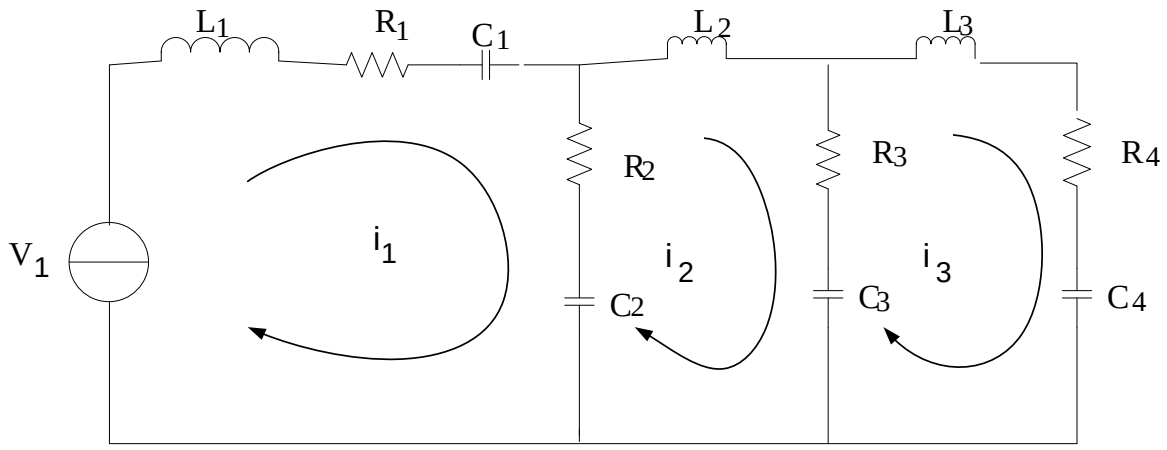

Fig 4.5. Equivalent electrical circuit for a vibrating conductor

4.6 The Input-Output Model

The input-output model for the circuit above is derived by using the sets of electrical differential equations used to form the system electrical circuit i.e. equations (4.29 a, b and c). The model is derived by applying Kirchhoff's voltage law to these sets of differential equations.

The damping was evaluated from the system's equivalent circuit based on the assumption that the total damping experience by the system as a result of the input voltage V_1 is the output voltage across resistor, R_4.

Taking the Laplace transform of the above equation

$$sL_1\, I_1(s) + \ (R_1 + \ R_2)I_1(s) - \ R_2 I_2(s) + \left(\frac{1}{SC_1} + \frac{1}{SC_2}\right) I_1(s) - \frac{1}{SC_2} I_2(s) = V_1(s)$$

$$sL_2\, I_2(s) - R_1 I_1(s) + \ (R_2 + \ R_3)I_2(s) - \ R_3 I_2(s) - \frac{1}{SC_1} I_1(s) + \left(\frac{1}{SC_2} + \right.$$

$$1SC3\, I2s - 1SC3I3(s) = 0$$

$$sL_3\, I_3(s) - R_3 I_2(s) + (R_3 + R_4) I_3(s) - \frac{1}{SC_3} I_2(s) + \left(\frac{1}{SC_1} + \frac{1}{SC_2}\right) I_1(s) = 0$$

Rearranging

$$I_1(s)\left[sL_1 + (R_1 + R_2) + \left(\frac{1}{SC_1} + \frac{1}{SC_2}\right)\right] + I_2(s)\left[-R_2 - \frac{1}{SC_2}\right] = V_1(s) \quad \ldots\ldots\ldots\ldots (4.25a)$$

$$I_1(s)\left[-R_1 - \frac{1}{SC_1}\right] + I_2(s)\left[sL_2 + (R_2 + R_3) + \left(\frac{1}{SC_2} + \frac{1}{SC_3}\right)\right] + I_3(s)\left[-R_3 - \frac{1}{SC_3}\right] = 0$$

$$\ldots\ldots\ldots\ldots\ldots (4.25b)$$

$$I_2(s)\left[-R_3 - \frac{1}{SC_3}\right] + I_3(s)\left[sL_3 + (R_3 + R_4) + \left(\frac{1}{SC_3} + \frac{1}{SC_4}\right)\right] = 0 \quad \ldots\ldots\ldots\ldots\ldots (4.25c)$$

Putting in matrix form it becomes

$$\begin{bmatrix} a_{11} & a_{12} & 0 \\ a_{21} & a_{22} & a_{23} \\ 0 & a_{32} & a_{33} \end{bmatrix} \begin{bmatrix} I_1(s) \\ I_2(s) \\ I_3(s) \end{bmatrix} = \begin{bmatrix} V_1(s) \\ 0 \\ 0 \end{bmatrix} \quad \ldots\ldots\ldots\ldots (4.26)$$

Where $a_{11} = \left[sL_1 + (R_1 + R_2) + \left(\frac{1}{SC_1} + \frac{1}{SC_2}\right)\right]$

$a_{12} = \left[-R_2 - \frac{1}{SC_2}\right]$

$a_{21} = \left[-R_1 - \frac{1}{SC_1}\right]$

$a_{22} = \left[sL_2 + (R_2 + R_3) + \left(\frac{1}{SC_2} + \frac{1}{SC_3}\right)\right]$

$a_{23} = \left[-R_3 - \frac{1}{SC_3}\right]$

$a_{32} = \left[-R_3 - \frac{1}{SC_3}\right]$

$a_{33} = \left[sL_3 + (R_3 + R_4) + \left(\frac{1}{SC_3} + \frac{1}{SC_4}\right)\right]$

If

$$D = \begin{bmatrix} a_{11} & a_{12} & 0 \\ a_{21} & a_{22} & a_{23} \\ 0 & a_{32} & a_{33} \end{bmatrix}$$

$$D_1 = \begin{bmatrix} V_1(s) & a_{12} & 0 \\ 0 & a_{22} & a_{23} \\ 0 & a_{32} & a_{33} \end{bmatrix}$$

$$D_2 = \begin{bmatrix} a_{11} & V_1(s) & 0 \\ a_{21} & 0 & a_{23} \\ 0 & 0 & a_{33} \end{bmatrix}$$

$$D_3 = \begin{bmatrix} a_{11} & a_{12} & V_1(s) \\ a_{21} & a_{22} & 0 \\ 0 & a_{32} & 0 \end{bmatrix}$$

Using Creamer rule

$$I_1 = \frac{D_1}{D}$$

$$I_2 = \frac{D_2}{D}$$

$$I_3 = \frac{D_3}{D}$$

The output voltage across R_4 is given as

$Vo\ (s)$ = $R_4\ I_3(s)$ …….. (4.27)

But $I_3(s) = \dfrac{V_1\ (s)(a_{21}a_{32})}{a_{11}(a_{12}a_{33}-a_{23}a_{32})-a_{12}(a_{21}a_{33})}$ …….. (4.28)

Hence, the transfer function for the electrical equivalent circuit will be given below as

$$\frac{Vo\ (s)}{V_1(s)} = \frac{R_4\ a_{21}a_{32}}{a_{11}a_{12}a_{33}-a_{11}a_{23}a_{32}-a_{12}a_{21}a_{33}} \qquad \text{…….. (4.29)}$$

By defining the conductor's equivalent circuit resistance, capacitance and inductance in terms conductor characteristics

$$R_m = \frac{c}{\sigma}$$

$$C_m = \frac{1}{K\sigma}$$

$$L_m = \frac{M}{\sigma}$$

Where K = stiffness of the conductor
M = the mass of the conductor
c = the damping constant
σ = electromechanical factor
m = 1, 2 3 4

The transfer function developed above was implemented in Matlab software with the calculated circuit element equivalents as defined above and the result of the simulation is presented in Chapter 5

CHAPTER 5

TESTING AND RESULTS

5.1 Vibration Research and Testing Centre (VRTC)

In verifying the analytical model analysed in chapter 3, experimental studies (vibration tests) were conducted. These tests were conducted at the Vibration Research and Testing Centre (VRTC) situated at the University of KwaZulu-Natal Westville Campus. The VRTC was set-up in 2004 in partnership between Eskom and the University of KwaZulu-Natal. The centre which is an indoor testing facility is aimed at testing and carrying research on power line conductors with regard to mechanical vibration. The VRTC laboratory facilities used for testing were designed, developed and constructed in line with the guideline provided in IEEE standard [37].
The laboratory consists of:

- A testing facility and a tunnel with temperature control, shown in figure 5.1
- A constant tension loading device
- A span–85m single conductor shown in figure 5.1
- A shaker–electro-dynamic in operation which is used to provide the input power to the conductor as shown in figure 5.3
- A control system which is used to analyse the output from the test facility

Because the VRTC is an indoor testing facility, tests conducted at the centre were used to simulate the wind-induced vibration on conductors that occurs in the real world. This is then used as the bases of comparison and predicts what actually occurs in real transmission lines. The tests that were conducted at the centre for this study were used mainly to determine the self damping capability of conductors according to the procedures described in IEEE standard on the Measurements of Conductor Self-damping [38]. Also based on the experimental data was the evaluation of dynamic stiffness of the conductor.

Figure 5.1 Facility tunnel and single span conductor at the VRTC

5.2 Methods of Testing

At the VRTC, the experiments that were carried out are on single span conductors as shown above. These were used to analyse and understand the conductor dynamic characteristics. For this purpose, two types of testing were done with the aim of verifying the analytical model. These are: free and forced vibrations.

5.2.1 Free vibration testing

The free vibration of a conductor is the natural response of the conductor to some form of impact or displacement and the amplitude of vibration decay with time due to damping. For this test the impact on the conductor was done using the impact hammer shown in the figure 5.2 below

Fig 5.2 Impact hammer

To evaluate the amount of damping from the conductor experiencing this form of vibration, the least square method [39] was used and the description of how this method was developed from log decrement techniques is given in appendix C

5.2.2 Forced vibration testing

The forced vibration of the conductor was done to obtain its response when the conductor is subjected to a repetitive forcing function. This caused the conductor to vibrate at the frequency of the excitation. For forced vibration test, it is assumed that the effective loading input that causes the conductor oscillation is concentrated at one point on the conductor. The excitation by this concentrated force is duplicated by a force at a single point (point loading), and this source of loading was simulated by the aerodynamic shaker. For this method of testing, a sweep test (resonance frequencies search) was done for frequency range between 6Hz and 50Hz for the Tern conductor and 5Hz and 50Hz for the Aero-Z conductor. The conductor damping was determined for each mode using the bandwidth method [40], also the description of this method is given in appendix C.

5.2.2.1 Methods of forced vibration testing

Two methods were employed for forced vibration testing at the VRTC in order to evaluate the conductor response and are explained in IEEE standard on power dissipation from conductors with respect to Aeolian vibration [37]. The two methods of forced vibration testing that were explained are the power method and the standing wave method.

The power method in which the conductor is forced into resonance by an electro-dynamic shaker and the power input into the system was determined directly from the product of the excitation force and the resulting velocity at the point of application of the load. This represents the power dissipated by the conductor, provided the two quantities are sinusoidal and are in phase with each other. It assumes also that the losses at the terminations are small compared with the dissipation within the conductor. The power method also permits the mechanical resistance per unit length of the conductor to be determined directly from the ratio of the force to the velocity.

The standing wave method in which the power transfer P_1 from the vibration generator towards the ends of the span at any particular node i.e. node 1, is derived from the inverse or the reciprocal of the standing wave ratio that is the ratio of the nodal and antinodal amplitudes and is given as follows

$$P_1 = \sqrt{Sm}\,\frac{V^2}{2}\left(\frac{a_1}{Y}\right)$$

Where

$\sqrt{Tm}$ = the wave or characteristic impedance (At very high frequencies this may be modified due to the effect of the stiffness of the conductor.)

$\frac{Y}{a_1}$ = standing wave ratio

V = single amplitude velocity at antinode

S = conductor tension

m = conductor mass per unit length

Then the power dissipated between two nodes 1 and 2 is simply

$$P = P_1 - P_2$$

5.2.2.2 Shaker conductor connection

The shaker-conductor connection for the forced vibration tests was by the flexible link connection as shown figure 5.3. This arrangement was used because it has the advantage of separating the conductor resonance from that of the shaker thereby decoupling them from each other. This set-up helps in setting the conductor alone into resonance for the purpose of

determining its resonance frequencies, conversely helping in ascertaining the amount of damping only from the vibrating conductor.

Figure 5.3 Shaker-Conductor flexible link connection

Note:

1. Before carrying out any test on the conductor, the conductor was initially strung to a tension 40% of the UTS, for ACSR and 30% of the UTS for the Aero-Z. Then the conductors were allowed to relax for 3 days before the test was done.
2. For both forms of testing: the free and the forced vibration, the point of impact and loading was at 1.2m from the load cell end for both conductors.
3. Two accelerometers where used for this study and they were placed at half (1/2) and at one-eight (1/8) of the span length from the load cell side of the conductor.
4. Also for both forms of testing, tests were done for tensions 19.96KN, 24.74KN and 29.64KN which are 20%, 25% and 30% of the UTS respectively for the case ACSR. While for Aero-Z the tests were done at 22.52KN, 30.02KN and 37.53KN which are 15%, 20% and 25% of the UTS respectively.
5. For both the free and the forced vibration test, the PUMA analyser [41] was used.

5.3 Results

For the experiential study conducted on the indoor single span conductor, two forms of testing were carried out: free and forced vibrations according to the explanation given in section 5.2. These were done for two conductors: the ACSR-Tern and the Aero-Z conductors. The results of the laboratory experiments for both testing methods and for the two conductors are given below.

Next, the results also presented are that from the finite element simulation using ABAQUS which was also done at the three different tensions with the same values used in the experimental studies for both conductors.

Finally, result for the free response was obtained from the simulation for the transfer function developed from the electrical equivalent circuit for the vibrating conductor.

5.3.1 Experimental Results for Free Vibration: Tern Conductor

For the experimental studies done on Tern conductor, the graphs below are the free vibration responses for Tern conductor at tensions of 20% UTS-19.64KN, 25% UTS-24.64KN and 30% UTS-29.71KN. The two tables accompanying each graph are used to evaluate the conductor damping using the least square method. The first table is used to evaluate damping for the first decay region and second table for the second decay region for each graph and they are labeled first decay and second decay respectively. Also for each tension used, two graphs are presented to evaluate the conductor damping labeled graph 1 and graph 2 respectively.

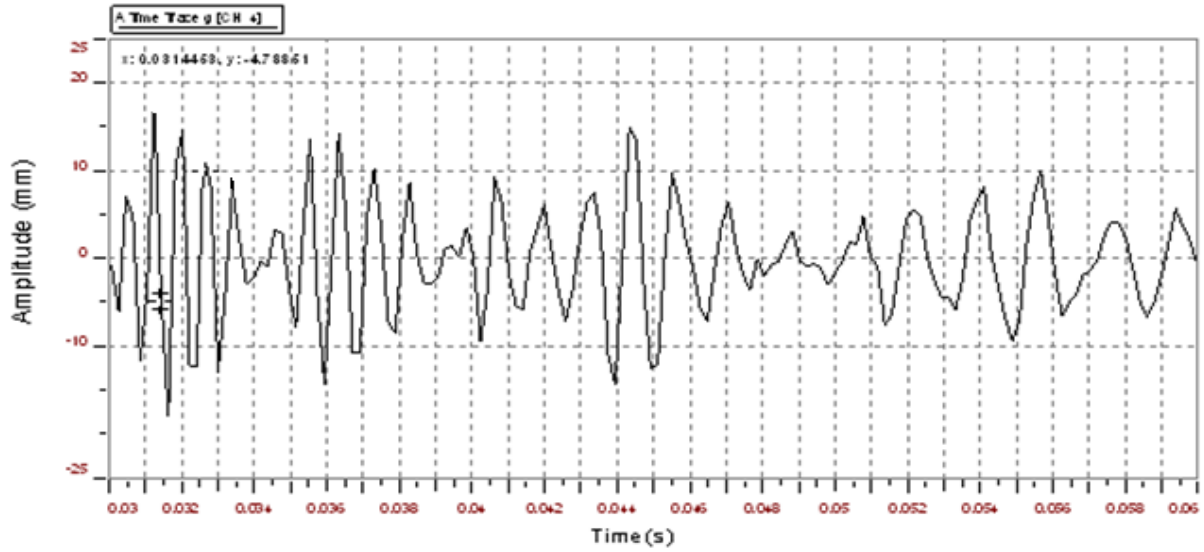

Fig 5.4 Free vibration for Tern conductor at 20% UTS-19.64KN (graph 1)

Table 5.1 Using the least square method to calculate damping for 20% UTS (first decay)

Integer j	Amplitude(mm) Y	LN(Y)	(j-1)	LN(Y)(j-1)	$(j-1)^2$
1	16.224	2.7865	0	0	0
2	14.823	2.6962	1	2.6962	1
3	11.924	2.4786	2	4.9571	4
4	9.732	2.2754	3	6.8263	9
Sum		10.2366	6	14.4795	14

The log-deg = 0.1751 and zeta = 0.0279

Table 5.2 Using the least square method to calculate damping for 20% UTS Tern (second decay)

Integer j	Amplitude(mm) Y	LN(Y)	j-1	LN(Y)(j-1)	$(j-1)^2$
1	12.624	2.5356	0	0	0
2	13.423	2.5970	1	2.5970	1
3	10.024	2.30450	2	4.6099	4
4	8.032	2.0834	3	6.2503	9
Sum		9.5210	6	13.4572	14

The Log-deg = 0.1649 and zeta = 0.0262

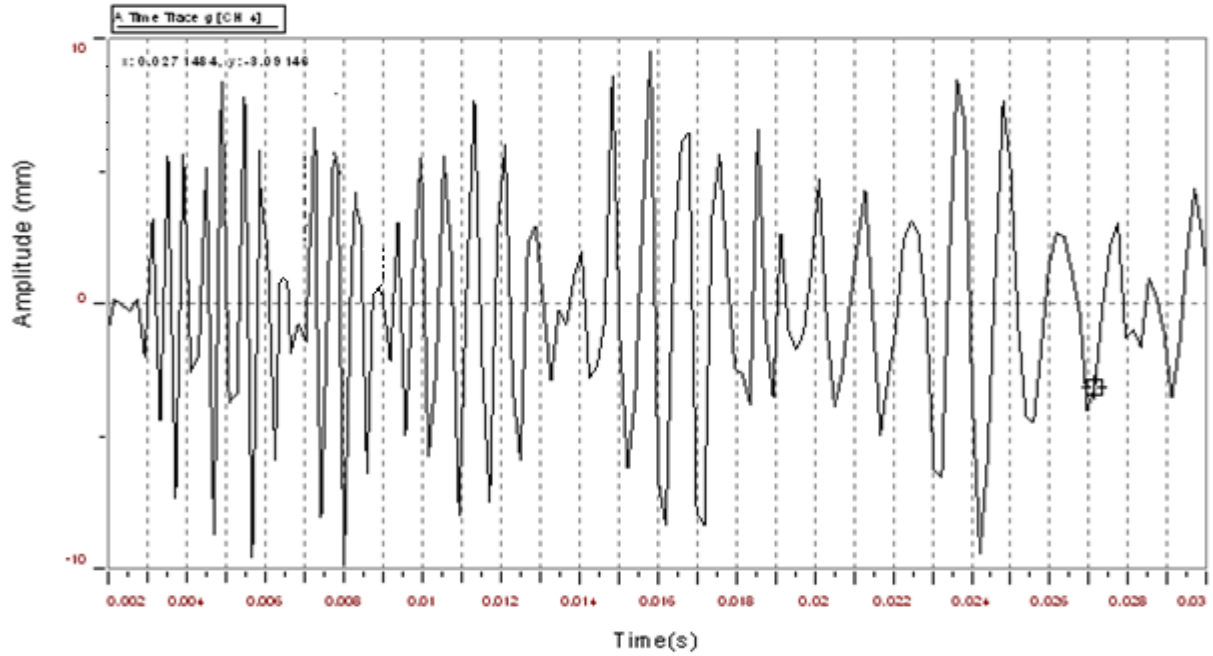

Fig 5.5 Free vibration for Tern conductor at 20% UTS-19.64KN (graph 2)

Table 5.3 Using the least square method to calculate damping for 20% UTS-Tern (first decay)

Integer j	Amplitude(mm) Y	LN(Y)	(j-1)	LN(Y)(j-1)	$(j-1)^2$
1	8.245	2.1096	0	0	0
2	7.623	2.0311	1	2.0312	1
3	5.949	1.7832	2	3.5664	4
Sum		5.9240	3	5.5976	5

The log-deg = 0.1392 and zeta = 0.0259

Table 5.4 Using the least square method to calculate damping for 20% UTS-Tern (second decay)

Integer j	Amplitude(mm) Y	LN(Y)	(j-1)	LN(Y)(j-1)	$(j-1)^2$
1	7.245	1.9803	0	0	0
2	6.823	1.9203	1	1.9203	1
3	4.899	1.5890	2	3.1781	4
Sum		5.4896	3	5.0984	5

The log-deg = 0.1956 and zeta = 0.0311

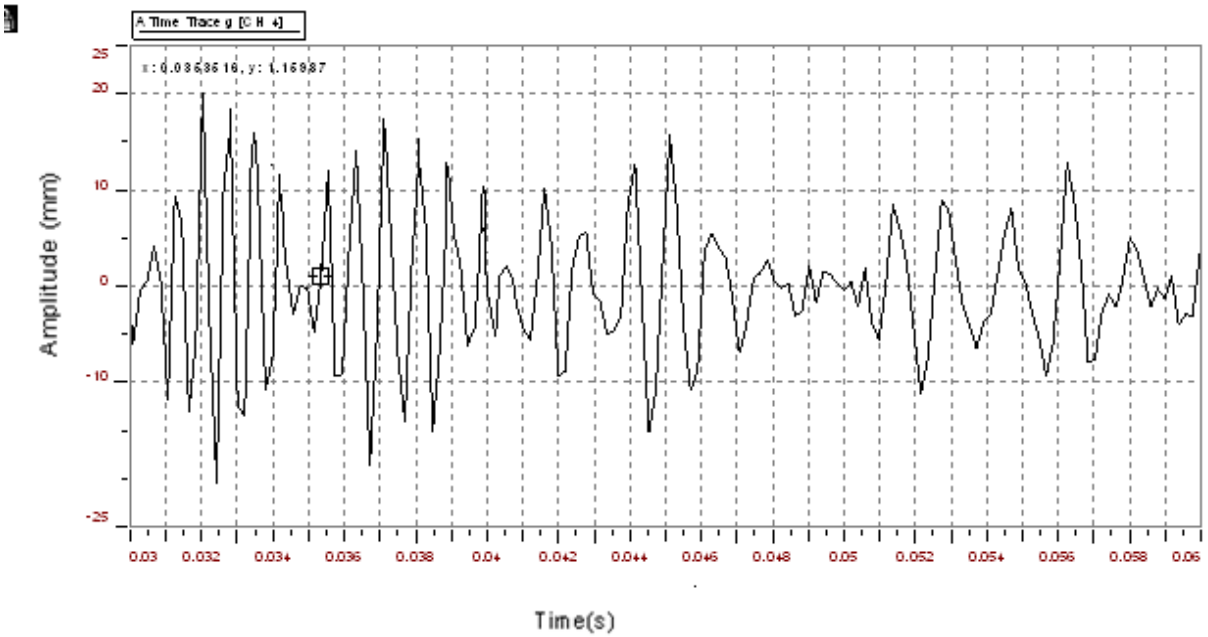

Figure 5.6 Free vibration for Tern conductor at 25% UTS-24.47KN (graph 1)

Table 5.5 Using the least square method to calculate damping for 25 %UTS-Tern (first decay)

Integer j	Amplitude(mm) Y	LN(Y)	(j-1)	LN(Y)(j-1)	$(j-1)^2$
1	20.176	3.0045	0	0	0
2	18.483	2.9169	1	2.9169	1
3	16.987	2.8324	2	5.6649	4
4	12.755	2.5459	3	7.6378	9
Sum		11.2997	6	16.2120	14

The log-deg = 0.1460 and zeta = 0.0232

Table 5.6 Using the least square method to calculate damping for 25% UTS-Tern (second decay)

Integer j	Amplitude(mm) Y	LN(Y)	(j-1)	LN(Y)(j-1)	$(j-1)^2$
1	17.276	2.8493	0	0	0
2	15.983	2.7715	1	2.7715	1
3	13.97	2.6369	2	5.2738	4
4	10.855	2.3846	3	7.1539	9
Sum		10.6424	6	15.1992	14

The log-deg = 0.1529 and zeta = 0.0243

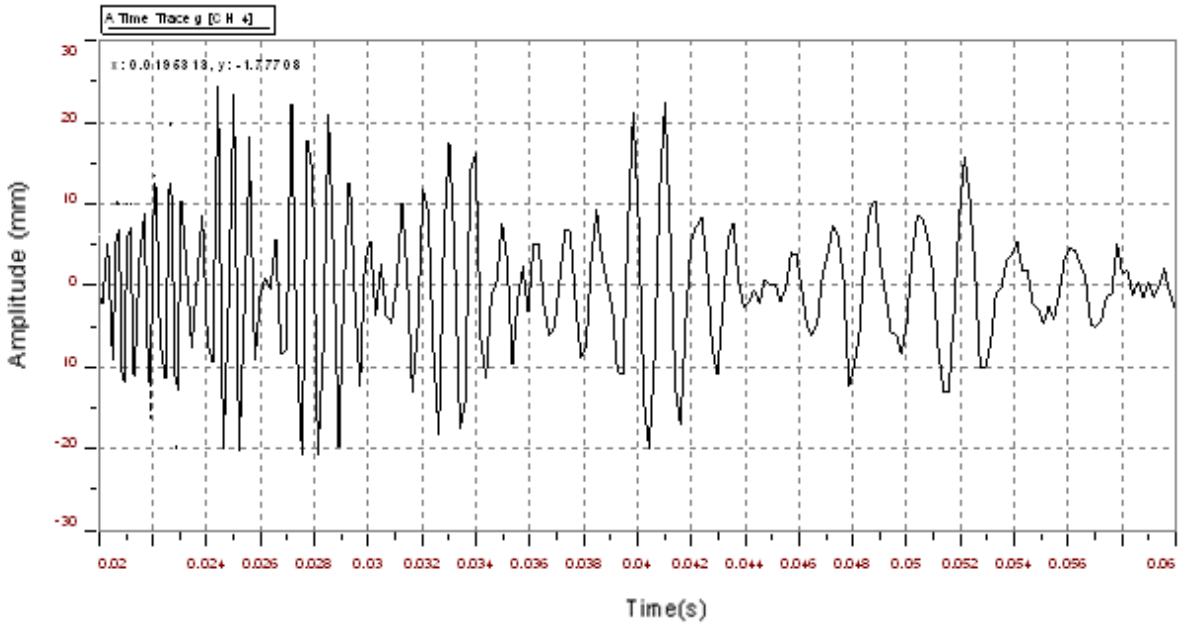

Figure 5.7 Free vibration for Tern conductor at 25% UTS-24.47KN (graph 2)

Table 5.7 Using the least square method to calculate damping for 25% UTS-Tern (first decay)

Integer j	Amplitude(mm) Y	LN(Y)	(j-1)	LN(Y)(j-1)	$(j-1)^2$
1	24.624	3.2037	0	0	0
2	23.249	3.1463	1	3.1463	1
3	18.637	2.9251	2	5.8503	4
Sum		9.2751	3	8.9966	5

The log-deg = 0.1393 and zeta = 0.0222

Table 5.8 Using the least square method to calculate damping fo 25% UTS-Tern (second decay)

Integer j	Amplitude(mm) Y	LN(Y)	(j-1)	LN(Y)(j-1)	$(j-1)^2$
1	22.417	3.1098	0	0	0
2	18.983	2.9435	1	2.9435	1
3	21.087	3.0487	2	6.0973	4
4	13.655	2.6141	3	7.8423	9
Sum		11.7161	6	16.8832	14

The log-deg = 0.1382 and zeta = 0.0219

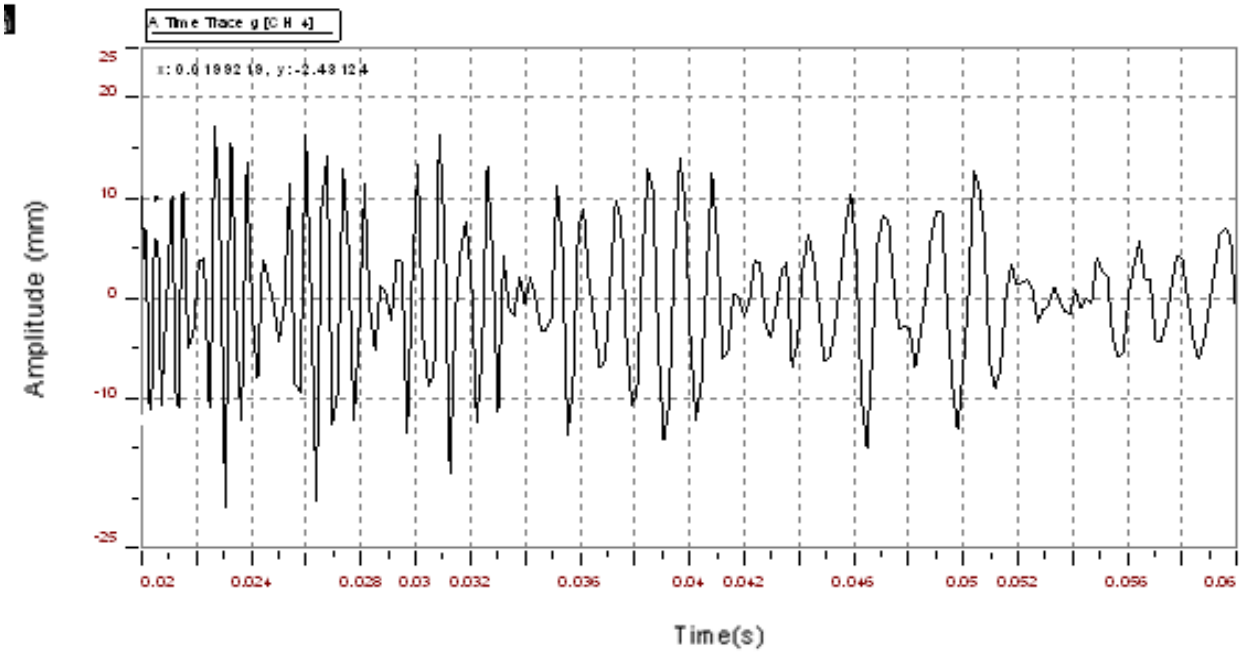

Figure 5.8 Free vibration for Tern conductor at 30% UTS -29.71KN (graph 1)

Table 5.9 Using the least square method to calculate damping for 30% UTS-Tern (first decay)

Integer j	Amplitude(mm) Y	LN(Y)	(j-1)	LN(Y)(j-1)	$(j-1)^2$
1	17.444	2.8590	0	0	0
2	16.809	2.8219	1	2.8219	1
3	14.737	2.6904	2	5.3807	4
Sum		8.3713	3	8.2026	5

The log-deg = -0.0843 and zeta = 0.0134

Table 5.10 Using the least square method to calculate damping for 30% UTS-Tern (second decay)

Integer j	Amplitude(mm) Y	LN(Y)	(j-1)	LN(Y)(j-1)	$(j-1)^2$
1	16.124	2.7803	0	0	0
2	15.223	2.7228	1	2.7228	1
3	13.924	2.6336	2	5.2672	4
4	12.732	2.5441	3	7.6324	9
Sum		10.6809	6	15.6224	14

The log-deg = 0.0798 and zeta = 0.0127

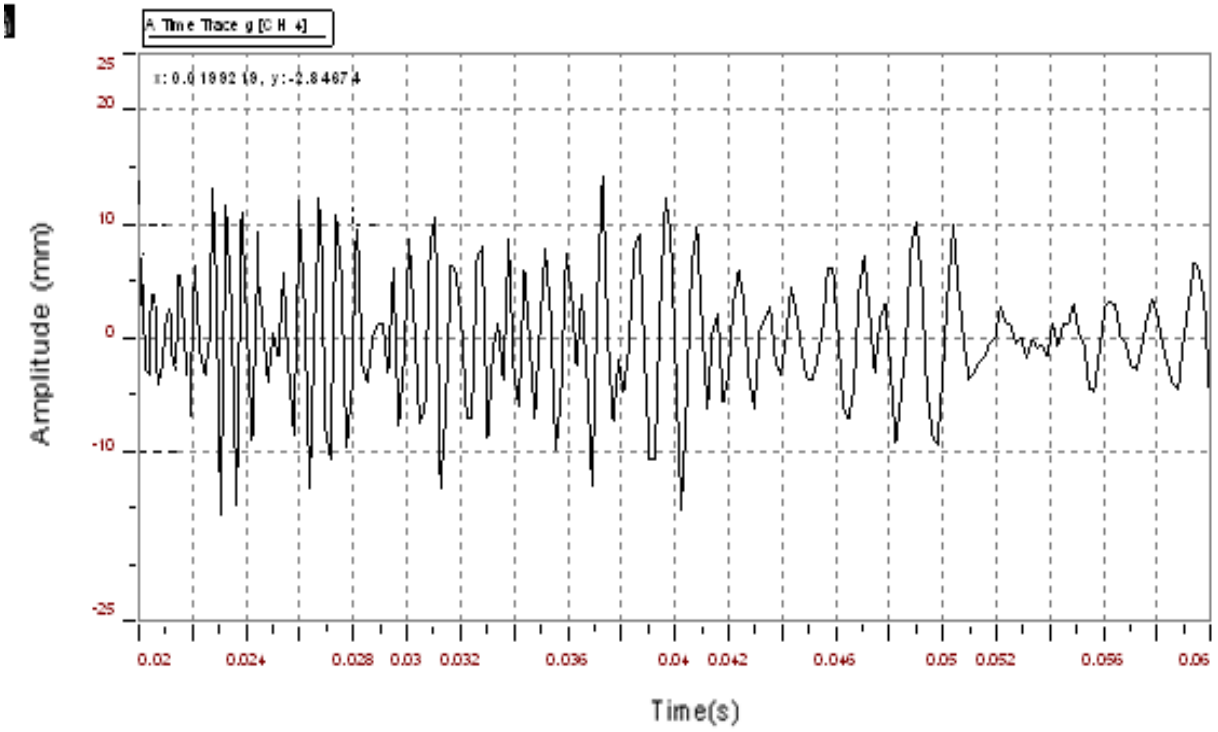

Figure 5.9 Free vibration for Tern conductor at 30% UTS-29.71KN (graph 2)

Table5.11 Using the least square method to calculate damping for 30% UTS-Tern (first decay)

Integer j	Amplitude(mm) Y	LN(Y)	(j-1)	LN(Y)(j-1)	$(j-1)^2$
1	13.276	2.5860	0	0	0
2	12.683	2.5403	1	2.5403	1
3	11.487	2.4412	2	4.8824	4
4	9.855	2.2880	3	6.8639	9
Sum		9.8554	6	14.2866	14

The log-deg = 0.0993 and zeta = 0.0158

Table 5.12 Using the least square method to calculate damping for 30% UTS-Tern (second decay)

Integer j	Amplitude(mm) Y	LN(Y)	(j-1)	LN(Y)(j-1)	$(j-1)^2$
1	12.524	2.5276	0	0	0
2	12.023	2.4868	1	2.4868	1
3	11.324	2.4269	2	4.8538	4
4	9.732	2.2754	3	6.8263	9
Sum		9.7168	6	14.1669	14

The log-deg = 0.0817 and zeta = 0.0130

5.3.2 Experimental Results for Forced Vibration (Sweep Test): Tern Conductor

To determine the dynamic response for the conductor, a sweep test was conducted for the Tern conductor. The graphs shown below are the forced vibration (sweep test) for Tern conductor at tensions 20% UTS-19.64KN, 25%UTS-24.64KN and 30%UTS-29.71KN. The table accompanying each graph is used to record the first ten resonance frequencies and also the evaluation of the conductor damping at each mode using the bandwidth method.

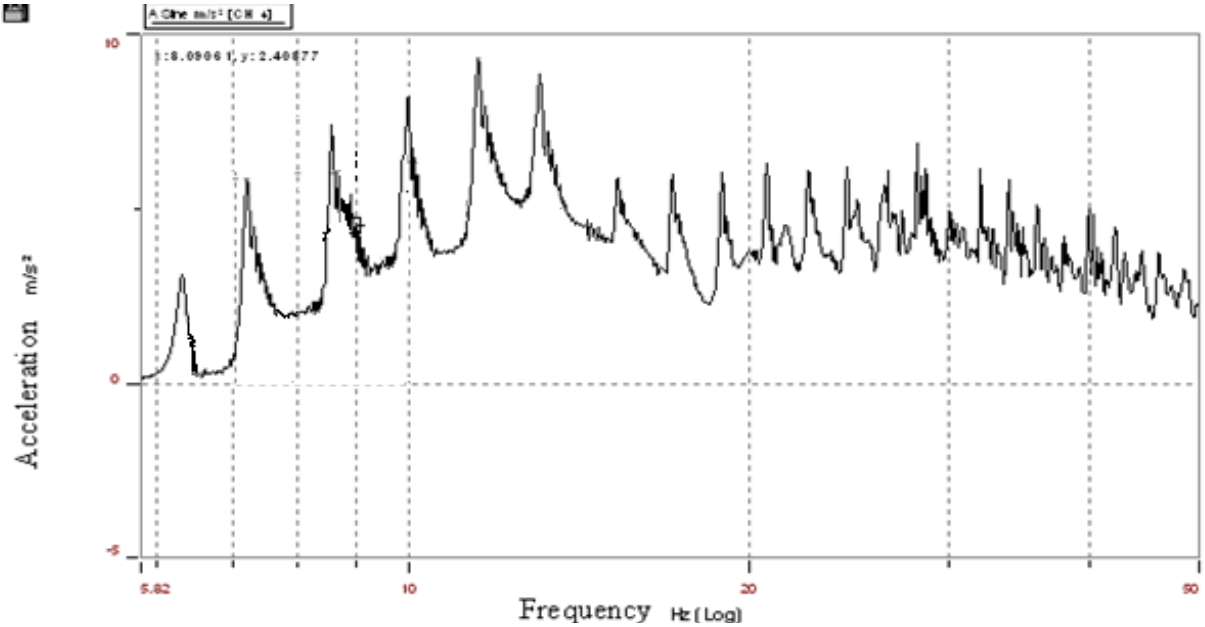

Figure 5.10 Forced vibration for Tern conductor at 20% UTS-19.64KN

Table 5.13 Showing Resonance frequencies and calculation for damping using bandwidth method

Resonance frequency R_f	Acceleration a(G)	$a/\sqrt{2}$	Half-Power F_1	Half-Power F_2	Bandwidth Δf	quality factor Q	damping factor ζ
6.39	3.910	2.7648	6.16	6.89	0.73	8.7534	0.0571
7.21	6.010	4.2498	6.87	7.58	0.71	10.1549	0.0492
8.61	7.970	5.6357	8.27	8.87	0.60	14.2167	0.0352
10.13	8.190	5.7913	9.83	10.38	0.55	18.4182	0.0271
12.92	9.080	6.4206	12.68	13.29	0.61	21.1803	0.0236
14.02	6.130	4.3346	13.77	14.39	0.62	22.6129	0.0221
16.99	6.290	4.4477	16.69	17.44	0.75	22.6533	0.0221
17.70	6.470	4.5750	17.47	18.14	0.67	26.4179	0.0189
19.21	6.640	4.6952	18.87	19.66	0.79	24.3165	0.0206
21.82	6.670	4.7164	21.35	22.29	0.94	23.2128	0.0215

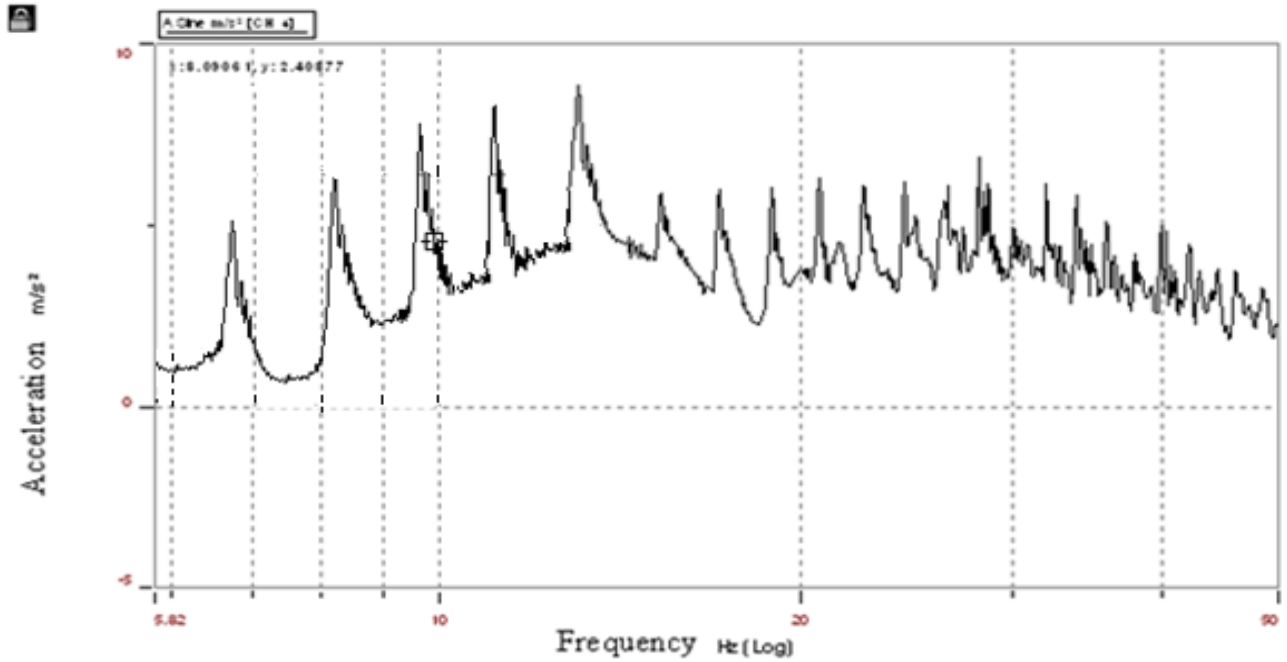

Figure 5.11 Forced vibration for Tern conductor at 25%UTS-24.47KN

Table 5.14 Showing Resonance frequencies and calculation for damping using bandwidth method

Resonance frequency R_f	Acceleration a(G)	$a/\sqrt{2}$	Half-Power F_1	Half-Power F_2	Bandwidth Δf	quality factor Q	damping factor ζ
6.78	5.210	3.6841	6.54	7.22	0.68	10.0441	0.0498
8.22	6.850	4.8437	7.88	8.62	0.74	11.1081	0.0450
9.82	8.270	5.8478	9.51	10.11	0.60	16.2000	0.0309
12.13	8.680	6.1377	11.87	12.51	0.64	18.9531	0.0264
14.83	9.040	6.3923	14.36	15.24	0.88	16.8523	0.0297
16.81	6.010	4.2498	16.38	17.12	0.74	22.7162	0.0220
18.24	6.460	4.5680	17.93	18.71	0.78	23.3846	0.0214
19.27	6.880	4.8649	19.02	19.85	0.83	23.2169	0.0215
21.61	6.910	4.8862	21.21	22.07	0.86	25.1279	0.0199
23.52	7.080	5.0064	23.21	24.12	0.91	25.8462	0.0193

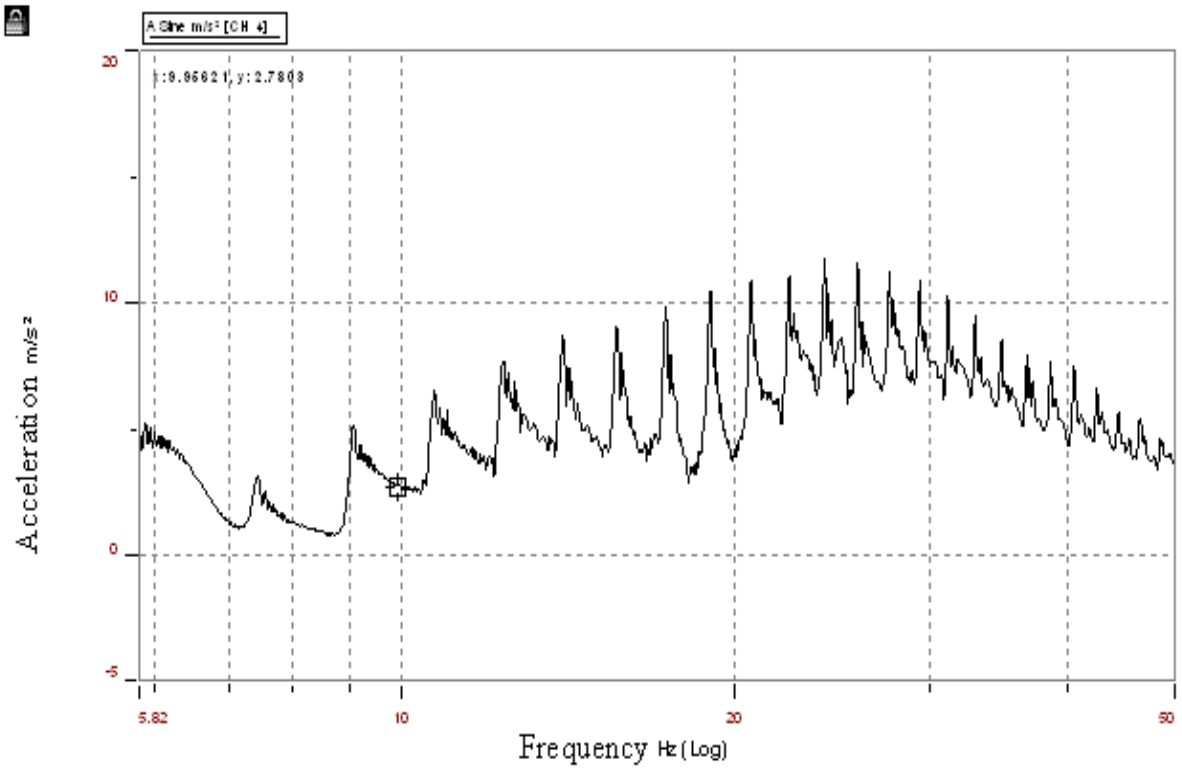

Figure 5.12 Forced vibration for Tern conductor at 30% UTS-29.71KN

Table 5.15 Showing Resonance frequencies and calculation for damping using bandwidth method

Resonance frequency R_f	Acceleration a(G)	$a/\sqrt{2}$	Half-Power F_1	Half-Power F_2	Bandwidth Δf	quality factor Q	damping factor ζ
7.46	3.106	2.1963	7.19	7.79	0.60	12.4333	0.0402
9.09	5.653	3.9973	8.85	9.48	0.63	14.4286	0.0347
11.43	6.270	4.4336	11.08	11.78	0.70	16.3286	0.0306
13.67	7.770	5.4943	13.17	14.03	0.86	15.8953	0.0315
15.74	8.640	6.1095	15.38	16.23	0.85	18.5176	0.0270
17.41	9.210	6.5125	17.03	17.71	0.68	25.6029	0.0195
18.10	10.000	7.0711	17.71	18.39	0.68	26.6176	0.0188
19.22	10.480	7.4106	18.88	19.69	0.81	23.7284	0.0211
21.07	10.610	7.5025	20.59	21.41	0.82	25.6951	0.0195
23.26	10.880	7.6934	22.92	23.73	0.81	28.7160	0.0174

5.3.3 Experimental Results for Free Vibration: Aero-Z Conductor

Similar to Tern conductor, the same free vibration test was also done for Aero-Z conductor. The results are presented in a format similar to that of the Tern conductor.

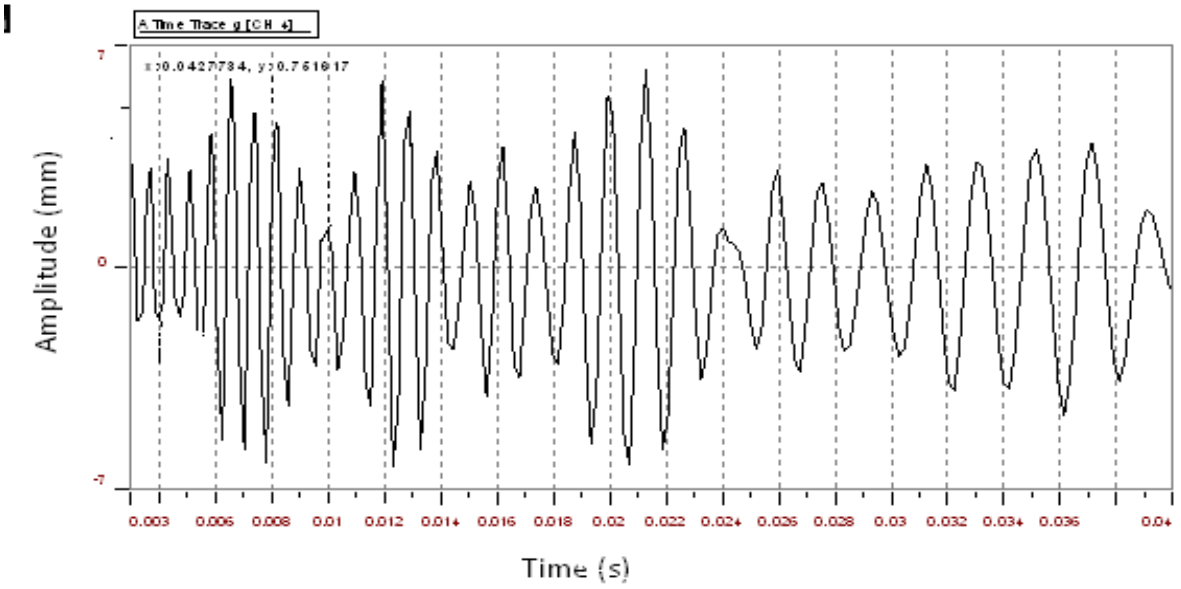

Figure 5.13 Free vibration for Aero-Z conductor at 15%UTS-22.52KN (graph 1)

Table 5.16 Using the least square method to calculate damping for 15% UTS-Aero-Z (first decay)

Integer j	Amplitude(mm) Y	LN(Y)	(j-1)	LN(Y)(j-1)	$(j-1)^2$
1	6.524	1.8755	0	0	0
2	4.823	1.5734	1	1.5734	1
3	4.240	1.4446	2	2.8891	4
4	2.843	1.0449	3	3.1348	9
Sum		5.9384	6	7.5973	14

The log-deg = -0.2262 and zeta = 0.0417

Table 5.17 Using the least square method to calculate damping for 15% UTS-Aero-Z (second decay)

Integer j	Amplitude(mm) Y	LN(Y)	(j-1)	LN(Y)(j-1)	$(j-1)^2$
1	6.124	1.8120	0	0	0
2	5.023	1.6140	1	1.6140	1
3	3.781	1.3301	2	2.6602	4
4	2.909	1.0679	3	3.2038	9
Sum		5.8243	6	7.4780	14

The log-deg = -0.2517 and zeta = 0.0400

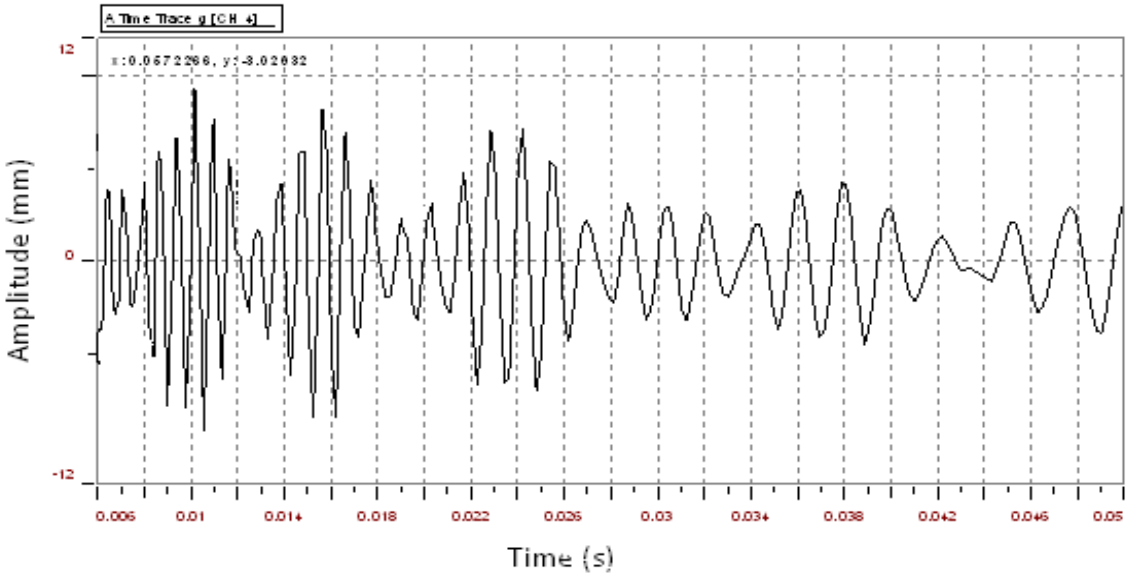

Figure 5.14 Free vibration for Aero-Z conductor at 15% UTS-22.52KN (graph 2)

Table 5.18 Using the least square method to calculate damping for 15% UTS-Aero-Z (first decay)

Integer j	Amplitude(mm) Y	LN(Y)	(j-1)	LN(Y)(j-1)	$(j-1)^2$
1	9.920	2.2946	0	0	0
2	7.763	2.0494	1	2.049369	1
3	5.785	1.7553	2	3.510537	4
Sum		6.0992	3	5.559906	5

The log-deg = -0.2696 and zeta = 0.0429

Table 5.19 Using the least square method to calculate damping for 15% UTS-Aero-Z (second decay)

Integer j	Amplitude(mm) Y	LN(Y)	(j-1)	LN(Y)(j-1)	$(j-1)^2$
1	8.720	2.1656	0	0	0
2	6.663	1.8966	1	1.8966	1
3	4.995	1.6084	2	3.2169	4
Sum		5.6706	3	5.1134	5

The log-deg = -0.27859 and zeta = 0.0443

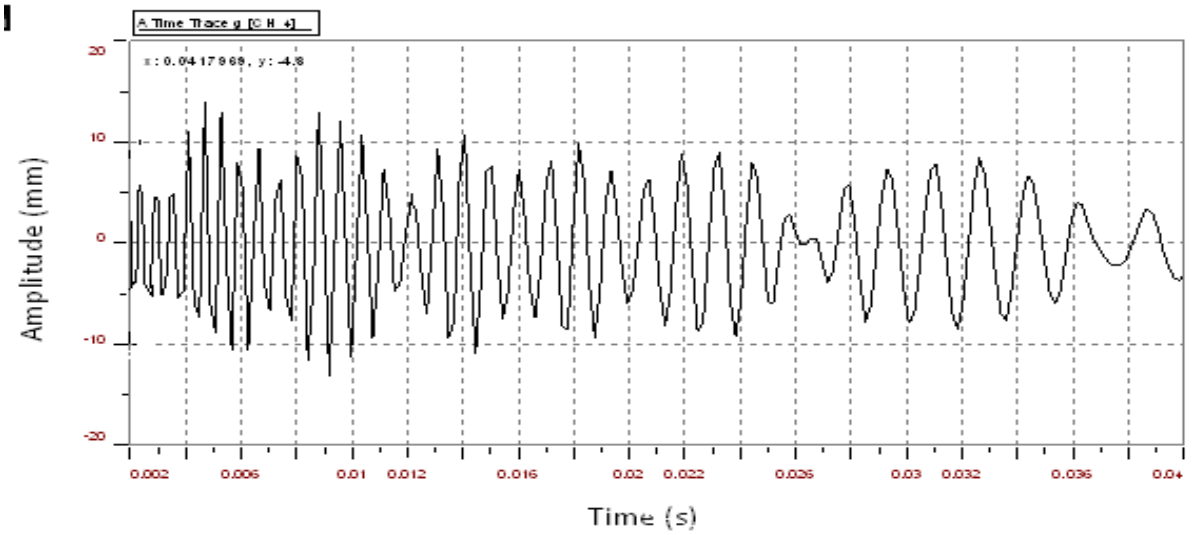

Figure 5.15 Free vibration for Aero-Z conductor at 20% UTS-30.02KN (graph 1)

Table 5.20 Using the least square method to calculate damping for 20% UTS-Aero-Z (first decay)

Integer j	Amplitude(mm) Y	LN(Y)	(j-1)	LN(Y)(j-1)	$(j-1)^2$
1	14.324	2.6619	0	0	0
2	13.823	2.6263	1	2.6263	1
3	8.0924	2.0909	2	4.1819	4
4	9.532	2.2547	3	6.7640	9
5	6.272	1.8361	4	7.3444	16
Sum		11.4700	10	20.917	30

The log-deg = -0.2023 and zeta = 0.0322

Table 5.21 Using the least square method to calculate damping for 20% UTS-Aero-Z (second decay)

Integer j	Amplitude(mm) Y	LN(Y)	(j-1)	LN(Y)(j-1)	$(j-1)^2$
1	13.324	2.5896	0	0	0
2	12.4823	2.5243	1	2.5243	1
3	10.484	2.3499	2	4.6997	4
4	7.732	2.0454	3	6.1361	9
5	4.972	1.6038	4	6.4153	16
Sum		11.11292	10	19.7754	30

The log-deg = -0.24504 and zeta = 0.0390

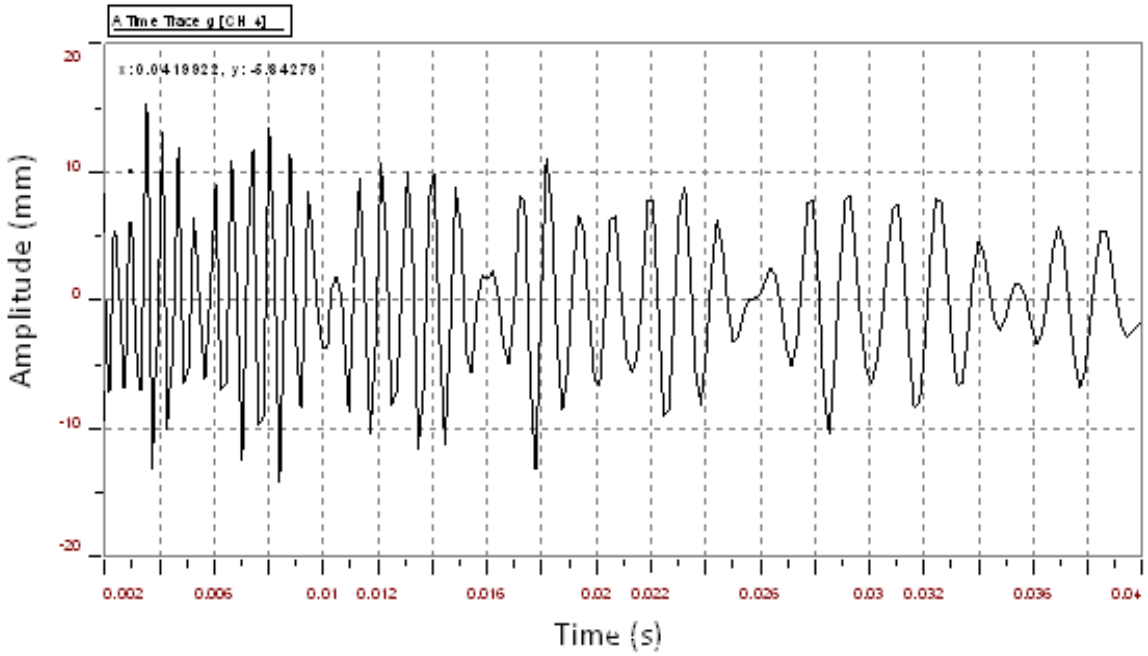

Figure 5.16 Free vibration for Aero-Z conductor at 20% UTS-30.02KN (graph 2)

Table 5.22 Using the least square method to calculate damping for 20% UTS-Aero-Z (first decay)

Integer j	Amplitude(mm) Y	LN(Y)	(j-1)	LN(Y)(j-1)	$(j-1)^2$
1	15.342	2.7306	0	0	0
2	13.823	2.6263	1	2.6263	1
3	12.202	2.5016	2	5.0033	4
4	7.732	2.0454	3	6.1361	9
Sum		9.9039	6	13.7657	14

The log-deg = -0.2180 and zeta = 0.0347

Table 5.23 Using the least square method to calculate damping for 20% UTS-Aero-Z(second decay)

Integer j	Amplitude(mm) Y	LN(Y)	(j-1)	LN(Y)(j-1)	$(j-1)^2$
1	14.018	2.6403	0	0	0
2	12.920	2.5588	1	2.5588	1
3	8.700	2.1633	2	4.3266	4
Sum		7.3624	3	6.8854	5

The log-deg = -0.2385 and zeta = 0.0379

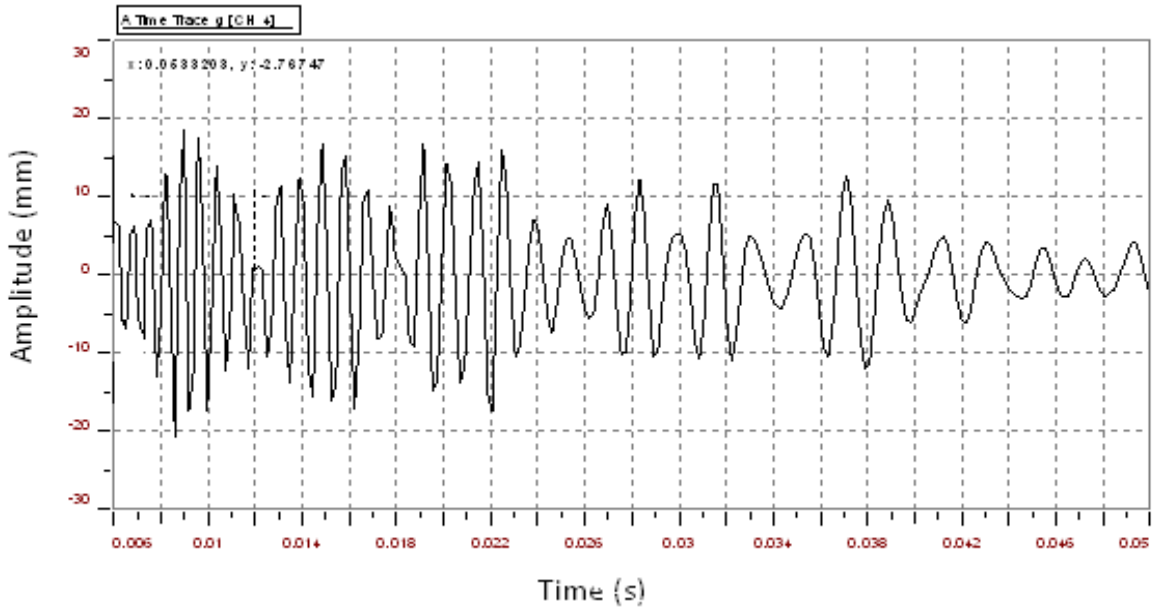

Fig 5.17 Free vibration for Aero-Z conductor at 25% UTS-37.53KN (graph 1)

Table 5.24 Using the least square method to calculate damping for 25% UTS-Aero-Z (first decay)

Integer j	Amplitude(mm) Y	LN(Y)	(j-1)	LN(Y)(j-1)	$(j-1)^2$
1	19.024	2.9457	0	0	0
2	18.423	2.9136	1	2.9136	1
3	14.224	2.6549	2	5.3099	4
4	10.832	2.3825	3	7.1475	9
Sum		10.8970	6	15.3710	14

The log-deg = -0.1948 and zeta = 0.0310

Table 5.25 Using the least square method to calculate damping for 25% UTS-Aero-Z (second decay)

Integer j	Amplitude(mm) Y	LN(Y)	(j-1)	LN(Y)(j-1)	$(j-1)^2$
1	16.724	2.8168	0	0	0
2	15.823	2.7615	1	2.7615	1
3	13.224	2.5820	2	5.1641	4
4	9.402	2.2409	3	6.7228	9
Sum		10.4013	6	14.6483	14

The log-deg = -0.1907 and zeta = 0.0303

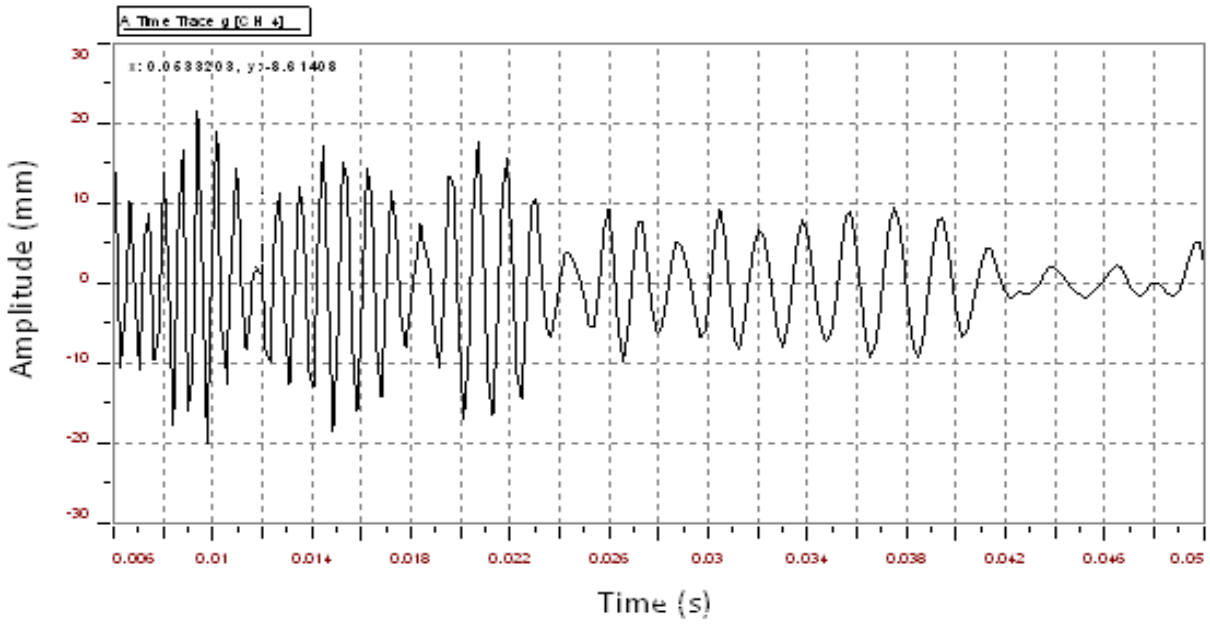

Fig 5.18 Free vibration for Aero-Z conductor at 25% UTS-37.53KN (graph 2)

Table 5.26 Using the least square method to calculate damping for 25% UTS-Aero-Z(first decay)

Integer j	Amplitude(mm) Y	LN(Y)	(j-1)	LN(Y)(j-1)	$(j-1)^2$
1	22.141	3.0974	0	0	0
2	19.232	2.9565	1	2.9565	1
3	15.120	2.7160	2	5.4320	4
Sum		8.7699	3	8.3885	5

The log-deg = -0.1906and zeta = 0.0303

Table 5.27 Using the least square method to calculate damping for 25% UTS-Aero-Z (second decay)

Integer j	Amplitude(mm) Y	LN(Y)	(j-1)	LN(Y)(j-1)	$(j-1)^2$
1	16.524	2.8048	0	0	0
2	14.823	2.6962	1	2.6962	1
3	13.924	2.6336	2	5.2672	4
4	11.732	2.4623	3	7.3870	9
5	7.072	1.9561	4	7.8246	16
Sum		12.55307	10	23.1749	30

The log-deg = -0.1903 and zeta = 0.0307

5.3.4 Experimental Results for Forced Vibration (Sweep test): Aero-Z Conductor

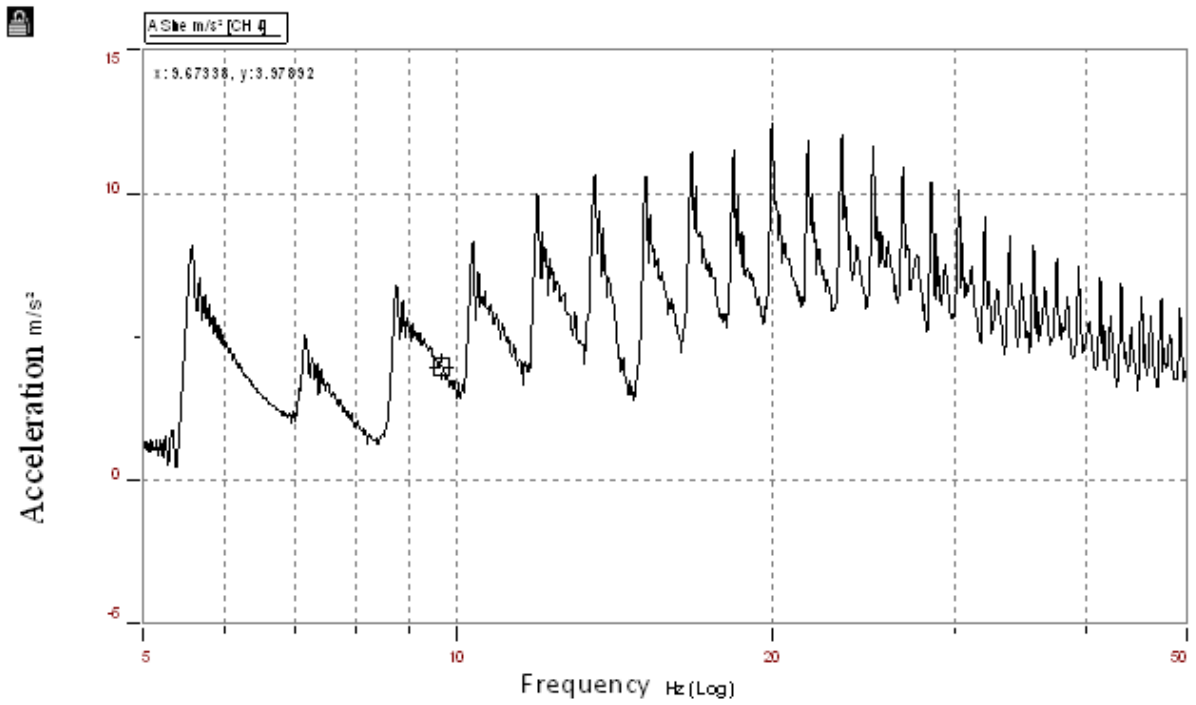

Fig 5.19 Forced vibration for Aero-Z conductor at 15% UTS-22.52KN

Table5.28 Showing Resonance frequencies and calculation for damping using bandwidth method For 15% UTS Aero-Z

Resonance Frequency R_f	Acceleration $a(m/s^2)$	$a/\sqrt{2}$	Half-Power F_1	Half-Power F_2	Half-Power F_2	quality factor Q	damping factor ζ
5.63	7.960	5.6286	5.48	5.95	0.47	11.9787	0.0417
7.23	4.960	3.5073	7.00	7.59	0.59	12.2542	0.0408
8.85	6.770	4.7872	8.65	9.53	0.88	10.0568	0.0497
10.26	8.050	5.6923	9.76	10.54	0.78	13.0256	0.0384
13.28	10.600	7.4954	12.83	13.76	0.93	14.2796	0.0350
14.63	10.810	7.6439	13.94	14.97	1.03	14.2039	0.0352
16.30	10.650	7.5308	15.95	16.82	0.87	18.7356	0.0267
17.39	12.330	8.7187	16.79	17.67	0.88	19.7614	0.0253
18.81	12.030	8.5066	18.19	19.03	0.84	22.1548	0.0226
20.04	12.820	9.0652	19.54	20.52	0.98	20.4490	0.0245

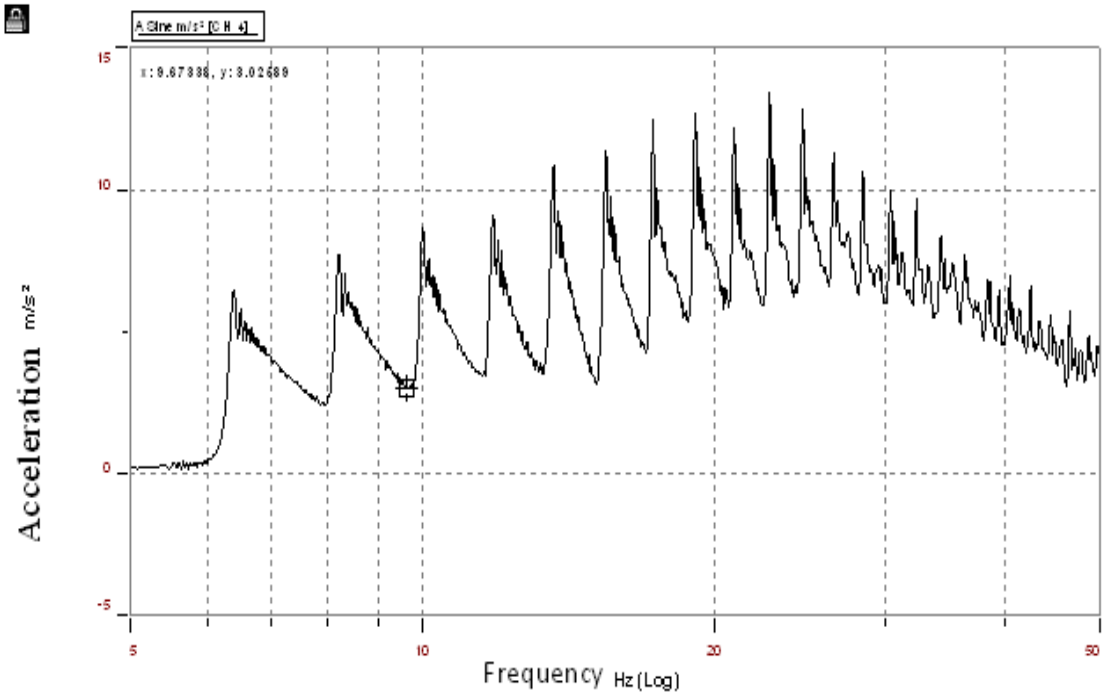

Fig 5.20 Forced vibration for Aero-Z conductor at 20%UTS-30.02KN

Table 5.29 Showing Resonance frequencies and calculation for damping using bandwidth method for 20% UTS Aero-Z

Resonance Frequency R_f	Acceleration $a(m/s^2)$	$a/\sqrt{2}$	Half-Power F_1	Half-Power F_2	Half-Power F_2	quality factor Q	damping factor ζ
6.46	6.760	4.7801	6.21	6.78	0.57	11.3333	0.0441
8.23	7.290	5.1549	8.04	8.67	0.63	13.0635	0.0383
10.09	8.070	5.7064	9.87	10.49	0.62	16.2742	0.0307
12.41	9.250	6.5408	11.63	12.39	0.76	15.8026	0.0316
14.83	12.060	8.5278	14.31	15.25	0.94	15.7766	0.0317
16.70	12.610	8.9167	16.21	17.22	1.01	16.5347	0.0302
18.11	13.150	9.2985	17.83	18.97	1.14	15.9737	0.0313
19.49	13.330	9.4258	18.93	20.36	1.43	13.7692	0.0363
21.43	12.930	9.1430	20.74	21.92	1.18	18.1610	0.0275
23.30	13.920	9.8430	22.69	24.06	1.37	17.0073	0.0294

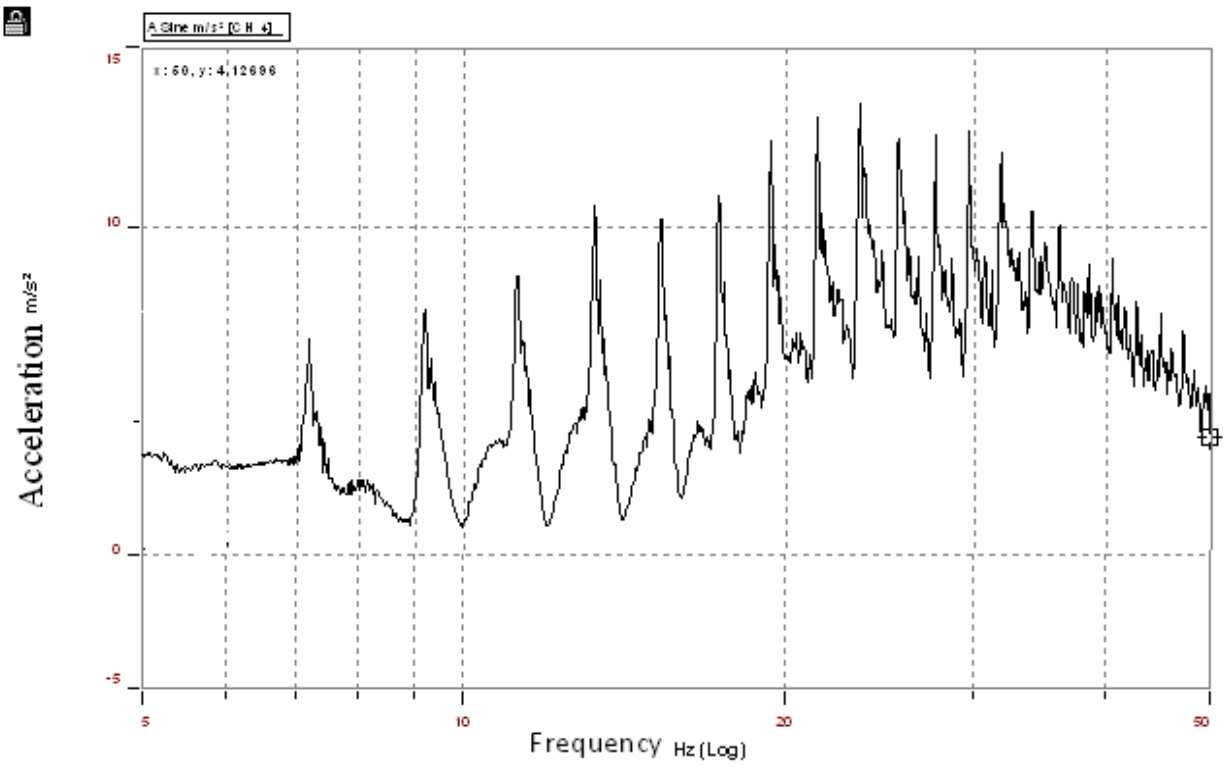

Fig 5.21 Forced vibration for Aero-Z conductor at 25%UTS-37.53KN

Table 5.30 Showing Resonance frequencies and calculation for damping using bandwidth method for 25% UTS Aero-Z

Resonance Frequency R_f	Acceleration $a(m/s^2)$	$a/\sqrt{2}$	Half-Power F_1	Half-Power F_2	Half-Power F_2	quality factor Q	damping factor ζ
7.21	6.960	4.9215	6.98	7.33	0.35	20.3714	0.0245
9.16	7.090	5.0134	8.96	9.41	0.45	20.3556	0.0246
12.57	8.570	6.0600	10.92	11.49	0.57	19.5965	0.0255
14.21	10.450	7.3893	12.99	13.67	0.68	19.4265	0.0257
16.24	10.060	7.1136	14.82	15.74	0.92	16.5652	0.0302
17.91	10.810	7.6439	16.82	17.83	1.01	17.1386	0.0292
19.82	13.050	9.2278	18.71	19.98	1.27	15.2126	0.0329
21.37	13.730	9.7087	20.66	22.02	1.36	15.7132	0.0318
23.43	14.030	9.9208	22.67	23.82	1.15	20.3739	0.0245
25.47	13.120	9.2773	24.96	26.32	1.36	18.7279	0.0267

5.4 Finite Element Analysis (FEA) Results

The finite element analysis modeling of transmission lines conductor simulation can be found in [27], in which the simulations of conductor vibrations were done using ABAQUS software. Similarly, in this study ABAQUS software was also used for the conductor vibration simulation but only for Aeolian vibration. Thus, finite element analysis for the mechanical oscillation for transmission line conductors was simulated using the code for beam properties. The values for physical properties of the test conductors used for the simulation are found in table-B-1 and table-B-2 in appendix B.

In simulating conductor vibration using ABAQUS, the eigenvalues were searched and computed in the frequency range for both conductors. For the Tern conductor, the first ten natural frequencies for the conductor between the frequency ranges of 6 to 50Hz were obtained and are recorded in table 5.33 in comparison to the values obtained for the analytical model at tensions 20%, 25%, and 30% of its UTS. Similar simulations were also done for the Aero-z conductor but for the frequency ranges of 5 to 50Hz at 15%, 20% and 25% of its UTS. The results also in comparison with the values obtained from the analytical model are recorded in table 5.34.

To compute the damping constants that were used for these simulations was by the derived equation (4.22) in relation to experimental values. Thus, using the experimental resonance frequencies values, the least squares method (pseudo-inverse routine) was used to compute the damping constants using Matlab. The values obtained were then used as proportional damping constants in ABAQUS to simulate the conductor vibration for damping.

The ABAQUS simulation results for the eigenvalues and the natural frequencies for both conductors are presented in appendix D.

Table 5.31. Showing comparison Natural frequencies values obtained from the analytical mode and FEA for Tern conductor

Mode	Natural Frequency (Hz) 20% UTS			Natural Frequency (Hz) 25% UTS			Natural Frequency (Hz) 30% UTS		
	Analytical Model	FEA	Exp. value	Analytical Model	FEA	Exp. value	Analytical Model	FEA	Exp. value
9	6.394	6.406	6.39	7.114	6.754	6.78	7.911	7.380	7.46
10	7.110	6.957	7.21	7.909	7.387	8.22	8.796	8.067	9.09
11	7.829	7.501	8.61	8.707	8.008	9.82	9.68	8.741	11.43
12	8.549	8.038	10.13	9.506	8.619	12.13	10.569	9.400	13.67
13	9.272	8.568	12.92	10.308	9.216	14.83	11.458	10.044	15.74
14	9.997	9.610	14.02	11.111	9.802	16.81	12.350	10.673	17.41
15	10.725	10.121	16.99	11.917	10.375	18.24	13.244	11.285	18.10
16	11.455	10.626	17.70	12.725	10.935	19.27	14.140	11.881	19.22
17	12.188	11.124	19.21	13.537	11.481	21.61	15.039	12.461	21.07
18	12.925	11.614	21.82	14.351	12.015	23.52	15.941	13.567	23.26

Table 5.32 Showing comparison Natural frequencies values obtained from analytical model and FEA for Aero-Z conductor

Mode	Natural Frequency (Hz) 15% UTS			Natural Frequency (Hz) 20% UTS			Natural Frequency (Hz) 25% UTS		
	Analytical Model	FEA	Exp. Value	Analytical Model	FEA	Exp. Value	Analytical Model	FEA	Exp. Value
8	6.385	5.646	5.63	7.372	6.515	6.46	8.243	7.281	7.21
9	6.922	6.311	7.23	7.985	7.280	8.23	8.923	8.969	9.16
10	7.698	6.961	8.85	8.878	8.028	10.09	9.920	9.781	12.57
11	8.475	7.595	10.26	9.773	8.757	12.41	10.918	10.571	14.21
12	9.255	8.211	13.28	10.669	9.465	14.83	11.918	11.335	16.24
13	10.037	8.810	14.63	11.569	10.515	16.70	12.920	12.071	17.91
14	10.822	9.387	16.30	12.470	10.813	18.11	13.923	12.778	19.82
15	11.610	9.943	17.39	13.373	11.449	19.49	14.929	13.455	21.37
16	12.401	10.477	18.81	14.280	12.058	21.43	15.938	14.099	23.43
17	13.195	10.988	20.04	15.188	12.640	23.30	16.949	14.709	25.47

5.5 Equivalent circuit results

To simulate the transfer function for the electrical equivalent circuit developed in chapter 4 for the vibrating conductor, the equivalent parameters for the electrical circuit in equivalence to its mechanical parameters have to be obtained. From [9] the value of the unit transverse stiffness of a pinned-pinned beam of modulus *E*, area moment of inertia *I* and unit length l, for a load applied at a point a, from its end is given as

$$K_i = \frac{3EIl}{a^2(l-a)^2} \qquad i = 1, 2, 3 \; and \; 4$$

With the unit length l= 21.25m and a =1.2m

The values of the mass per unit length of both conductors are given in table-B-1 in appendix B, using the dimensionless numbers as defined by the author [36] and simply using the assumed scale factor of one to obtain the corresponding electrical equivalent values. To determine the values for the resistance in equivalent damping was by iterative process. This process was used to obtain the values of resistance which in equivalence corresponds to the damping value for free vibration of 20% UTS of Tern. Using these electrical equivalent values obtained, the transfer function for the impulse response for the circuit was simulated using Matlab and the result is shown in figure 5.22 below.

To simulate the impulse response that corresponds to 25% and 30% UTS, a linear relationship was adopted in which the stiffness increases with increase in tension. Damping was evaluated by the assumption that change in resistance of the conductor is a function of temperature.

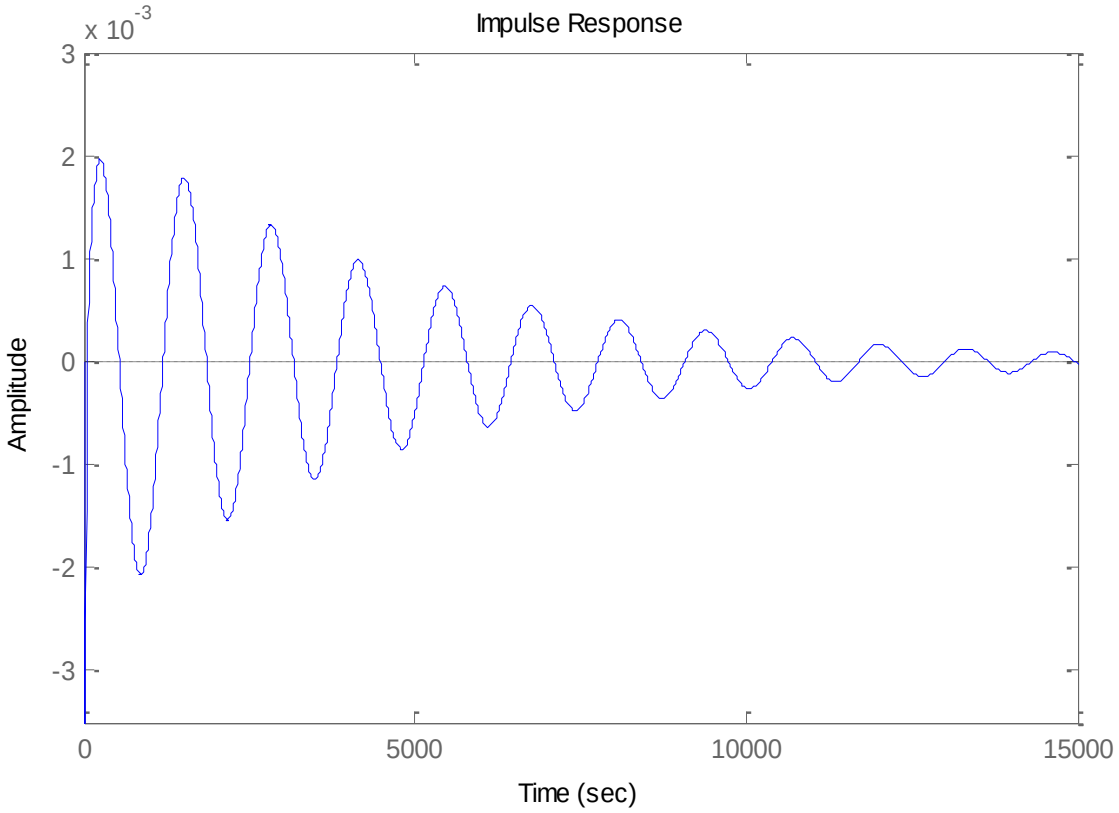

Figure 5.22 Impulse responses for the transfer function

The same concept was also used to simulate the impulse response for Aero-Z conductor but at 15%, 20% and 25% of its UTS

5.6 Analysis of Results

In studying the vibration of a body, the actual reproduction of the test is very difficult; however in any test conducted, the vibration test results are always specific for a particular excitation. This study conducted with regards to wind-induced vibration experienced by power line conductor is of threefold, done with respect to the two forms of vibration: free and forced.

The first is the analysis of the analytical model describing the transverse vibration of conductors. This involved analysing the developed analytical model of the transverse vibration of a conductor as a simply supported beam i.e. flexural rigidity of the conductor was not is ignored. Although, this model was used to predict the transverse vibration of the conductor, the fact was that a precise model was very difficult due to the non-linear response of the conductor. In some literature [17][18], the experiments conducted were done in wind tunnels in which the concept of

fluid-solid interaction was used to determine wind loading on the conductor which distributed along the conductor span length. This aspect was not covered in this study instead the loading was assumed to be a point loading and this input force was provided by a shaker. This model was used to obtain the conductor natural frequencies and its associated mode shapes. The values of the ten natural frequencies for the analytical model for both conductors at the three different tensions are presented in tables 5.31 and 5.32. Also obtained is conductor self-damping equation. This was achieved by incorporating two damping models into the equation of motion of the conductor.

The second was the development of finite element method (FEM) and the electrical equivalence using mechanical-electrical analogy, for the conductor and compared with data obtained from experimental results (natural frequencies). The FEM entailed the formulation of global equation for the conductor. The single span length conductor was developed and implemented on a computer program using ABAQUS software. The program was simulated using beam properties and the system damping was simulated by using proportional damping. The constant damping values were calculated using equation (4.22) and the values was used for the simulations. The computer program was used to simulate the response of the conductor and the mode of vibration was limited to the vertical plane. From the computer program simulations the values for the natural frequencies were obtained. Table 5.31 and table 5.32 showed the comparison between the natural frequencies obtained from the analytical model and that from the FEA. Comparing the results, there was a good agreement between the analytical and the FEM frequencies for the two conductors done at the three different tensions. Also both tables are also used to compare the values of the resonance frequencies obtained from resonance search test. In comparison the first few lower modes tend to be close to both the analytical and FEM values but as the mode number increase there were deviations and the deviations also increases as the mode increase.

Also obtained was the development of the electrical analogy for the power line conductor. Due to the fact that the model for the finite element method and electrical equivalence were dimensionally equal, similar results were obtained from both methods. The impulse response was obtained by the simulation using Matlab, and the calculation for damping was by using the ratios of decaying amplitudes. The results were in good agreement with the experimental results for free vibration.

The final aspect of this study was the experimental verification of the analytical model. The experimental data available for verification was for Aeolian vibration. The verification experiments were done on the 84.6m span conductor at three different tensions for the two conductors used for the experimental testing.

The laboratory results have shown that conductor vibration is characterised by a high mode density and a narrow bandwidth. For the free vibration test, a time history domain was used to

present the capture system's response due to the impact loading. This was then used to calculate the amount of damping from the system, while for the forced vibration test; a frequency history domain was used to determine the resonance frequencies for the system caused by excitation from the sinusoidal force. Based on these values, the amount of damping for each mode was calculated.

For the free vibration test, the average value for damping for Tern at 20% UTS, 25% UTS and 30% UTS were 0.0278, 0.0229 and 0.0137 respectively. Similarly, for Aero-Z conductor, the average value for damping at 15% UTS, 20% UTS and 25% UTS were 0.0422, 0.0360 and 0.0305 respectively.

In chapter one, besides this study seeking to gain more understanding into the mechanism of wind-induced vibration, the main goal was the determination of self-damping of the conductor and this prompted the research question. This intention has been achieved and a methodology established for the determination of conductor self-damping. In this vain, this process will help to determine at a particular stringing tension, the conductor self-damping capability and to ascertain whether the value for damping at that particular tension should be ignored or not. This will also helped in determining the type and number of vibration absorber that will be required to counter the effect of dynamic loading in order to keep the conductor safe. It has been highlighted through the literature reviewed in chapter two that some parameters were particularly important as related to the Scruton number, to the prediction of the response of a system to some form of excitation. Some of these parameters are mass density and damping. From all aspects of the study, for Tern conductor it was noticed that the conductor damping value decreases as the axial tension was increased. Due to this very low inherent damping at higher tension greater than the recommended UTS value, the conductor tends to be more prone to mechanical oscillation. For Aero-Z conductor, it was observed that at higher tensions greater than the recommended UTS tension value, the damping value was okay to the string line. But stringing of this conductor is done at lower tension based on the less capability of the conductor to withstand both the dynamic loading and the static tensile stress due to the absent of steel in the conductor.

Hence, from this analysis it was established that Aero-z conductor has a higher damping capacity compared to Tern and this was confirmed in all aspects of this study. Therefore, in this study the values of the conductor self-damping were determined using shorter span indoor conductor.

So far in this study, two methods of damping identification have been developed to enable in the estimation of dynamic action of Aeolian vibrations on overhead transmission lines. For the experimental studies, the free vibration present results for the damping values for the system at three different tensions while forced vibration present the damping values at the resonance frequencies also at the same three different tensions for free vibration. Both results show that the

damping decreases as the cable tension was being increased. In section 2.4.2, the various damping mechanisms in a vibrating conductor were explained. The explanation stated that damping can be caused by relative motion between conductor strands and also between the conductor accessories. Thus, this form of damping is caused by the frictional force that exist due motion relatively between each strand and also between members like the clamps, dampers, spacers, spacer-dampers, and suspension assemblies. As the axial tension was being increased the inter-strand motion was highly being restricted. This consequently led to the reduction in damping from this damping mechanism.

For the other means, this is material damping which has to do with the conductor property i.e. the conductor stiffness. As the tension was also increased, the conductor stiffness was also increased which invariably led to reduction in damping. Section 3.5 explains how these two mechanisms have been modeled in order to determine the conductor damping: viscous and material damping models respectively.

The experimental and finite element results have also shown the great influence of both cable tensioning and stiffness and it was noticed that damping tend to decrease as the axial tension was being increased in both cases. In the mathematical model in section 3.5, these mechanisms were model in relation to the damping parameters βI *and* C. These parameters tend to servers as the means to determine the contribution of both damping mechanism to the total damping at various tensions. Because, the foregoing analysis in this study lacks some important issues which can be addressed by conducting more investigations, on the bases of the findings with regards to further investigations, then these damping constants can then be used to ascertain the contributions of each damping mechanism to the total damping as the cable tension is being increased or varied.

Hence, further studies need be carried out and also some form of non-linear concepts introduced. The outcome can then be used in analysis of actual transmission lines to determine how best they agree. This will involve, using these generated responses for the analytical model for the system, finite element simulation and experiment data from the laboratory and compared with data from actual transmission lines. Based on the comparison between these responses and that on the real overhead power lines, conclusions can then be drawn on how self-damping occurred and how it can be incorporated into transmission lines design and construction.

CHAPTER 6

CONCLUSIONS AND RECOMMENDATIONS

6.1 Conclusions

From the research study, as well as the tests conducted and compiled in this report and also from the inferences drawn based on analysis done in the last chapter, the following were established from the theoretical (analytical) model, finite element method, and experimental study

- Natural Frequencies of the vibrating conductor increases with the increase in the axial tension of the conductor.
- Damping decreases with the increase in tension.

- In comparison there was close agreement of the values of the natural frequencies and damping obtained in theoretical, FEM and that from the laboratory experiments.
- The parameters obtained from the above, to some degree of accuracy can be used to predict the response of conductors to wind loading.

The main objective of this report was the evaluation of bare conductor self-damping. In this study, two methods were used to evaluate damping at different tensions: free and forced vibration. The experimental data showed that self-damping of Aero-Z conductor is higher than that of Tern conductor. However, because Tern has higher resistances to structural failure due to the presence of steel, stringing at higher tension is recommended.

6.2 Recommendations

From results compiled in this study it could be observed that in order to improve future research relating to this area of wind-induced vibration some modifications are needed. Some of them are as follows:

- In all aspects of this study ranging from analysis of the analytical model, finite element analysis, and electrical analogy, the linear concept was used. This concept is actually contrary to what happens to conductors when they are exposed to the dynamic forces of nature like wind. In the real world, conductor response is non-linear; therefore to improve on the conductor modeling some concept of non-linearity should be introduced.
- Also in modeling structural damping the viscous damping model was used in this study. The hysteresis or dry or coulomb model should be considered in order to improve on the accuracy of the value of this type of damping. This is because these forms of damping models can help represent in terms of non-linearity with regard to modeling damping.
- Boundary conditions in both analytical models and FEA and effect of end termination should also be examined to improve on the accuracy of results.

With respect to axial loading, at the lower tension the wind power input into the conductor does not exceed the power loss. As the tension is increased, the input power tends to exceed the power loss from the conductor. Therefore, based on the outcome of study, the ability to evaluate self-damping of bare conductors can determined. However, further study could be done to determine the critical point in which the conductor damping (power loss) balances the input power at a given tension. This process will help determine the types and amount of damper needed on the line in order to prevent damage that could be caused by the conductor oscillation.

Further study could also be done to ascertain and developed a method that can be used to obtain a value for bending stiffness which varies along the conductor length in the area of finite element analysis. This can then be used to formulate a computer program that can be used as a design parameter for designing transmission lines.

Finally, because of the experimental data available, verification of the analytical model was done for Aeolian vibration only. Similarly, these three concepts covered in this study should also be extended to the analysis of wake-induced vibration.

All the above areas for future study will form the basis of my PhD studies.

References

[1] E.S Duocy Etal, "Wind induced conductor motion" Transmission Line Reference Book, Electrical Power Research Institute 1979

[2] SABS 0280, "Code of practice for overhead power lines for conditions prevailing in South Africa", 1998.

[3] P. Du Plessis. "Mechanical oscillation on overhead transmission line", PhD in Mechanical Engineering, Rand Afrikaans University, June 1994

[4] EPRI "Transmission Line Reference Book: Wind-Induced Conductor Motion" Final Report, November, 2006

[5] R. Claren and G Diana, "Mathematical Analysis of Transmission Line Vibration" IEEE transactions on power apparatus and systems, vol. pas-88 No. 12, December, 1968

[6] Cigrè Study Committee 22-Working Group o1, "Report on Aeolian Vibration" Electra, no 124, pp-101, May 1989

[7] IEC 62219 Overhead Electrical Conductors - Formed Wire, Concentric Lay, Stranded Conductors, February 1, 2002

[8] K. Govender "Digital analysis of Vibration and Nonlinear Systems" Msc in Electrical Engineering thesis, University of Natal, 1992

[9] J. I. Daniel "Engineering Vibration" Prentice Hall, 1996.

[10] A.D. Nashif, D.I. Jones and J.P. Henderson "Vibration Damping" Wiley, Canada. 1985.

[11] C. Hardy,. "Analysis of Self-damping Characteristic of Stranded Cables in Transverse Vibrations" CSME Mechanical Engineering Forum. 1990

[12] J. Vecchiarelli, I.G. Currie and D.G. Havard, "Computational Analysis of Aeolian Conductor Vibration with a Stockbridge-type Damper" Journal of fluids and Structures 14, 489-509, 2000.

[13] V. Stronhal, "on Aeolian tones" Ann of Phys, Edition 5, pp, 216, 1878.

[14] S. Kumarasema, P.N. Jones, P. Irwin and P.Taylor " Wind-Induced Vibration of Stay Cables" publication no. FHWA-HRT-05-083. August, 2007.

[15] R E.D Bishop "Vibration" Cambridge University press, England, 1965

[16] R. D. Blevins, *Flow - Induced Vibration.* New York, Van Nostrand Reinhold, 1977

[17] F.B Faquharon and R.E McHugh, "Wind Tunnel Investigationof conductor Vibration of Rigid Model" IEEE, Transaction paper. Pp. 871-7, October 1956

[18] G. Diana and M. Falco, "On the Forces Transmitted to a Vibrating Cylinder b a Blowing Fliud" Meccanica, vol. 6 pp. 9-22, 1971

[19] F. Kiessling, P. Nefzger, J. F. Nolasco and U. Kaintzyk, "Overhead Power Lines: Planning, Design and Construction" Springer, 2003.

[20] C.F. Beards "Engineering Vibration Analysis with Application to Control Systems" Edwards Arnold, London, 1995.

[21] L. Meirovitch. "Principle and Techniques of Vibrations" Prentice Hall. 1997

[22] F.J. Shaker. "Effect of End Load on Mode Shape and Frequencies of Beams" Lewis research Centre Report NASA-TN_8109, 1975.

[23] H. T. Banks, D.J Inman, "On Damping Mechanisms in Beams" Transactons of the ASME pp. 716 Vol. 58, September, 1991

[24] K.O. Papailiou, "On the Bending Stiffness of Transmission Line Conductors" 6102 Malters, Switzerland, IEEE 1996

[25] Aberdare Power cables Division, Aberdare cables (Pty) Ltd South Africa, Catalogue of Conductors

[26] C. K Günther "The Finite Element Modelling of the Dynamic Behaviour of a Transmission Line Conductor" Msc in Electrical Engineering thesis, University of Cape Town, 1996

[27] Nexans Trade (Pty) Ltd

[28] M.N. Newmark, "A Method of Computation for Structural Dynamics" Journal of the Engineering Mechanics Division, Proceedings ASCE, vol. 85, N0.EM3, July 1959.

[29] E. L Wilson and R. W. Clough "Dynamic Response by Step-by-step Matrix Analysis" Proceedings, Symposium on the Use of Computers in Civil Engineering, Paper No.45, Lisbon, Portugal, October 1-5. 1962.

[30] H.M Hilber, Th.J.R Hughes and R.L Taylor, "Improved Numerical Dissipation for Time Integration algorithms in Structural Dynamics" Earthquake Engineering and Structural Dynamics, 5, p. 283-292, 1977.

[31] O. C. Zienkiewcz, “The Finite Element Method” McGraw-Hill Book Company, 3rd Edition, New York, 1979

[32] J.N. Reddy, “An Introduction to the Finite Element Method” McGraw-Hill International Edition, 1984.

[33] Y.W. Kwon and H. Bang, “Finite Element Method using Matlab” 2nd Edition CRC Press, 1997.

[34] H. H Cudney and D. J Inman “ Determining Damping Mechanisms in a composite beams by Experimetal Modal Analysis” State university of New York at Buffalo, Amberst, NY 14260, April 27, 1989.

[35] W. W. Seto “Mechanical Vibration” Schaums outline series, McGraw Hill, 1964.

[36]. Measurement Analysis Corporation, “Electrical Analogies and the Vibration of Linear Mechanical System” Los Angeles, California.

[37] The Institute of Electrical and Electronics Engineers “Guide for Laboratory Measurement of the Power Dissipation Characteristics of Aeolian Vibration” IEEE std 664-1993

[38] The Institute of Electrical and Electronics Engineers, “Guide on Conductor Self-damping Measurements” IEEE std 563-1978 (R2002)

[39] L. Meirovitch “Fundamentals of Vibrations” McGraw-Hill International Edition, 2001

[40] C. W. De silva, “Vibration Monitoring, Testing, and Instrumentation” The University of British Columbia, Vancouver, Canada, CRC press, 2007

[41] PUMA, “Vibration Control and Analysis Systems” 2003

Appendix A: Derivation of the Simple Beam Equation: Euler-Bernoulli Equation
(The Simple Beam Theory)

The beam is an example distribute-parameter system and such system has infinite number of natural frequencies. For this kind of system, when there is vibration, each of these infinite numbers of elements moves relative to each other in continuous manner. Vibration of a beam in the perpendicular direction to the length is often referred to transverse vibration or flexural vibration.

Deriving the flexural vibration of a uniform beam shown in figure 3.1 with cross-sectional area *A*, flexural rigidity *EI*, material density ρ, and length *L*.

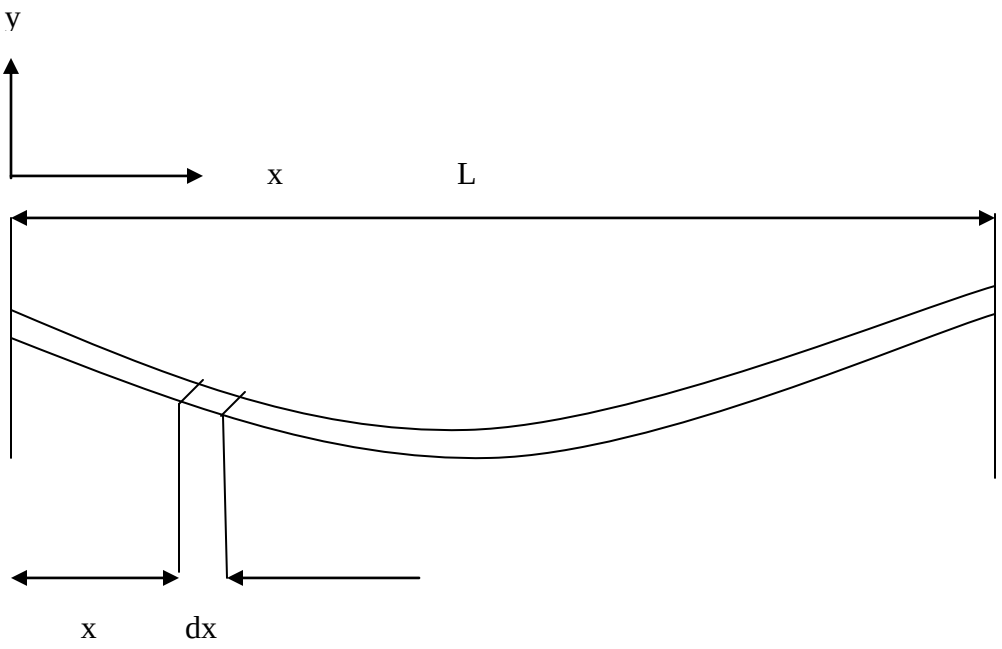

Fig A-1 A Uniform Beam.

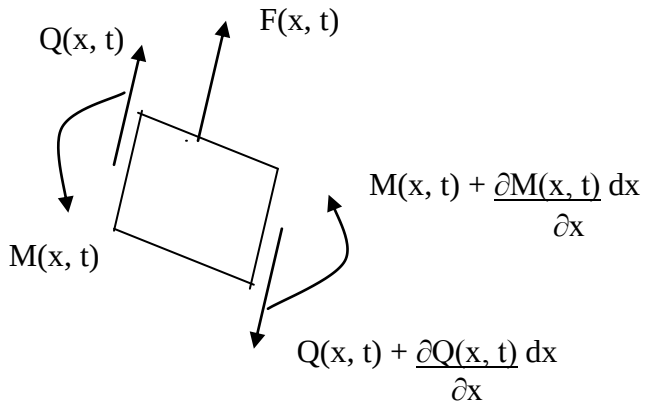

Figure A-2 Differential Element of the Beam

Considering small element with length dx as shown in figure 3.2 which is subject to an external force *f(x, t)*

Where M is the bending moment
Q is the shear force
F is the applied force
From mechanics of materials

$$M(x,t) = EI(x)\frac{\partial^2 y(x,t)}{\partial x^2} \quad \text{..... (A1)}$$

Summation of force in the y-direction

$$\left[Q(x,t) + \frac{\partial Q(x,t)dx}{\partial x}\right] - Q(x,t) + f(x,t) = \rho A(x)dx\frac{\partial^2 y(x,t)}{\partial x} \quad \text{……..…… (A2)}$$

Summation of moment about z-axis

$$\left[M(x,t) + \frac{\partial M(x,t)dx}{\partial x}\right] - M(x,t) + \left[Q(x,t) + \frac{\partial Q(x,t)dx}{\partial x}\right]dx + \left[f(x,t)\right]dx = 0$$

$$\left[\frac{\partial M(x,t)}{\partial x} + Q(x,t)\right]dx + \left[\frac{\partial Q(x,t)}{\partial x} + f(x,t)\right](dx)^2 = 0$$

Because dx is assumed to be small, then $(dx)^2$ is assumed to be almost zero

$$Q(x,t) = -\frac{\partial M(x,t)}{\partial x} \quad \text{… …… (A3)}$$

Substituting Eq (3.3) into Eq (3.2)

$$\left[\frac{-\partial M(x,t)}{\partial x} + \frac{\partial}{\partial x}\left(\frac{-\partial M(x,t)}{\partial x}\right)dx\right] - \left[\frac{-\partial M(x,t)}{\partial x}\right] + f(x,t) = \rho A(x)dx\frac{\partial^2 y(x,t)}{\partial t^2}$$

$$\frac{-\partial^2}{\partial x^2}\left[M(x,t)\right]dx + f(x,t) = \rho A(x)dx\frac{\partial^2 y(x,t)}{\partial t^2} \quad \text{.....…….. (A4)}$$

Dividing through by dx and substituting Equation (3.1) into Equation (3.4)

$$\rho A(x)\frac{\partial^2 y(x,t)}{\partial t^2} + \frac{\partial^2}{\partial x^2}\left[EI(x)\frac{\partial^2 y(x,t)}{\partial x^2}\right] = f(x,t) \quad \text{…….. (A5)}$$

If EI(x) and A(x) are assumed constant and no external force applied f(x, t) = 0 then Eq (A5) becomes

$$\frac{\partial^2 y(x,t)}{\partial t^2} = C^2 \frac{\partial^4 y(x,t)}{\partial x^4} \qquad \text{..... (A6)}$$

Where C is the wave speed for the beam and is given as

$$C = \sqrt{\frac{EI}{\rho A}}$$

Note: Equation (A6) is the free vibration for the beam, also known as Euler-Bernoulli equation.

The solutions to equation (A6) of a simple beam require four boundary conditions and two initial conditions to solve the free wave equation. Using separation-of-variable where the solution is assumed in the following form

$$Y(x,t) = X(x)T(t) \qquad \text{..... (A.7)}$$

Then Equation (3.6) becomes

$$C^2 \frac{X''''(x)}{X(x)} = -\frac{\ddot{T}(t)}{T(t)} = \omega^2 \qquad \text{..... (A.8)}$$

Where ω^2 is the separation constant
The right hand side of eq (3.8) becomes

$$\ddot{T}(t) + \omega^2 T(t) = 0 \qquad \text{..... (A.9)}$$

This is the temporal equation and because the beam perform a harmonic vibration with time, the solution of equation is

$$T(t) = A_1 \sin \omega t + B_1 \cos \omega t \qquad \text{..... (A.10)}$$

The constants A_1 and B_1 are determined from the initial conditions of the equation.
Also the left hand side of equation (3.8) becomes

$$X''''(x) + \frac{\omega^2}{C^2} X(x) = 0 \qquad \text{..... (A11)}$$

This is known as spatial equation

$$\text{If} \quad \Psi^4 = \frac{\omega^2}{C^2} = \frac{\rho A \omega^2}{EI} \qquad \text{.....(A.12)}$$

If $X(x) = Ae^{mx}$ therefore $X''''(x) = Am^4 e^{mx}$

$X''''(x) - \Psi^4 X(x) = 0\ \Omega^2$

$Zm^4e^{ma} - ,\Psi^4 Ze^{ma} = 0 \quad Am^4e^{mx} - \Psi^4 Ae^{mx} = 0$

$Ze^{ma}(m^4 - ,\Psi^4) = 0 \quad Ae^{mx}(m^4 - \Psi^4) = 0$

$Ae^{mx} \neq 0$, it implies that $(m^4 - \Psi^4) = 0$

$(m^4 - ,\Psi^4) = (m^2 + ,\Psi^2)(m^2 - ,\Psi^2) = 0$

If $(m^2 + ,\Psi^2) = 0$ then $m^2 = - ,\Psi^{2,}$ it then implies that $m^2 = \pm j,\Psi^2$

Therefore $X(x) = C_1 \sin x,\Psi + C_2 \cos,\Psi x$ ……. (A.13)

Also if $(m^2 - \Omega^2) = 0$, then $m^2 = \Omega^{2,}$ it implies that $m^2 = \pm \Omega^2$

Therefore $X(x) = C_3 \sinh \Omega x + C_4 \cosh \Omega x$

Hence, the general solution becomes

$X(x) = C_1 \sin \Omega x + C_2 \cos \Omega x + C_3 \sinh \Psi x + C_4 \cosh \Psi x$ …..... (A.14)

The constants C_1, C_2, C_3 and C_4 are determined from the boundary conditions.

To determine the natural frequencies and mode shapes for the transverse vibration of a simply supported or pinned at both end ends as shown below with the four boundary conditions

Substituting these boundary condition into equation (3.14)

At $x = 0$ and $X''(0) = 0$

$C_1 + C_3 = 0$

At $x = 0$ and $X''(0)$

$C_1 - C_3 = 0$

Therefore $C_1 = C_3 = 0$

Then eq (3.14) becomes

$X(x) = C_2 \cos \Omega x + C_4 \cosh \Psi x$ ..…… (A.15)

At $x = L$ and $X(L) = 0$

$X(L) = C_2 \cos \Omega L + C_4 \cosh \Omega L$

At $x = L$ and $X''(L) = 0$

$X(L) = C_2 \cos \Omega L - C_4 \cosh \Omega L$

Hence $X(x) = C_2 \sin \Psi L - C_4 \sinh \Psi L = 0$

Based on the fact that sinh Ψ L $\neq 0$ C_4 =0. Then equation (3.14) becomes

$$X(x) = C_2 \sin \Psi x \qquad \ldots\ldots\ldots\ldots\ldots\ldots \text{(A.16)}$$

But since $C_2 \sinh \lambda L = 0$ and $C_2 \neq 0$ and because X(x) will be zero for values of x then

$$Sin\Psi l = 0$$

$$\lambda l = 0, \pi, 2\pi, 3\pi, 4\pi, \ldots\ldots\ldots \text{ or } \lambda = 0, \frac{\pi}{l}, \frac{2\pi}{l}, \frac{3\pi}{l}, \frac{4\pi}{l}, \ldots\ldots\ldots$$

$$\Psi_n = \frac{nx}{l}$$

So that

$$\omega = 0, \quad \left(\frac{\pi}{l}\right)^2 \sqrt{\left(\frac{EI}{A\rho}\right)}, \quad \left(\frac{2\pi}{l}\right)^2 \sqrt{\left(\frac{EI}{A\rho}\right)}, \quad \left(\frac{3\pi}{l}\right)^2 \sqrt{\left(\frac{EI}{A\rho}\right)}, \quad \text{rad/s} \qquad \ldots\ldots\ldots\ldots\ldots \text{(A.17)}$$

Appendix B: Physical Properties of Test Conductors

Code name: Tern [25]
Conductor type – aluminum conductor steel reinforced (Stranded) (ACSR)
Conductor properties:
Diameters: O. Dia - 27 mm, Core dia– 6.75 mm
Stranding number & wire diameters:
Aluminium: 45, 3.37 mm
Steel: 7, 2.25 mm
Cross section:
Aluminium: 402.58 square millimeters
Steel: 27.83 square millimeters
Total: 430.32 square millimeters
Mass per unit length: 1.334 kg/m

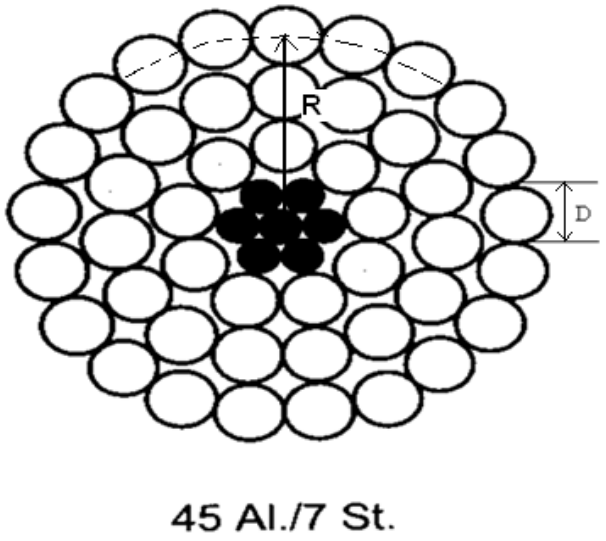

Fig B-1 Tern Conductor

Table –B-1Physical Properties for Tern Conductor

Quantity		Unit
Radius of conductor	0.014	m
Total cross-sectional area	431.60×10^{-6}	m^2
Conductor density	3090.82	kg/m^3
Conductor Span length	84.6	m
Conductor Chord Length	85.0	m
Conductor mass per length	1.334	Kg/m
Poisson's ratio	0.33	
Maximum bending stiffness	1350	Nm^2

To calculate for the maximum and minimum bending stiffness values for Tern.
Given:
$E_a = 6.895 \times 10^{10}$ Nm^2
$E_s = 20.68 \times 10^{10}$ Nm^2

Using equation 5.1 and values of young modulus for steel and aluminium given above, the minimum EI value is given as

$$EI_{min} = 7 \times 20.68 \times 10^{10} \times \frac{\pi(2.25\times10^{-3})^4}{64} + 45 \times 6.895 \times 10^{10} \times \frac{\pi(3.37\times10^{-3})^4}{64}$$

$EI_{min} = 21.47$Nm^2

The value for maximum bending stiffness for Tern is calculated using equation 5.4 and analysis is given in table 5.1

The table is used to calculate the EI_{max} for Tern conductor

	Steel		Aluminiun		
n	1	6	9	15	21
d	0.00225	0.00225	0.00338	0.00338	0.00338
R	0	0.00225	0.005065	0.008445	0.011825
E	2.07E+11	2.07E+11	6.90E+10	6.90E+10	6.90E+10
I	1.26E-12	6.79E-11	1.09365E-09	4.8961E-09	1.33102E-08
EI	2.60E-01	1.41E+01	7.54E+01	3.38E+02	9.18E+02

$EI_{max} = 1350$Nm^2

Code name: 445-A3F-26 [27]
Conductor type – Aero-Z
Conductor properties:
Diameters: O. Dia – 26.10 mm, Core dia– 14.5 mm
Stranding number & z-wires diameters:
Round aluminiun wires: 19, 2.9 mm
Z-shape aluminun wires 42, 2.9mm
Cross section:
Total aluminium: 461.73 square millimeters
Mass per unit length: 1.284 kg/m

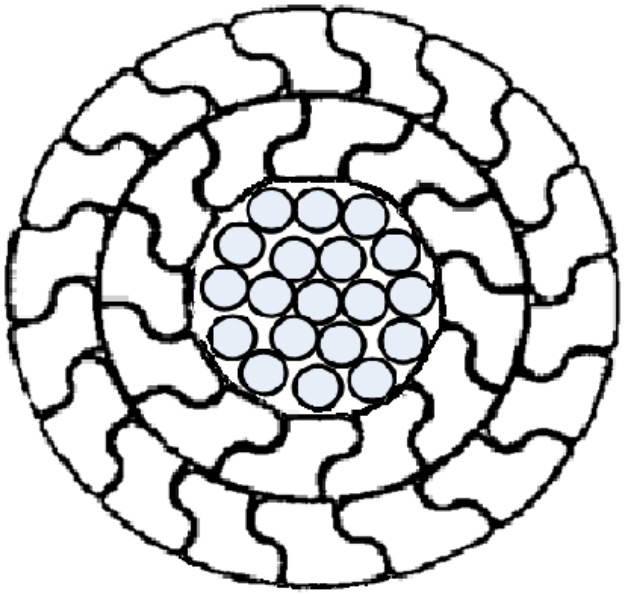

Fig B-2 Aero-Z Conductor

Table-B-2 Physical Properties for Aero-Z (445-A3F-261) Conductor

Quantity		Unit
Radius of conductor	0.01305	m
Young's Modulus	5.4×10^{10}	N/m^2
Total cross-sectional area	461.73×10^{-6}	m^2
Conductor density	2780.85	kg/m^3
Conductor Span length	84.6	m
Conductor Chord Length	85.0	m
Conductor mass per length	1.284	Kg/m
Poisson's ratio	0.35	
Bending stiffness	1198.8	Nm^2

To calculate the bending stiffness for the Aero-Z conductor using equation (3.25) from chapter 3 given below

$EI = EI_x + EI_{zs} = E(I_x + I_{zs})$

Where $I_x = \frac{n\pi d^2}{8}\left(\frac{d^2}{8} + R^2\right)$

$$I_{zs} = \frac{\pi(d_o^4 - d_i^4)}{64}$$

The table below is used to for I_x

n	1	6	12
d	2.90E-03	2.90E-03	2.90E-03
R	0	2.90E-03	5.80E-03
I	3.47231E-12	1.88E-10	1.38E-09

$I_x = 1.57 \times 10^{-9}\ \text{Nm}^2$

Calculating for $I_{zs} = \frac{3.142[(266.1\times10^{-3})^4 - (14.5\times10^{-3})^4]}{64} = 2.0612 \times 10^{-8}\ \text{m}^4$

Give $E = 5.4 \times 10^{10} N/m^2$

Therefore

$EI = 5.4 \times 10^{10}(1.57 \times 10^{-9} + 2.0612 \times 10^{-8})$

$EI = 1198.8\text{Nm}^2$

Appendix C: DAMPING MEASUREMENT

Measurement of Damping: Free Vibration [39]

To measure the damping of a system experiencing free vibration, with decaying amplitude at the completion of one cycle of vibration as shown in the diagram below.

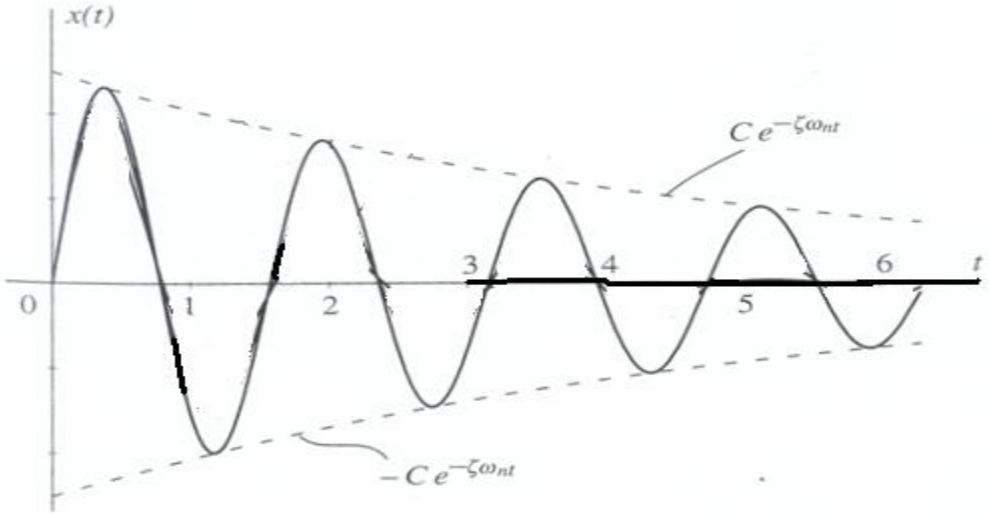

Considering t_1 and t_2 to be the times corresponding to the first and second peak, denoted the peak displacement x_1 and x_2 respectively, and the ratio

$$\frac{x_1}{x_2} = \frac{x(t_1)}{x(t_2)} = \frac{Ce^{-\varsigma\omega_n t_1}\cos(\omega_d t_1 - \phi)}{Ce^{-\varsigma\omega_n t_2}\cos(\omega_d t_2 - \phi)} = \frac{Ce^{-\varsigma\omega_n t_2}\cos(\omega_d t_1 - \phi)}{Ce^{-\varsigma\omega_n t}\cos(\omega_d t_2 - \phi)} \quad \text{.....C1}$$

From the plot above of the response x (t) as a function of time, $Ce^{-\varsigma\omega_n t}$ represents the exponentially decay function and cos $(\omega_d t - \phi)$

$$\frac{x_1}{x_2} = \frac{e^{-\varsigma\omega_n t_1}\cos(\omega_d t_1 - \phi)}{e^{-\varsigma\omega_n (t+T)}\cos[\omega_d (t_1+T) - \phi]} = \frac{e^{\varsigma\omega_n T}\cos(\omega_d t_1 - \phi)}{\cos(\omega_d t_1 - \phi + 2\pi)} \quad \text{.....C2}$$

$$\frac{x_1}{x_2} = e^{\varsigma\omega_n T} = e^{2\pi\varsigma\omega_n/\omega_d} = e^{2\pi\varsigma/\sqrt{1-\varsigma^2}} \quad \text{.....C3}$$

In view of the exponential form of the right side of the equation (C3), then taking the natural logarithm on both sides, it becomes

$$\delta = In\frac{x_1}{x_2} = \frac{2\pi\varsigma}{\sqrt{1-\varsigma^2}} \quad \text{.....C4}$$

Where δ is known as the logarithmic decrement, solving for the damping factor

$$\varsigma = \frac{\delta}{\sqrt{(2)^2 + \delta^2}} \qquad \text{……C5}$$

The damping factor, such that $\varsigma << 1$ equation (C5) yields directly

$$\varsigma \cong \frac{\delta}{2\pi} \qquad \text{… ……..C6}$$

The damping factor ς can be determine more accurately be developing the least square method from the log decrement techniques. To develop this technique is by measuring the values the displacements of the decaying amplitudes at two different times separated by a given number of periods. Letting x_1 and x_{j+1} be the peak displacements corresponding to the times t_1 and t_{j+1}, where j is an integer. Taking the ratio of any two consecutive peak displacement, not only for x_1/x_2, we conclude that

$$\frac{x_1}{x_{j+1}} = \frac{x_1 x_2}{x_2 x_3} \dots \frac{x_j}{x_{j+1}} = \left(e^{2\pi\varsigma/\sqrt{1-\varsigma^2}} \right)^j = e^{j2\pi\varsigma/\sqrt{1-\varsigma^2}} \qquad \text{.. ……C7}$$

$$\varsigma = \frac{\delta}{\sqrt{(2)^2 + \delta^2}} = \frac{1}{j} In \frac{x_1}{x_{j+1}}$$

$$Inx_j = Inx_1 - \delta(j-1), \quad j = 1, 2, \dots, l \qquad \text{…… C8}$$

On semilog paper, a plot Inx_j versus j of equation base on equation C8 has a straight line with the slope $-\delta$

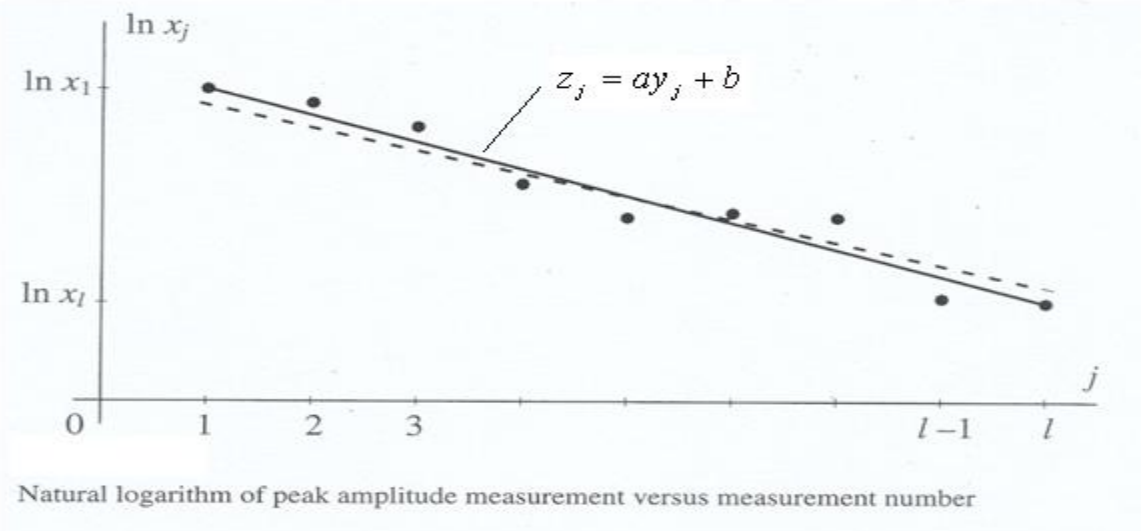

Natural logarithm of peak amplitude measurement versus measurement number

To determine the damping factor for the measurement of peak amplitudes of $x_1\, x_2 \dots x_n$ of a vibrating lightly damped system

From the above diagram, the equation of the straight line is expressed as

$$z_j = ay_j + b \qquad \text{.....C9}$$

Where z_j corresponds to Inx_j, a to $-\delta$ and b to Inx_1
The sum of the squares of the difference as the error is given as

$$\in = \sum_{j=1}^{n}\left(Inx_j - z_j\right)^2 = \sum_{j=1}^{n}\left(Inx_j - ay_j + b\right)^2 \qquad \text{.....C10}$$

To minimize the error, we write

$$\frac{\partial \in}{\partial a} = 2\sum_{j=1}^{n}\left(Inx_j - ay_j + b\right)\left(-y_j\right) = 0 \qquad \text{.....C11a}$$

$$\frac{\partial \in}{\partial b} = 2\sum_{j=1}^{n}\left(Inx_j - ay_j + b\right)(-1) = 0 \qquad \text{.....C11b}$$

Equations (C11) represent two algebraic equations in the unknown a and b, which can be written in the more explicit form

$$\left(\sum_{j=1}^{n} y_j^2\right)a + \left(\sum_{j=1}^{n} y_j\right)b = \sum_{j=1}^{n}\left(Inx_j\right)y_j \qquad \text{.....C12}$$

$$\left(\sum_{j=1}^{n} y_j\right)a + nb = \sum_{j=1}^{n} Inx_j \qquad \text{.....C13}$$

Solving for a and b simultaneously from equations C12 and C13 from the above equations, where a corresponds to $-\delta$ and b to Inx_1. Hence, the damping constant can then be obtained using equation (C5)

Measurement of Damping: Forced Vibration [40]

The bandwidth method of damping measurements based on frequency-response. Consider the frequency-response function magnitude given in the diagram below of an oscillatory system with some form of damping. The peak magnitude (amplification factor, Q) is given by equation for low damping.

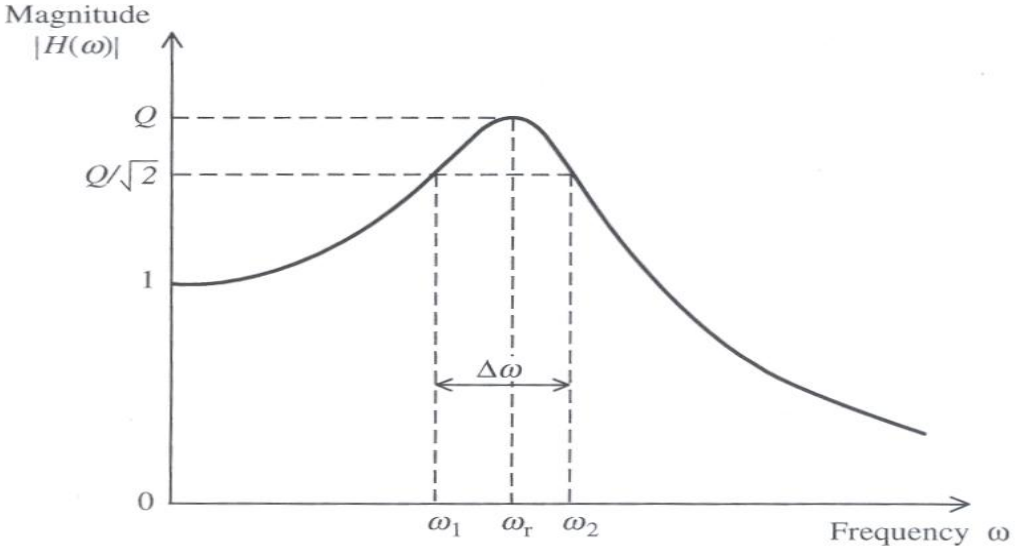

Bandwidth method of damping measurement in a single-DoF system.

$$|H(\omega)| = \frac{\omega_n^2}{\left[\left(\omega_n^2 - \omega^2\right)^2 + 4\varsigma^2\omega_n^2\omega^2\right]^{1/2}} \qquad \text{..……..C14}$$

$$Q = \frac{1}{2\varsigma} \qquad \text{…….C15}$$

For $\Delta\omega = \omega_1 - \omega_2$ is obtained below using equation C14. By definition ω_1 and ω_2 are the roots of the equation

$$\frac{\omega_n^2}{\left[\left(\omega_n^2 - \omega^2\right)^2 + 4\varsigma^2\omega_n^2\omega^2\right]^{1/2}} = \frac{1}{\sqrt{2\times 2\varsigma}} \qquad \text{……..... C16}$$

for ω. Equation C16 can be expressed in the form

$$\omega^4 - 2(1-2\varsigma^2)\omega_n^2\omega^2 + (1-8\varsigma^2)\omega_n^4 = 0 \qquad \text{……..... C17}$$

This is a quadratic equation inω_2, having roots ω_1^2 and ω_2^2 which satisfy

$$(\omega^2 - \omega_1^2)(\omega^2 - \omega_2^2) = \omega^4 - (\omega_1^2 + \omega_2^2)\omega^2 + \omega_1^2\omega_2^2$$

Consequently,

$$\omega_1^2 + \omega_2^2 = 2(1-2\varsigma^2)\omega_n^2$$

and
$\omega_1^2\omega_2^2 = (1-8\varsigma^2)\omega_n^4$

It follows that

$(\omega_2-\omega_2)^2 = \omega_1^2 + \omega_2^2 - 2\omega_1\omega_2 = 2(1-2\varsigma^2)\omega_n^2 - \sqrt{1-8\varsigma^2\omega_n^2}$ ……..... C18

For small ς (in comparison to 1), we have

$\sqrt{1-8\varsigma^2\omega_n^2} \cong 1-4\varsigma^2$

Hence,
$(\omega_2-\omega_2)^2 = 4\varsigma^2\,\omega_n^2$

or, for low damping

$\Delta\omega = 2\varsigma\omega_n$ ……..... C19

From equation C19 it follows that the damping ratio can be estimated from the bandwidth using the relation

$\varsigma = \frac{1}{2}\frac{\Delta\omega}{\omega_n}$ ……..... C20

For a body with multiple degree of free freedom with widely spaced resonance, for such body with *i*th mode, the damping ratio is given by

$\varsigma_i = \frac{1}{2}\frac{\Delta\omega_i}{\omega_i}$ ..……..... C21

Appendix D: ABAQUS results for the simulation for both Tern and Aero-Z conductors0

Tern_condcutor@20%UTS
1

Abaqus 6.9-2 Date 15-Aug-2010 Time 17:36:41
For use at University of KwaZulu-Natal under license from Dassault Systemes or its subsidiary.

Analysis of Tern conductor at 20% of its UTS STEP 3 INCREMENT 1
To determine the natural frquencies of the conductor TIME COMPLETED IN THIS STEP 0.00

S T E P 3 C A L C U L A T I O N O F E I G E N V A L U E S

F O R N A T U R A L F R E Q U E N C I E S

To determine the natural frquencies of the conductor

THE LANCZOS EIGENSOLVER IS USED FOR THIS ANALYSIS
Abaqus WILL COMPUTE UNCOUPLED
STRUCTURAL AND ACOUSTIC MODES
ALL EIGENVALUES IN THE SPECIFIED RANGE WILL BE EXTRACTED
HIGHEST FREQUENCY OF INTEREST 50.000
LOWEST FREQUENCY OF INTEREST 6.0000
MAXIMUM NUMBER OF STEPS WITHIN RUN 35
BLOCK SIZE FOR LANCZOS PROCEDURE 7
THE EIGENVECTORS ARE SCALED SO THAT
THE LARGEST DISPLACEMENT ENTRY IN EACH VECTOR IS UNITY
INITIAL STRESS AND DISPLACEMENT EFFECTS ARE INCLUDED IN THE STIFFNESS MATRIX

THIS IS A LINEAR PERTURBATION STEP.
ALL LOADS ARE DEFINED AS CHANGE IN LOAD TO THE REFERENCE STATE

LARGE DISPLACEMENT THEORY WILL BE USED

M E M O R Y E S T I M A T E

PROCESS	FLOATING PT OPERATIONS PER ITERATION	MINIMUM MEMORY REQUIRED (MBYTES)	MEMORY TO MINIMIZE I/O (MBYTES)
1	5.14E+004	20	28

E I G E N V A L U E O U T P U T

MODE NO	EIGENVALUE	FREQUENCY (RAD/TIME)	FREQUENCY (CYCLES/TIME)	GENERALIZED MASS
9	1547.0	39.331	6.406	79.811
10	1728.6	41.576	6.957	79.382
11	1899.9	43.587	7.501	79.344
12	2056.6	45.350	8.038	78.987
13	2194.6	46.847	8.568	80.765
14	2309.3	48.055	9.610	78.826
15	2396.1	48.950	10.121	78.597
16	2450.2	49.499	10.626	78.758
17	4558.1	67.514	11.124	79.634
18	5788.2	76.080	11.616	80.969

1

Abaqus 6.9-2 Date 15-Aug-2010 Time 17:23:51

For use at University of KwaZulu-Natal under license from Dassault Systemes or its subsidiary.

Analysis of Tern conductor at 25% UTS STEP 3 INCREMENT 1

To determine the first 10 natural frequencies TIME COMPLETED IN THIS STEP 0.00

S T E P 3 C A L C U L A T I O N O F E I G E N V A L U E S F O R N A T U R A L F R E Q U E N C I E S

To determine the first 10 natural frequencies

THE LANCZOS EIGENSOLVER IS USED FOR THIS ANALYSIS
Abaqus WILL COMPUTE UNCOUPLED
STRUCTURAL AND ACOUSTIC MODES
ALL EIGENVALUES IN THE SPECIFIED RANGE WILL BE EXTRACTED
HIGHEST FREQUENCY OF INTEREST 50.000
LOWEST FREQUENCY OF INTEREST 6.0000
MAXIMUM NUMBER OF STEPS WITHIN RUN 35
BLOCK SIZE FOR LANCZOS PROCEDURE 7
THE EIGENVECTORS ARE SCALED SO THAT
THE LARGEST DISPLACEMENT ENTRY IN EACH VECTOR IS UNITY
INITIAL STRESS AND DISPLACEMENT EFFECTS ARE INCLUDED IN THE STIFFNESS MATRIX

THIS IS A LINEAR PERTURBATION STEP.
ALL LOADS ARE DEFINED AS CHANGE IN LOAD TO THE REFERENCE STATE

LARGE DISPLACEMENT THEORY WILL BE USED

M E M O R Y E S T I M A T E

PROCESS	FLOATING PT OPERATIONS PER ITERATION	MINIMUM MEMORY REQUIRED (MBYTES)	MEMORY TO MINIMIZE I/O (MBYTES)
1	5.14E+004	20	28

E I G E N V A L U E O U T P U T

MODE NO	EIGENVALUE	FREQUENCY (RAD/TIME)	FREQUENCY (CYCLES/TIME)	GENERALIZED MASS
9	1689.0	41.097	6.754	80.829
10	1921.0	43.830	7.387	79.790
11	1921.1	43.830	8.008	79.756
12	2145.0	46.314	8.619	79.397
13	2145.0	46.314	9.216	79.390
14	2355.6	48.534	9.802	79.339
15	2355.6	48.534	10.375	79.325
16	2547.5	50.473	10.935	78.933
17	2547.5	50.473	11.481	78.872
18	2715.7	52.112	12.015	80.665

Tern-conductor-30%

Abaqus 6.9-2 Date 09-Jun-2010 Time 10:49:43
For TIME COMPLETED IN THIS STEP 0.00

Abaqus 6.9-2 Date 09-Jun-2010 Time 10:49:49
For use at University of KwaZulu-Natal under license from Dassault Systemes or its subsidiary.
Analysis of Tern conductor at 30%UTS STEP 3 INCREMENT 1
To determine the natural frrequencies of the conductor TIME COMPLETED IN THIS STEP 0.00

S T E P 3 C A L C U L A T I O N O F E I G E N V A L U E S

F O R N A T U R A L F R E Q U E N C I E S

To determine the natural frrequencies of the conductor

THE LANCZOS EIGENSOLVER IS USED FOR THIS ANALYSIS
Abaqus WILL COMPUTE UNCOUPLED
STRUCTURAL AND ACOUSTIC MODES
ALL EIGENVALUES IN THE SPECIFIED RANGE WILL BE EXTRACTED
HIGHEST FREQUENCY OF INTEREST 50.000
LOWEST FREQUENCY OF INTEREST 6.0000
MAXIMUM NUMBER OF STEPS WITHIN RUN 35
BLOCK SIZE FOR LANCZOS PROCEDURE 7
THE EIGENVECTORS ARE SCALED SO THAT
THE LARGEST DISPLACEMENT ENTRY IN EACH VECTOR IS UNITY
INITIAL STRESS AND DISPLACEMENT EFFECTS ARE INCLUDED IN THE STIFFNESS MATRIX

THIS IS A LINEAR PERTURBATION STEP.
ALL LOADS ARE DEFINED AS CHANGE IN LOAD TO THE REFERENCE STATE

LARGE DISPLACEMENT THEORY WILL BE USED

M E M O R Y E S T I M A T E

PROCESS	FLOATING PT OPERATIONS PER ITERATION	MINIMUM MEMORY REQUIRED (MBYTES)	MEMORY TO MINIMIZE I/O (MBYTES)
1	8.06E+004	20	29

E I G E N V A L U E O U T P U T

MODE NO	EIGENVALUE	FREQUENCY (RAD/TIME)	FREQUENCY (CYCLES/TIME)	GENERALIZED MASS
9	2150.3	46.371	7.3802	76.627
10	2569.4	50.689	8.0674	74.910
11	3016.3	54.921	8.7410	74.640
12	3488.5	59.063	9.4002	77.801
13	3982.9	63.110	10.044	75.403
14	4497.0	67.060	10.673	74.338
15	5027.9	70.908	11.285	74.234
16	5573.1	74.653	11.881	74.199
17	6129.8	78.293	12.461	74.154
18	7266.4	85.243	13.567	74.834

Aero-Z-conductor-15%UTS

Abaqus 6.9-2 Date 09-Jun-2010 Time 12:34:52
For use at University of KwaZulu-Natal under license from Dassault Systemes or its subsidiary.

Analysis of Aero-Z conductor at 15%UTS STEP 3 INCREMENT 1
To determine the natural frequencies of the conductor TIME COMPLETED IN THIS STEP 0.00

STEP 3 CALCULATION OF EIGENVALUES FOR NATURAL FREQUENCIES

To determine the natural frequencies of the conductor

THE LANCZOS EIGENSOLVER IS USED FOR THIS ANALYSIS
Abaqus WILL COMPUTE UNCOUPLED
STRUCTURAL AND ACOUSTIC MODES
ALL EIGENVALUES IN THE SPECIFIED RANGE WILL BE EXTRACTED
HIGHEST FREQUENCY OF INTEREST 50.000
LOWEST FREQUENCY OF INTEREST 5.000
MAXIMUM NUMBER OF STEPS WITHIN RUN 35
BLOCK SIZE FOR LANCZOS PROCEDURE 7
THE EIGENVECTORS ARE SCALED SO THAT THE LARGEST DISPLACEMENT ENTRY IN EACH VECTOR IS UNITY
INITIAL STRESS AND DISPLACEMENT EFFECTS ARE INCLUDED IN THE STIFFNESS MATRIX

THIS IS A LINEAR PERTURBATION STEP.
ALL LOADS ARE DEFINED AS CHANGE IN LOAD TO THE REFERENCE STATE

LARGE DISPLACEMENT THEORY WILL BE USED

MEMORY ESTIMATE

PROCESS	FLOATING PT OPERATIONS PER ITERATION	MINIMUM MEMORY REQUIRED (MBYTES)	MEMORY TO MINIMIZE I/O (MBYTES)
1	8.06E+004	20	29

EIGENVALUE OUTPUT

MODE NO	EIGENVALUE	FREQUENCY (RAD/TIME)	FREQUENCY (CYCLES/TIME)	GENERALIZED MASS
8	1258.9	35.480	5.6469	63.343
9	1572.5	39.654	6.3112	63.005
10	1912.9	43.737	6.9609	64.265
11	2277.1	47.719	7.5948	62.975
12	2661.8	51.592	8.2112	62.747
13	3063.4	55.348	8.8089	65.448
14	3478.4	58.978	9.3866	63.364
15	3903.1	62.475	9.9432	62.477
16	4333.8	65.831	10.477	62.380
17	4766.7	69.041	10.988	62.326

Abaqus 6.9-2 Date 09-Jun-2010 Time 16:13:30
For use at University of KwaZulu-Natal under license from Dassault Systemes or its subsidiary.

Analysis of Areo-Z conductor at 20% of its UTS STEP 3
INCREMENT 1
To determine the natural frequencies of the conductor TIME COMPLETED IN THIS STEP 0.00

STEP 3 CALCULATION OF EIGENVALUES FOR NATURAL FREQUENCIES

To determine the natural frequencies of the conductor

THE LANCZOS EIGENSOLVER IS USED FOR THIS ANALYSIS
Abaqus WILL COMPUTE UNCOUPLED
STRUCTURAL AND ACOUSTIC MODES
ALL EIGENVALUES IN THE SPECIFIED RANGE WILL BE EXTRACTED
HIGHEST FREQUENCY OF INTEREST 50.000
LOWEST FREQUENCY OF INTEREST 5.000
MAXIMUM NUMBER OF STEPS WITHIN RUN 35
BLOCK SIZE FOR LANCZOS PROCEDURE 7
THE EIGENVECTORS ARE SCALED SO THAT
THE LARGEST DISPLACEMENT ENTRY IN EACH VECTOR IS UNITY
INITIAL STRESS AND DISPLACEMENT EFFECTS ARE INCLUDED IN THE STIFFNESS MATRIX

THIS IS A LINEAR PERTURBATION STEP.
ALL LOADS ARE DEFINED AS CHANGE IN LOAD TO THE REFERENCE STATE

LARGE DISPLACEMENT THEORY WILL BE USED

MEMORY ESTIMATE

PROCESS	FLOATING PT OPERATIONS PER ITERATION	MINIMUM MEMORY REQUIRED (MBYTES)	MEMORY TO MINIMIZE I/O (MBYTES)
1	8.06E+004	20	29

EIGENVALUE OUTPUT

MODE NO	EIGENVALUE	FREQUENCY (RAD/TIME)	FREQUENCY (CYCLES/TIME)	GENERALIZED MASS
8	1675.8	40.937	6.5153	63.349
9	2092.5	45.744	7.2804	63.014
10	2544.5	50.443	8.0282	64.217
11	3027.5	55.023	8.7571	62.973
12	3536.9	59.471	9.4652	62.759
13	4067.9	63.780	10.151	65.457
14	4615.6	67.938	10.813	63.342
15	5174.9	71.937	11.449	62.489
16	5740.4	75.766	12.058	62.417
17	6307.4	79.419	12.640	62.329

Abaqus 6.9-2 Date 09-Jun-2010 Time 16:49:26
For use at University of KwaZulu-Natal under license from Dassault Systemes or its subsidiary.

STEP 3
INCREMENT 1
To determine the natural frequencies of the conductor TIME COMPLETED IN THIS STEP 0.00

S T E P 3 C A L C U L A T I O N O F E I G E N V A L U E S

F O R N A T U R A L F R E Q U E N C I E S

To determine the natural frequencies of the conductor

THE LANCZOS EIGENSOLVER IS USED FOR THIS ANALYSIS
Abaqus WILL COMPUTE UNCOUPLED
STRUCTURAL AND ACOUSTIC MODES
ALL EIGENVALUES IN THE SPECIFIED RANGE WILL BE EXTRACTED
HIGHEST FREQUENCY OF INTEREST 50.000
LOWEST FREQUENCY OF INTEREST 5.000
MAXIMUM NUMBER OF STEPS WITHIN RUN 35
BLOCK SIZE FOR LANCZOS PROCEDURE 7
THE EIGENVECTORS ARE SCALED SO THAT
THE LARGEST DISPLACEMENT ENTRY IN EACH VECTOR IS UNITY
INITIAL STRESS AND DISPLACEMENT EFFECTS ARE INCLUDED IN THE STIFFNESS MATRIX

THIS IS A LINEAR PERTURBATION STEP.
ALL LOADS ARE DEFINED AS CHANGE IN LOAD TO THE REFERENCE STATE

LARGE DISPLACEMENT THEORY WILL BE USED

M E M O R Y E S T I M A T E

PROCESS	FLOATING PT OPERATIONS PER ITERATION	MINIMUM MEMORY REQUIRED (MBYTES)	MEMORY TO MINIMIZE I/O (MBYTES)
1	8.06E+004	20	29

E I G E N V A L U E O U T P U T

MODE NO	EIGENVALUE	FREQUENCY (RAD/TIME)	FREQUENCY (CYCLES/TIME)	GENERALIZED MASS
8	2092.6	45.745	7.2806	63.343
9	2612.4	51.111	8.1346	63.010
10	3175.8	56.354	8.9690	64.179
11	3777.5	61.461	9.7818	62.931
12	4411.5	66.419	10.571	62.758
13	5071.9	71.218	11.335	65.452
14	5752.2	75.843	12.071	63.335
15	6446.0	80.287	12.778	62.470
16	6624.5	81.391	12.954	63.275
17	7146.7	84.538	13.455	62.359